S2S4E
Climate Services for Clean Energy

Research and Innovation action
H2020-SC5-2017

Validation of observational dataset and recommendations to the energy users

Deliverable D3.1

Version N°3

Authors: Irene Cionni (ENEA), Jaume Ramon (BSC), Llorenç Lledó (BSC), Harilaos Loukos (TCDF), Thomas Noël (TCDF).

Disclaimer

This project received funding from the Horizon 2020 programme under the grant agreement n°776787.

Document Information

Grant Agreement	776787
Project Title	Sub-seasonal to Seasonal climate forecasting for Energy
Project Acronym	S2S4E
Project Start Date	01/12/2017
Related work package	WP 3 Observational datasets
Related task(s)	Task 3.1 Analysis and verification of observational data sets
Lead Organisation	ENEA
Submission date	31/08/2018
Dissemination Level	Public

History

Date	Submitted by	Reviewed by	Version (Notes)
04/06/2018	Jaume Ramon (BSC)	Llorenç Lledó (BSC)	V0: First draft of reanalysis intercomparisons
06/08/2018	Irene Cionni (ENEA)	Llorenç Lledó (BSC)	V1: Add reanalysis intercomparison for all ECVs. First comparisons with independent observations
28/08/2018	Irene Cionni (ENEA)	Llorenç Lledó (BSC)	V2: Include regridding benchmark. Finalize all sections.
10/01/2020	Irene Cionni (ENEA)	Llorenç Lledó (BSC)	V3 : revised version according to the Review Report

Table of content

List of figures

List of tables

Executive summary

Reanalysis datasets will be employed within S2S4E project for several purposes: a) verify and bias adjust seasonal and sub-seasonal predictions, b) compute weather regimes and teleconnection indices, c) derive indicators of electricity generation and demand, and d) understand the impact of weather regimes and teleconnection indices in the electricity generation and demand.

Therefore, evaluating the quality of the available reanalysis products that will be used as ground-truth observations is key to guarantee credible conclusions. For that purpose, four Essential Climate Variables (ECV) that heavily impact the energy sector have been selected: 2 meters temperature for energy demand, surface solar radiation for solar power generation, surface wind speed for wind power generation and precipitation for hydropower generation. The quality of those four ECVs has been compared in six different global reanalyses. First, an intercomparison of the climatology, variability and long-term trends has been carried out in order to establish the main differences between datasets. Then, independent observations have been employed to assess the quality of the reanalyses in terms of biases, correlation, variability and centered root mean square errors.

Some of the analyses required a regridding or interpolation procedure in order to compare datasets in different grids. To that end, a study of the more suitable regridding methods for each ECV has been conducted.

For variables that assimilate observations (i.e. 2m temperature), large differences in climatology and variability are found in regions characterized by scarcity of observed data. Indeed, in regions where the availability of data for assimilation is extensive (e.g. Europe), reanalyses are in good agreement with each other and with observed independent dataset in terms of high spatio-temporal correlation and comparable variability. Forecasted variables (i.e. precipitation, solar radiation or surface wind) show large discrepancies over regions where the role of the model parametrizations (e.g. convective schemes, radiative transfer model or planetary boundary layer parametrization) is more relevant. Observed spatio-temporal variability of solar radiation is generally underestimated by most of the reanalysis over Europe and North Africa. European precipitation is not always well correlated with data from inland stations. For surface wind speed, broad discrepancies are found among reanalyses, although all models tend to underestimate wind speed. Different behaviours can be seen inland and over oceans, and for tropical and extratropical regions. The scores obtained when comparing reanalysis wind speed with observations strongly depend on the terrain complexity of the observational sites.

In general, high-resolution reanalyses are in better agreement with observed data.

Keywords

Global reanalysis. Reanalysis verification. Reanalysis intercomparison. Regridding methodologies. Observational uncertainty. Energy-relevant essential climate variables. Climatology. Interannual Variability. Long-term trends. Renewable energy.

Introduction

Renewable energy is the fastest growing source of electricity globally. Within the European Union, it represents more than 80% of the new installed capacity. In the case of wind power, it is expected to be the main source of electricity shortly after 2030 (IEA, 2017). Nevertheless, the diffusion of these energy sources still faces important challenges due to the high impact of weather and climate oscillations on energy generation (Brayshaw et al., 2011).
In recent decades climate and weather information has been widely used in several economic sectors impacted by climate variability, including the energy sector. The use of station observations is constantly decreasing respect to the use of gridded products, especially meteorological reanalysis datasets. On the one hand spatio-temporally varying gaps restrict the effective application of observations. Meteorological observations suffer from incomplete spatiotemporal coverage and observation errors, including systematic, random and representation errors. Recent satellite-based observations, that have much better coverage, suffer from other notable limitations, including temporal inhomogeneities (e.g. satellite drift) and retrieval errors (Bengtsson et al., 2007). On the other hand, reanalysis datasets are usually available globally; they provide several decades of coverage; and they are usually freely available. A major advantage is that reanalyses can provide data for locations or times where no direct observations are available through the integration of measurements and numerical models. However, potential problems like model errors, insufficient spatial resolution or quantity and quality of assimilated data make it necessary to validate reanalyses against measured data for applications where high accuracy is necessary. In this report six global reanalysis datasets are intercompared in terms of climatology, variability and trends, and thereafter validated against well-established observational datasets in order to build a knowledge-base about their characteristics and limitations. This information will be very useful within the project for WP4 and WP5, were a reanalysis dataset needs to be used for bias adjusting and verifying seasonal and sub-seasonal predictions.
The focus of this report is the Essential Climate Variables (ECV) directly related with renewable energy production and energy demand. The concept of Essential Climate Variables (ECVs) has been developed under the auspices of United Nations organizations and the International Council for Science to help ensure the availability of systematic observations of climate. Following (GCOS, 2010), a ECV is a physical, chemical, or biological variable or a group of linked variables that critically contributes to the characterization of Earth's climate. ECV data records are intended to provide reliable, traceable, observation-based evidence for a range of applications, including monitoring, mitigating, adapting to, and attributing climate changes, as well as the empirical basis required to understand past, current, and possible future climate variability. In this report, we analyze the following ECVs: 2 meter temperature, solar surface radiation, surface wind speed and total precipitation.

1 Reanalyses and observational datasets

This section provides details of the analyzed reanalyses and the various gridded and station observation datasets used to assess the quality of this reanalyses. Where applicable, a reference to a paper or report describing the dataset is given.

1.1 Reanalyses

The widely used reanalysis products have appeared as an efficient alternative to in-situ observations to investigate the past atmospheric conditions, both for monitoring and research purposes (Gregow et al., 2016; Compo et al., 2011; Dee et al., 2011). These global datasets are the result of combining a state-of-the-art numerical model with the assimilation of past observations from several sources to recreate the state of the atmosphere in a gridded three-dimensional mesh (Fujiwara et al., 2017). The numerical model (a geophysical fluid-dynamical model of the atmosphere containing important processes like radiative transfer and convection) enforces the results to follow the laws of physics, while the assimilation of observations constrains the recreation to be as close as possible to the measurements. A reanalysis uses a frozen model version to generate a dynamically consistent analysis over an extended period of time. However, the quantity and quality of observations varies greatly with time and location, which has an impact on final quality. The core of a reanalysis model is the data assimilation model, which uses past records to limit and guide the predictions. During the data assimilation, prior information on uncertainties in the observations and model are used to perform quality checks, derive bias adjustments and assign proportional weights. Therefore, such reanalyses add value to the instrumental record through the inclusion of bias adjustments, a broadened spatiotemporal coverage and an increased dynamical integrity or consistency. Assimilated variables vary among products but typically include air temperature, wind speed, pressure or relative humidity (analyzed fields), but the geophysical fluid-dynamical model also produces a vast list of parameters that are not directly observed and are just outputs of the numerical model (forecast fields).

The main four representative organizations that produce global reanalysis datasets are the National Centers for Environmental Prediction (NCEP), the European Centre for Medium-Range Weather Forecasts (ECMWF), the National Aeronautics and Space Administration (NASA) Goddard Space Flight Center (GSFC)'s Global Modeling and Assimilation Office (GMAO), and the Japan Meteorological Agency (JMA). Six reanalysis products (NCEP/NCAR-R1 and NCEP/DOE-R2 reanalyses from NCEP; ERA5 and ECMWF Interim Reanalysis (ERA-Interim) from ECMWF; Modern-Era Retrospective Analysis for Research and Applications (MERRA-2) reanalysis from GSFC; and JRA-55 from JMA) have been selected in this study. These products differ in many aspects, such as the numerical schemes, spatial resolution, the physical parameterizations in their numerical models, the quality and quantity of observational data assimilated, and the assimilation schemes (See Table 1 and (Fujiwara et al., 2017)). Other global reanalyses were disregarded for several reasons: discontinued products such as JRA-25, MERRA or ERA-40 are not available anymore for the recent years and are superseded by new datasets. Reanalyses that cover the whole 20th century, such as ERA-20C or NOAA's 20CR have bigger uncertainty as they assimilate only surface observations. One of the use of the reanalysis dataset in this project is the classification of the main modes of variability that largely impact the European weather. Methodologies to calculate these patterns are based on the analysis of variability in a domain between 90W and 50 E, therefore is not possible use regional reanalysis, such as UERRA that only covers a domain up to 20° W. Finally, CFSR (Saha et al., 2010), which is published by NCEP, has been produced with two different model versions before and after 2011, producing detectable changes in mean fields. Therefore, CFSR dataset has not been considered here.

Reanalysis	**ERA5**	**ERA-Interim**	**NCEP/DOE R2**	**NCEP/NCAR R1**	**JRA-55**	**MERRA-2**
Producing center	ECMWF	ECMWF	NCEP/DOE	NCEP/NCAR	JMA	NASA GMAO
Coverage	Global	Global	Global	Global	Global	Global
Spatial resolution	~ 30km	~79 km	~205 km	~205 km	~55 km	~ 55km
Time resolution	hourly	6-hourly	6-hourly	6-hourly	6-hourly	hourly
Available period	1950-present*	1979-present	1979-present	1948-present	1958-present	1980-present
Assimilation scheme	4D-Var with ensemble data assimilation	4D-Var	3D-Var	3D-Var	4D-Var	3D-Var with incremental updates
Year of model and assimilation scheme	2015	2006	1998	1995	2009	2015
Vertical levels	137 (hybrid σ-p)	60 (hybrid σ-p)	28 (σ)	28 (σ)	60 (hybrid σ-p)	72 (hybrid σ-p)
Top of model	0.01 hPa	0.1 hPa	3 hPa	3 hPa	0.1 hPa	0.01 hPa
Operational availability	Daily updates, <1 week of delay	monthly updates, 2/3 months of delay	monthly updates, <1 week of delay	monthly updates, <1 week of delay	daily updates, <1 week of delay	monthly updates, 15th/20th of next month
Commercial applications	allowed	allowed	allowed	allowed	not allowed	allowed

*whole period still not available

Table 1: Configuration details of the reanalysis datasets analyzed in this study (adapted from Fujiwara et al., 2017, and other sources).

ERA-Interim (Dee et al., 2011) has become a very used dataset for the energy sector (Gregow et al. 2016; Bett and Thornton 2016; Jones et al. 2017). The dataset covers the 1979-2017 period, and the temporal resolution is either 3 h (forecast) or 6 h (analysis), depending on the variable (see Dee et al., 2011, for details). The spatial resolution of the data set is 0.75 ° (approximately 80 km) on 60 vertical levels from the surface up to 0.1 hPa. The data assimilation method used to produce ERA-Interim is based on an updated version of the ECMWF forecasting model. ERA-Interim includes a four-dimensional variational analysis (4DVar). The assimilation includes in situ observations of near-surface air temperature, pressure and relative humidity, upper-air temperature, wind, specific humidity and rain-affected SSM/I radiances.

ERA-Interim uses climatological values for aerosols, carbon dioxide, trace gases and ozone, while it takes prognostic information from the forecasting model for the water vapor and a suite of SST and sea ice data from observations and NCEP.
https://www.ecmwf.int/en/forecasts/datasets/archive-datasets/reanalysis-datasets/era-interim

ERA5 is the new climate reanalysis dataset from ECMWF. The most substantial upgrades compared to ERA-Interim are: a finer spatial grid (31 km vs. 79 km), a higher time resolution (hourly vs. 3-hourly), a higher number of vertical levels (137 vs. 60), a new Numerical Weather Prediction model (IFS Cycle 41r2) and the increase of the amount of data assimilated. The radiative and SST forcings have also been improved, which can make a difference for climate scales. The dataset will cover from 1950 to near real time, but at this time only data for the period 2000–2017 is available. ERA5 is the first global reanalysis that produced several realizations (10 ensemble members at a lower resolution) to estimate observational uncertainty. The deterministic high-resolution version has been employed in this study.
https://www.ecmwf.int/en/forecasts/datasets/archive-datasets/reanalysis-datasets/era5

JRA-55 (Kobayashi et al. 2015) is the latest reanalysis project conducted by JMA. Compared to its predecessor, JRA-25, JRA-55 is based on a new data assimilation and prediction system that mitigates many deficiencies in the JRA-25 reanalysis. These improvements include a higher spatial resolution of T319 Gaussian grids (0.5625), a new radiation scheme, 4D-Var with Variational Bias Correction (VarBC) for satellite radiances, and introduction of greenhouse gases with time varying concentrations. JRA-55 uses in situ observation-base estimates of the COBE SST data and sea ice. The JRA-55 covers 60 years, spanning from 1958 to 2017. This dataset is not very well known in the energy sector, as its usage license does not allow commercial exploitation.
http://jra.kishou.go.jp/JRA-55/index_en.html

MERRA-2 (Gelaro et al., 2017) is a reanalysis project from NASA for the satellite era, from 1980 to present, using an updated new version of the Goddard Earth Observing System Data Assimilation System Version 5 (GEOS-5, Molod et al., 2015). MERRA-2 was created to replace the former MERRA reanalysis (Rienecker et al., 2011) and solves the limitations of the later in the assimilation of the newest sources of satellite data. MERRA-2 uses AMIP-II and Reynolds SST. One notable change is the assimilation of aerosol data to analyze five aerosol species including black and organic carbon, dust, sea salt and sulfates.
https://gmao.gsfc.nasa.gov/reanalysis/MERRA-2/

NCEP/NCAR R1 (Kalmay et al., 1996), is the first reanalysis that became available. Although using a very outdated dynamical model and data assimilation scheme and a low spatial resolution, it is convenient for its small size and fast run time. It is still routinely produced and used for several purposes, for instance it is used at NCEP Climate Prediction Center to compute Northern-Hemisphere teleconnection indices. Moreover, it spans a longer period than the other datasets presented here. It is also good as a benchmarking reference to understand the value of the enhancements the other datasets incorporate. This dataset has been used only for surface wind.
https://www.ncdc.noaa.gov/data-access/model-data/model-datasets/reanalysis-1-reanalysis-2

NCEP/DOE R2 (Kanamitsu et al., 2002), is mainly an error-correcting version or NCEP R1. It has the same resolution and assimilates a very similar observation database. However the

dynamical model incorporates some enhancements in terms of model physics. The temporal span is shorter, covering only the satellite era. NCEP R2 uses AMIP-II prescribed SST. This dataset has been used only for temperature, precipitation and radiation.
https://www.ncdc.noaa.gov/data-access/model-data/model-datasets/reanalysis-1-reanalysis-2
In order to compare and verify those reanalyses, a common period 1980-2017 has been selected. For ERA5, only data since 2000 is available at the time of writing this report, so for some analyses the shorter 2000-2017 period has been used. Table 2 summarizes the details of the employed grids, periods and time resolutions for each model. Notice also that R1 has been used for wind, while R2 has been employed for the other ECVs.

Reanalysis	**ERA5**	**ERA-Interim**	**NCEP/DOE R2**	**NCEP/NCAR R1**	**JRA-55**	**MERRA-2**
Employed period	2000-2017	1980-2017	1980-2017	1980-2017	1980-2017	1980-2017
ECVs	- 2m temp - solar rad - sfc wind - precip	- 2m temp - solar rad - sfc wind - precip	- 2m temp - solar rad - precip	- sfc wind	- 2m temp - solar rad - sfc wind - precip	- 2m temp - solar rad - sfc wind - precip
Employed grid	gaussian N320 (1280x640 points)	gaussian N128 (512x256 points)	gaussian F47 (192x94 points)	gaussian F47 (192x94 points)	regular 1.25ºx1.25º (288x145 points)	regular 0.625ºx0.5º (576x361 points)
Employed time resolution	daily & monthy means	daily & monthy means	daily & monthy means	daily & monthy means	daily & monthy means	daily & monthy means

Table 2: Details of the variables, grids and periods used in this study.

1.2 Observations

The quality of the selected reanalysis datasets has been verified with independent observations for each ECV (see Table 3). For temperature and precipitation, the E-OBS gridded dataset has been employed. For solar radiation, the CMSAF SARAH2 satellite product has been selected, while for wind speed a collection of station observations from tall towers has been used. As far as the authors know those datasets have not been ingested into the reanalyses datasets compared here. This is important to ensure a fair comparison, as a verification with observations employed in the assimilation of a reanalysis would lead to better scores.

Observa-tional Dataset	ECVs	Covera ge	Source	Grid	Time resolution	Available period
E-OBS	2 meter temperature	Europe	Meteorologi-cal stations	Regular 0.22°x0.22°	Daily	1950-2017

Observa-tional Dataset	ECVs	Covera ge	Source	Grid	Time resolution	Available period
	Precipitation					
CMSAF SARAH2	Surface solar radiation downward	Europe & Africa	Satellite	Regular 0.05°x0.05°	Instanta-neous, daily & monthly	1983-2015
Tall Tower Database	Surface wind	Global	Instrumented tall towers	Unstructured grid (213 sites)	Sub-daily, daily & monthly	1979-2018

Table 3: Details of the observational datasets used to verify the reanalysis quality.

E-OBS (Haylock et al. 2008) is a gridded daily dataset derived from ECAD surface stations (more than 7500) over Europe spanning the period from 1 January 1950 to the present, at four different grid resolutions. The area covered by E-OBS land grid squares is the area between 12º W and 45º E, and 30º N and 75º N, supplemented by Iceland (25º W to 12º W and 63º N to 67º N). The E-OBS data set was developed as part of the European Union Framework 6 ENSEMBLES project (van der Linden and Mitchell, 2009), with the aim to provide data for validation of Regional Climate Models (RCMs) and for climate change studies. The station data go through a series of basic quality checks to remove obvious problems and outliers. In order to construct time series that are as long and as complete as possible, a "blending" step is made in which ECAD data can be integrated through data available via the GTS (Global Telecommunication System). Although the station data from ECAD are not used by reanalysis in their assimilation processes, the operational GTS data are used by ERA-Interim, ERA5, JRA-55, R1, R2 and MERRA-2 reanalyses. Independence of E-OBS dataset respect to the reanalysis is also discussed in Jones et al. 2017.

CMSAF SARAH2 (Surface Solar Radiation Data Set) solar radiation data set (Müller et al., 2015) is provided by the CM SAF consortium and is derived from geostationary satellite images of the two METEOSAT geostationary satellites (0° and 57° E) covering Europe and Africa. SARAH-2 (Surface Solar Radiation Data Set-Heliosat, Edition 2, Pfeifroth et al., 2017), is the latest CM SAF climate data record of surface radiation based on the geostationary Meteosat satellite series covering Africa, Europe, and the Atlantic Ocean. SARAH-2 covers the time period 1983–2015 and offers global and direct radiation parameters as well as the effective cloud albedo. SARAH-2 is provided as daily and monthly means and as half-hourly instantaneous data. Data are limited to the part of the Earth seen by the satellites used (+/- 65° lat and lon), with the additional restriction that the calculation methods have reduced accuracy in areas that are seen at a very sharp angle by the satellite.

Tall Tower Database is an ongoing effort at BSC within the INDECIS project (www.indecis.eu) to build a unique archive of tall tower wind observations collected around the world. Most of the existing tall towers in the world belong to private companies that develop new wind farm projects and are reluctant to share their measurements. However, many public institutions,

research centers, universities and even some private initiatives also have instrumented tall towers that can be used for research purposes under diverse data policies. The basic structure of these masts is a high vertical tower (reaching heights of around 100 meters above ground level and even more in some cases) with different instrumented platforms or booms along the mast. The placement of high sensitivity sensors along these levels of measurement allows the characterization of the vertical wind profile within the area. In addition, for each level they usually have several booms, pointing to different directions. This allows the placement of more than one sensor for a given height. Therefore, failures in measurement by a sensor and shadows can be corrected by replacing these observations with those of a sensor at its same height. This helps to ensure the homogeneity of the time series. The database is composed by 213 meteorological masts so far (**¡Error! La autoreferencia al marcador no es válida.**). The period of record of these masts is quite diverse. Although it ranges from 37 to 1 year, most of the time series do not cover more than 20 years. These data have been processed to a common format and prepared for further usage. This collection of observations aims to be publicly accessible by 2019.

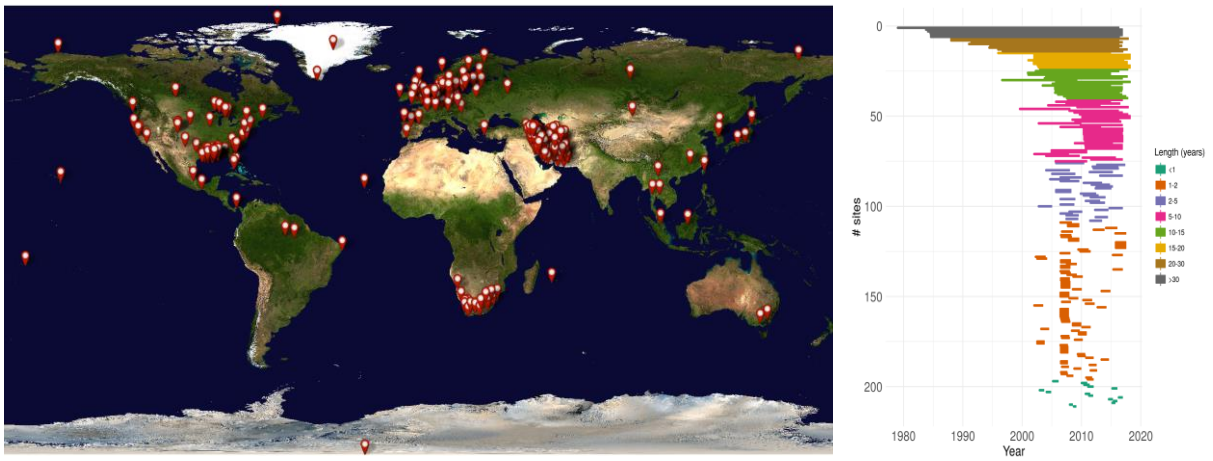

Figure 1: Spatial distribution and time span of the tall towers in the database.

1.3 Regridding methodologies

1.3.1 Rationale

Regridding methodologies are necessary in this project for two tasks:

- Intercompare various reanalysis datasets to understand differences among them and benchmark those reanalysis products with gridded or unstructured observations.
- Evaluate forecast products with an operational reanalysis product (this will be performed later in this project).

The partners decided to test and use existing tools for since the development of new methodologies is not central to this project. The obvious choice was to adopt the extensively

used Climate Data Operators (or CDO) available from the Max Planck Institute for Meteorology (https://code.mpimet.mpg.de/projects/cdo/) and already used by most partners of the project.

The available algorithms in CDO are:

- Bilinear interpolation (remapbil).
- Bicubic interpolation (remapbic)
- Nearest neighbor remapping (remapnn).
- Distance-weighted average remapping (remapdis).
- First order conservative remapping (remapycon).
- First order conservative remapping (remapcon).
- Second order conservative remapping (remapcon2).
- Largest area fraction remapping (remaplaf).

One will note that all functions are presented as "remapping" techniques (remap prefix). Indeed, they were originally developed to regrid different type of grids (regular, rectilinear, curvilinear regular, or unstructured) of similar resolution, hence the term "remap". The graphical examples of each function show for example the regridding from a regular to an unstructured triangular grid (Figure 2).

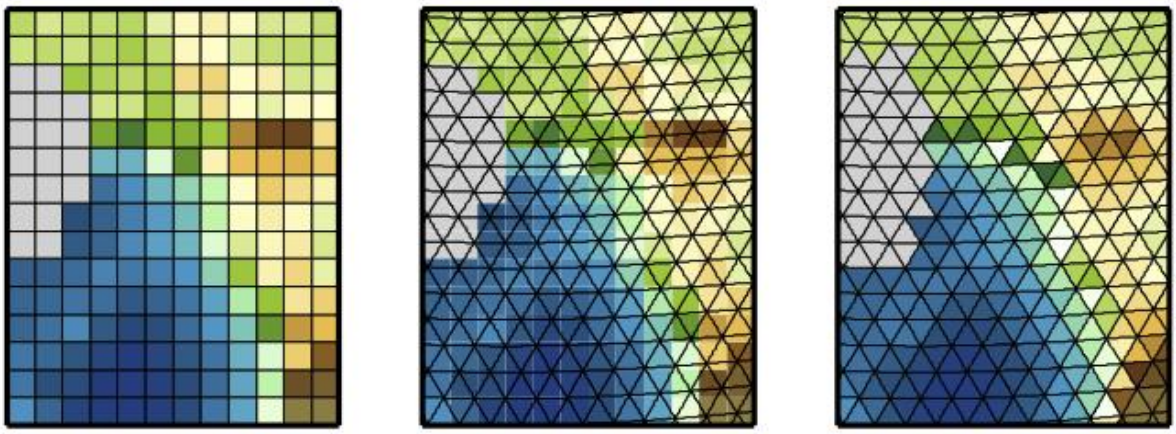

Figure 2: The figure on the left side shows the input data on a regular lon/lat source grid and on the right side the remapped result on an unstructured triangular target grid. The figure in the middle shows the input data with the target grid. Grid cells with missing value are grey colored (extracted from the CDO users Guide Version 1.9.4).

For both mentioned tasks of this project the regridding will be used to interpolate finer grids to coarser grids:

- the benchmark of reanalysis is done to the coarser grid.

- the evaluation of the forecast will be done with reanalysis products (probably ERA5) that have a finer resolution of the subseasonal and seasonal forecast products (typically 1°x1° to 2.5°x2.5°).

This makes some methods irrelevant to our case ("Largest area fraction remapping" for example). In addition, to avoid some redundancy between similar methods, we focus only to a subset of functions:

- Bilinear interpolation (remapbil).
- Bicubic interpolation (remapbic).
- Nearest neighbor remapping (remapnn).
- Second order conservative remapping (remapcon2).

To evaluate each algorithm, we have performed a "doubleback" experiment (McGinnis et al. 2010; A. Frein EURO-CORDEX personal communication). The data is first interpolated from its native high resolution regular grid to the lower resolution grid (corresponding to the two tasks mentioned above) and then back again to the original grid. The original values are then subtracted to show where the doubleback regridding introduces differences in the data.

ERA5 daily averages covering Europe from 2001 to 2017 where used as test data for all project variables. The targeted grids where regular 1.0°x1.0° and 2.5°x2.5° grids. Because the finer grid is as much as 10 times finer (0.25° compared to 2.5°) we also tested a stepwise approach where regridding was done sequentially on grids of intermediary resolution when regridding back to the finer grid. We adopted a single intermediate step for the 1° grid (1.0°→0.75°→0.25°) and up to three intermediate steps for the 2.5° grid (2.5°→1.25°→0.25°, 2.5°→1.5°→0.75°→0.25° and 2.5°→2.0°→1.5°→0.75°→0.25°).

1.3.2 Comparison of regridding methodologies

Graphical results for temperature are shown in Figure 3 as an illustration. A summary table including error statistics for all ECVs and methods is provided later (Table 4).

Visual analysis of Figure 3 does not allow seeing major differences between methods except for the "Nearest Neighbor" method. Indeed, results are inherently more "pixelated" and less smooth. Also adding a step in the backward interpolation does not seem to bring any improvements..

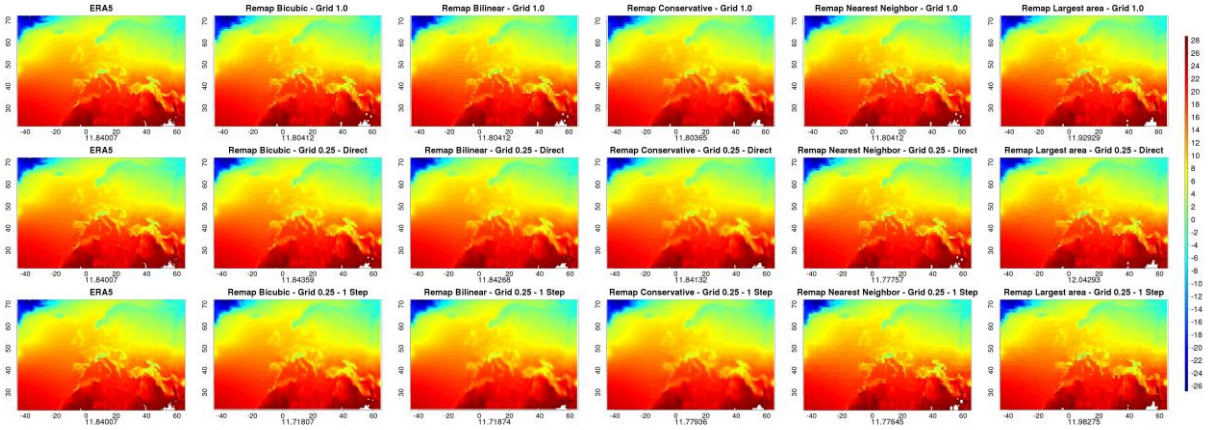

Figure 3: Doubleback interpolation for the 1° grid. All fields have been averaged over the test period. First column is the original ERA5 field; the four others are for the different remapping methods. First line is the direct remapping on the targeted grid. The second line is the "backwards" interpolation to the original grid, and the third one is again the backwards interpolation but with an intermediate single step.

Figure 4 shows the average absolute error for the temperature over the period for the 1° grid. Errors are concentrated over high elevations. Again, it is not possible to see major differences between methods except again for the "Nearest Neighbor" method.

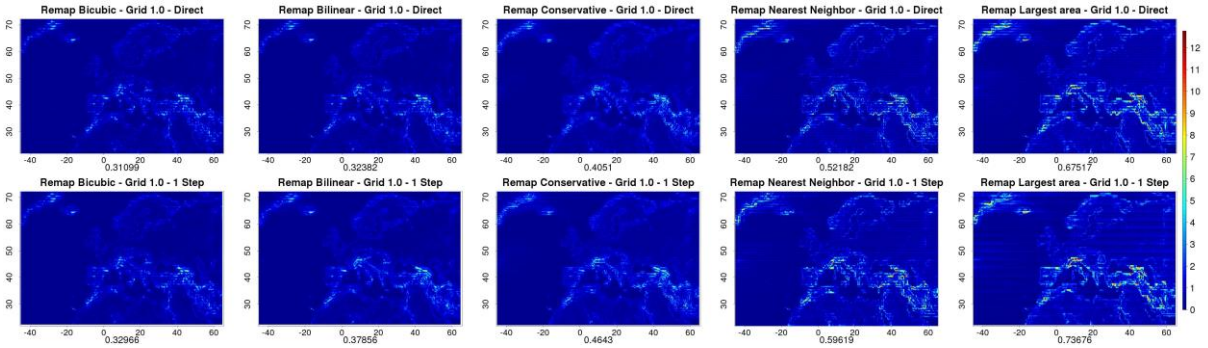

Figure 4: Absolute error fields from the doubleback interpolation for the 1° grid. All fields have been averaged over the period. Columns are the interpolation methods and lines the direct and one step approach.

As visual analysis does not convey a lot of information, Table 4 presents the statistics of the error fields and allows drawing some general remarks:

- remapnn has the worst results everywhere.
- remapbic seems to prevail for radiation.
- remapcon2 comes first for wind despite not having the smallest mean absolute error.

- Adding a step in the interpolation doesn't necessary improve the results.
- remapcon2 and remapbil have similar results depending on the variable and if the backwards interpolation is direct or stepwise. They should thus be considered as prefered methods;

		remapcon2		remapbil		remapbic		rempann	
		Direct	1 Step	Direct	1 Step	Direct	1 Step	Direct	1 Step
2m temperature	mean (abs)	0.41	0.47	0.34	0.39	**0.32**	0.34	0.53	0.61
	min	-15.9	-17.4	-18.0	**-15.5**	-18.2	-17.2	-24.8	-25.0
	max	15.6	**15.4**	16.5	16.5	16.1	16.1	24.7	28.7
	var	**0.17**	0.24	0.17	0.17	0.19	0.19	1.20	1.64
	std	**0.29**	0.32	0.30	0.30	0.30	0.30	0.45	0.50
Precipitation	mean (abs)	3.74E-04	4.25E-04	3.27E-04	3.81E-04	**3.16E-04**	3.36E-04	4.71E-04	5.29E-04
	min	-0.20	-0.22	-0.22	-0.24	-0.19	**-0.19**	-0.23	-0.31
	max	0.13	0.09	0.09	**0.07**	0.10	0.09	0.22	0.23
	var	**2.58E-12**	3.90E-12	3.06E-12	3.53E-12	2.81E-12	2.83E-12	1.19E-11	1.90E-11
	std	**5.27E-04**	5.86E-04	5.84E-04	5.67E-04	5.72E-04	5.52E-04	8.55E-04	9.67E-04
Mean sea level pressure	mean (abs)	21.1	25.7	10.0	12.3	**9.4**	10.3	32.3	38.2
	min	-897	-1054	**-856**	**-856**	-874	-996	-1352	-1599
	max	**909**	1006	998	998	963	1122	1759	2082
	var	2.19E+06	3.76E+06	**1.47E+06**	1.79E+06	2.07E+06	4.76E+06	1.45E+07	2.91E+07
	std	16.7	18.3	**14.3**	15.3	16.1	18.1	26.4	32.1
Surface Wind	mean (abs)	0.34	0.39	0.28	0.33	**0.25**	0.27	0.44	0.50
	min	**-12.0**	-14.0	-14.2	-15.7	-13.1	-13.2	-18.6	-21.0
	max	**12.9**	14.8	14.7	14.7	15.4	15.3	21.4	21.4
	var	**0.07**	0.10	0.07	0.08	0.07	0.07	0.39	0.60
	std	**0.21**	0.23	0.23	0.23	0.23	0.22	0.35	0.40

Surface solar radiation downwards	mean (abs)	1.42E+04	1.68E+04	9.95E+03	1.26E+04	**8.07E+03**	8.85E+03	1.89E+04	2.20E+04
	min	-4.81E+05	-5.70E+05	-4.96E+05	-5.45E+05	-5.01E+05	**-4.79E+05**	-8.33E+05	-1.01E+06
	max	5.01E+05	5.70E+05	4.88E+05	4.98E+05	4.95E+05	**4.84E+05**	8.52E+05	8.88E+05
	var	1.57E+17	3.10E+17	1.10E+17	1.38E+17	**7.55E+16**	8.28E+16	1.27E+18	2.71E+18
	std	7.89E+03	9.06E+03	8.20E+03	7.46E+03	7.30E+03	**6.80E+03**	1.56E+04	1.91E+04

Table 4: Error statistics for each variable from the doubleback interpolation experiment for the 1° grid. The "backwards" interpolation has been done directly and with a single step (at a 0.75° grid). Mean absolute error, minimal and maximal value, variance and standard deviation. Best values for each row are highlighted

The same experiment has been conducted for the 2.5º grid. The only appreciable difference is that for the 2.5º grid the stepwise approach with two intermediate steps delivered better results than direct in some cases. Also results, are more contrasted compared to the 1° grid. Figure S1 (see Supplementary Figures, ANNEX A) shows the average for temperature over the period for the 2.5° grid and Figure S2 shows the average for the temperature errors over the period for the 2.5° grid.

1.3.3 Discussion and recommendations on regridding methods

Second order conservative and bilinear interpolation are found as the best regridding methods in a doubleback experiment and can be safely used for the ECVs of the project. Obviously, these results depend on the experiment design and criterion adopted for selection. As simple statistics have been used here to infer the best method, this does not preclude other regridding or interpolation methods to perform well with other tests, for instance when interpolating reanalyses to single points. We have also found that if regridding for a coarser to a finer grid is needed, introducing a few intermediate steps (i.e. intermediate resolution grids) can improve results in some cases.

Two possible strategies can be adopted. Considering an optimal approach, one should pick the most adequate method form the two for each variable. Considering a simplified approach, one could decide to use the same method for all variables. In the last case, the conservative approach is usually preferred from a physical viewpoint because of the mass conservation constraint that is preferred for flux variables (like precipitation) and extended nonetheless to the non-flux variables.

Table 5 summarizes the selection of regridding or interpolation methods employed for each ECV in the remaining of this study for the comparison of the reanalyses with observations. For surface wind, several methods have been compared further (see section 3.3.4).

ECV	Reanalysis Grid	Observational Dataset Grid	Regridding or interpolation Methodologies
2 meter temperature	Regular	Regular	- bilinear interpolation
Surface solar radiation downward	Regular	Regular	- conservative interpolation
Surface wind	Regular	Unstructured	- nearest neighbor - bilinear interpolation - 9-point smoothing
Precipitation	Regular	Regular	- conservative interpolation

Table 5: Regridding methods per ECV used for the benchmarking of reanalysis products.

2 Methodologies

The ability of the different reanalyses to accurately reproduce the seasonal cycle and mean value, the interannual variability of seasonal averages, and the long-term trends have been studied. Each of those aspects is of importance for both seasonal forecasting evaluation and energy assessment purposes.

Seasonal averages have been computed from 6-hourly (ERA-Interim, JRA-55, R1 and R2) or hourly (ERA5 and MERRA-2) data samples. The usual seasons have been employed: December-January-February (DJF), March-April-May (MAM), June-July-August (JJA) and September-October-November (SON).

Some of the comparisons require a common grid to better contrast their performance. Consequently, the output of each model has been interpolated to the F47 (T62) horizontal grid, using the methodologies described in table 6 (previous section). This is R1's dataset grid and it is the coarsest of the four different grids used by the different datasets analyzed in this study.

For each ECV, climatology, variability and trends are studied for each season.

For climatology and variability, maps of multimodel mean (MM) have been computed, and the differences of each individual reanalysis with this MM analyzed. The spread amongst reanalyses (the standard deviation of those differences) is also presented to highlight the regions where there are stronger disagreements and higher uncertainty.

Trends have been presented in absolute or relative amount per decade, and statistical significance has been computed. Trends from 2000-2017 (ERA5 availability period) are not shown in this study. According to Hartmann et al. 2013 (AR5), trends based on short records are very sensitive to the beginning and end dates because of the natural variability and generally do not reflect long-term climate trends.

Interannual variability (IAV) is computed separately for each season as the standard deviation of the seasonal means for all years under consideration. Intraseasonal variability (ISV) is computed as the standard deviation of all the monthly means within a season for all years, and gives an idea of the amount of variability that exists between individual months of the same season (i.e. how good is the season in terms of grouping months of similar conditions).

The Taylor diagrams (Figure 5) provide a concise statistical summary to quantify the overall correspondence between variables of one or more test datasets (i.e. reanalysis A, B, C) and one or more reference datasets (observed dataset REF) (Taylor 2001). In the Taylor diagram the black dot (REF) on the x-axis identify the reference dataset. A single point (A) on the bidimensional plot indicates the ratio of the normalized variance (represented by the normalized ratio of their standard deviations), the correlation and the centered root-mean-square error (CRMSE) between test dataset and reference dataset. The standard deviation ratio of the test pattern is proportional to the radial distance from the arc at the point A and the arc at the REF. The centered root-mean-square error between the test and reference patterns is indicated by the semicircle contours centered on the REF. The correlation is given by the azimuthal position of A. Test patterns that agree well with reference pattern will lie near the black dot on the x-axis. In order to evaluate spatial climatological patterns Taylor diagrams are produced for annual climatologies and seasonal climatologies. In order to evaluate spatial and temporal patterns Taylor diagrams for daily, monthly and seasonal time series have been used. Informations about the percent bias are included in the taylor diagram by using triangles of different size and orientation (negative bias is indicated by upside down triagles), circles indicate bias below 1%.

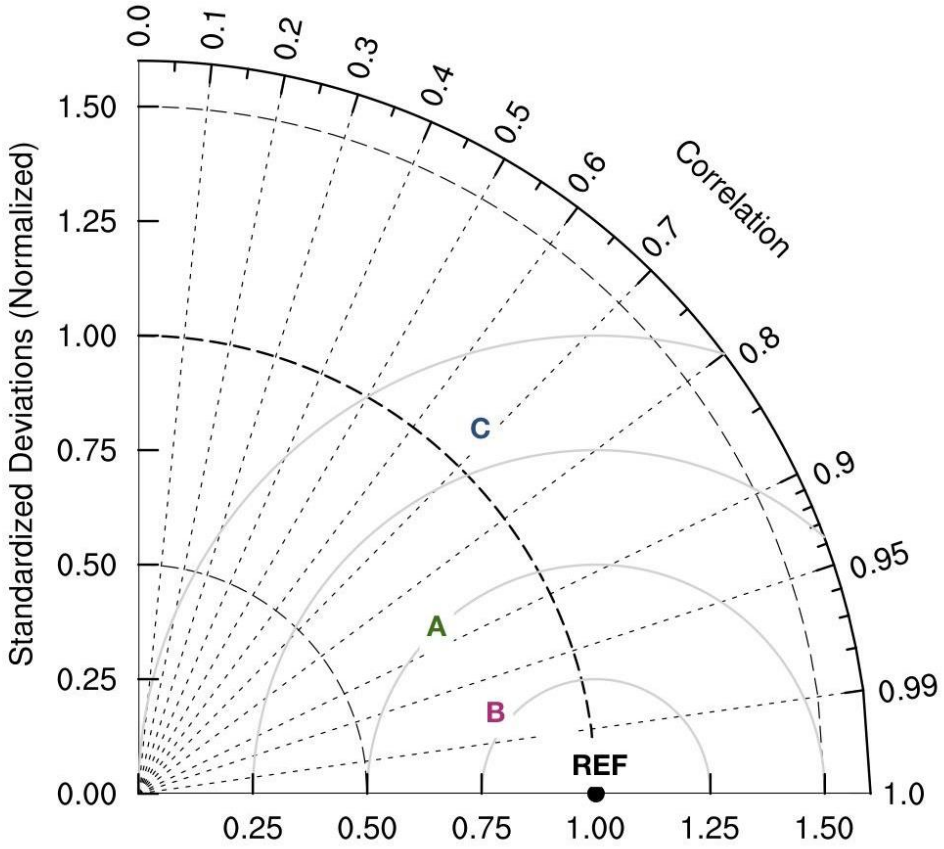

Figure 5: An example Taylor diagram

3 Verification of Reanalyses

3.1 Validation results for 2m temperature

Surface air temperature has profound and widespread impacts on human lives and activities, affecting health, agriculture, energy demand and much more. In particular, temperature is the dominant weather driver of electricity and residential gas demand in many developed countries, where lower temperatures produce heating demand and higher temperatures create air conditioning demand (Thornton et al. 2016, Hahn et al. 2009, De Felice 2013*)*. Energy demand is shown to vary across a range of timescales, with clear annual cycles and long-term trend. For this reason, seasonal climatology, seasonal interannual variability and intraseasonal variability of 2 meters temperature are investigated.

3.1.1 Intercomparison of 2m temperature climatology

The geographical distribution of seasonal and annual mean 2m temperature is well represented in all the datasets (Figure S3 and Figure S4). The differences between each single dataset and the ensemble mean are very similar in the annual mean (Figure 3S) and the seasonal mean (Figure 6) and generally are lower than 1°C, with slight departures from these values in locations where the observations assimilated are relatively scarce. Indeed, the multi reanalysis spread, computed as the standard deviation of the five climatologies, is highest at Poles, Africa and Asian Plateau (Figure 6). For the ocean based 2m temperature, which is strongly influenced by SST, the agreement is generally good. Differences in MERRA-2 and JRA-55 over the Arctic and Southern Oceans are expected and could also be due to differences in sea ice (Auger et al. 2018)

ERA-Interim and JRA-55 are positively biased in East Antarctica and slightly biased in North Africa and Europe. ERA-Interim has a warmer wintertime bias in Arctic (Simmons et al. 2015). The bias of ERA-Interim in North Asia is negative in DJF and positive in MAM.

MERRA-2 has a negative bias in Europe and North America especially in DJF and SON. MERRA-2 is generally warmer than the multi reanalysis mean over most of Africa, Australia, Central Asia, and South America. NCEP2 has a large negative bias in Africa during all the seasons and a strong positive bias in North America and North Europe during DJF. R2 is also the dataset less spatially correlated with the multi reanalysis mean.

In the seasonal climatological mean 2000-2017, ERA5 is very similar to ERA-Interim (Figure 7). ERA5 seems to be the dataset less biased respect to the multi reanalysis mean. In Arctic ERA5 is warmer over ice and colder over land. In Europe during JJA ERA5 is colder than ERA-Interim.

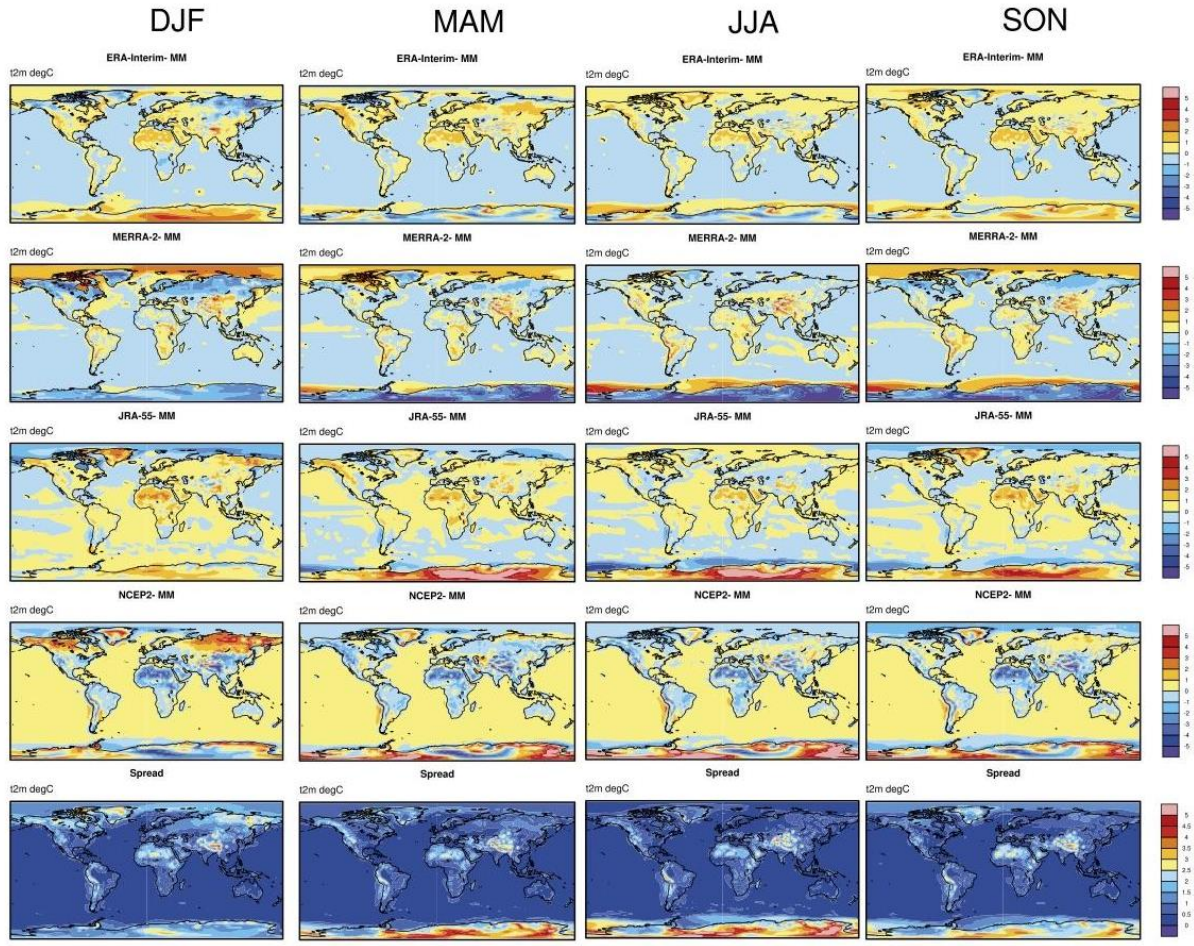

Figure 6: Differences of seasonal (DJF, MAM, JJA, SON) climatological mean 2 m temperature 1980-2017 between ERA-Interim, MERRA-2, JRA-55, NCEP/DOE R2 and multi reanalysis mean. (Bottom) Spread of the reanalysis ensemble

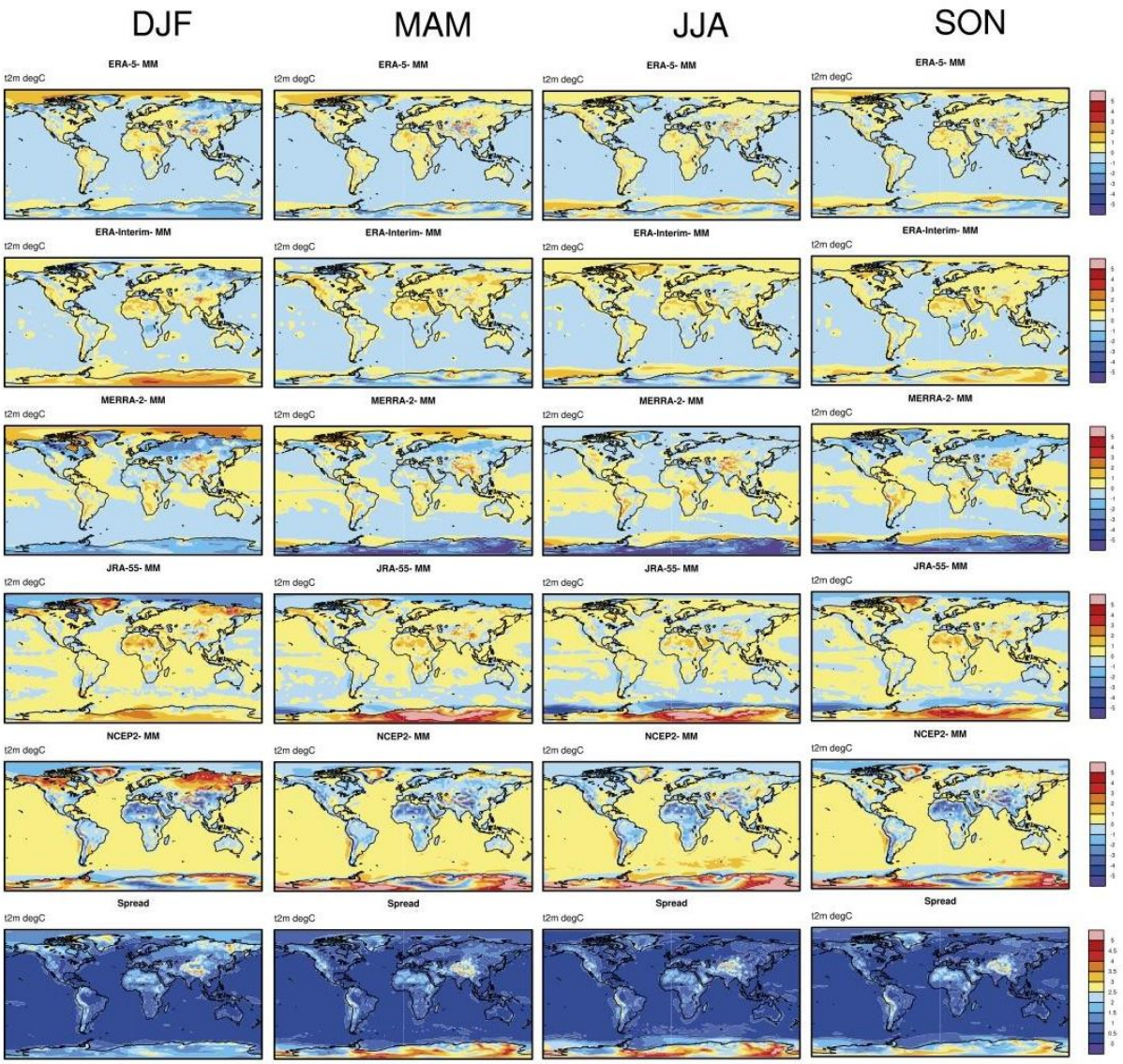

Figure 7: Differences of seasonal (DJF, MAM, JJA, SON) climatological mean 2 m temperature 2000-2017 between ERA5, ERA-Interim, MERRA-2, JRA-55, NCEP/DOE R2 and multi reanalysis mean. (Bottom) Spread of the reanalysis ensembles

3.1.2 Intercomparison of 2m temperature variability

Interannual Variability

The geographical distribution of the interannual variability shows very high values at extremes northern latitude and southern latitudes in seasonal and annual time series (Figure S5 and Figure S6). The intercomparison is based on Figure 8, where the differences of normalized interannual variability between single reanalysis and multi model mean are represented. Interannual variability has been normalized by the mean 2 m temperature of the season in Kelvin degrees. Generally, the multi reanalysis spread is higher where the interannual variability is higher (Figure S6). There is a low spread value in Europe during all the seasons, but not negligible values in Africa, Andes region and Asian Plateau. These are the same regions where the differences of climatological values are higher (Figure 8).

Differences between ERA-Interim and multi reanalysis mean are relevant only in North Asia during DJF. MERRA-2 has interannual variability higher than the multi reanalysis mean in Central Africa and Amazonia. JRA-55 has lower interannual variability in Antarctica and up to 60° latitude in DJF. R2 shows the highest variability in Antarctica, in Arctic, in North Africa and Andes mountain range especially in DJF and SON. These high values largely contribute to the multi reanalysis spread in those regions.
In the period from 2000-2017 (Figure 9), ERA5 has less inter annual variability than ERA-Interim during DJF and MAM over North Asia and Arctic and in better agreement with the others reanalysis.

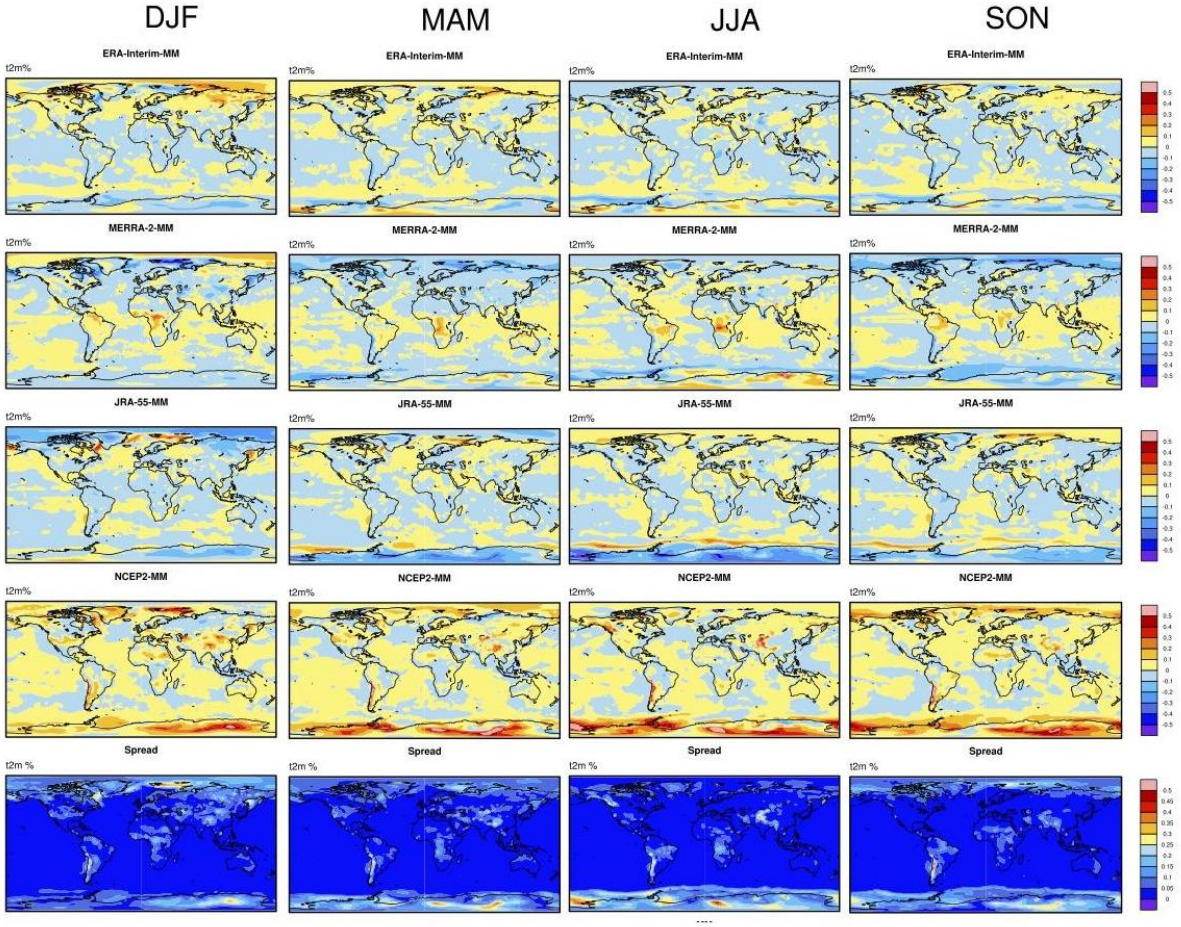

Figure 8: Differences of normalized interannual variability 1980-2017 2 m temperature between ERA-Interim, MERRA-2, JRA-55, NCEP/DOE R2 and multi reanalysis mean. (Bottom) Multi reanalysis spread of interannual variability.

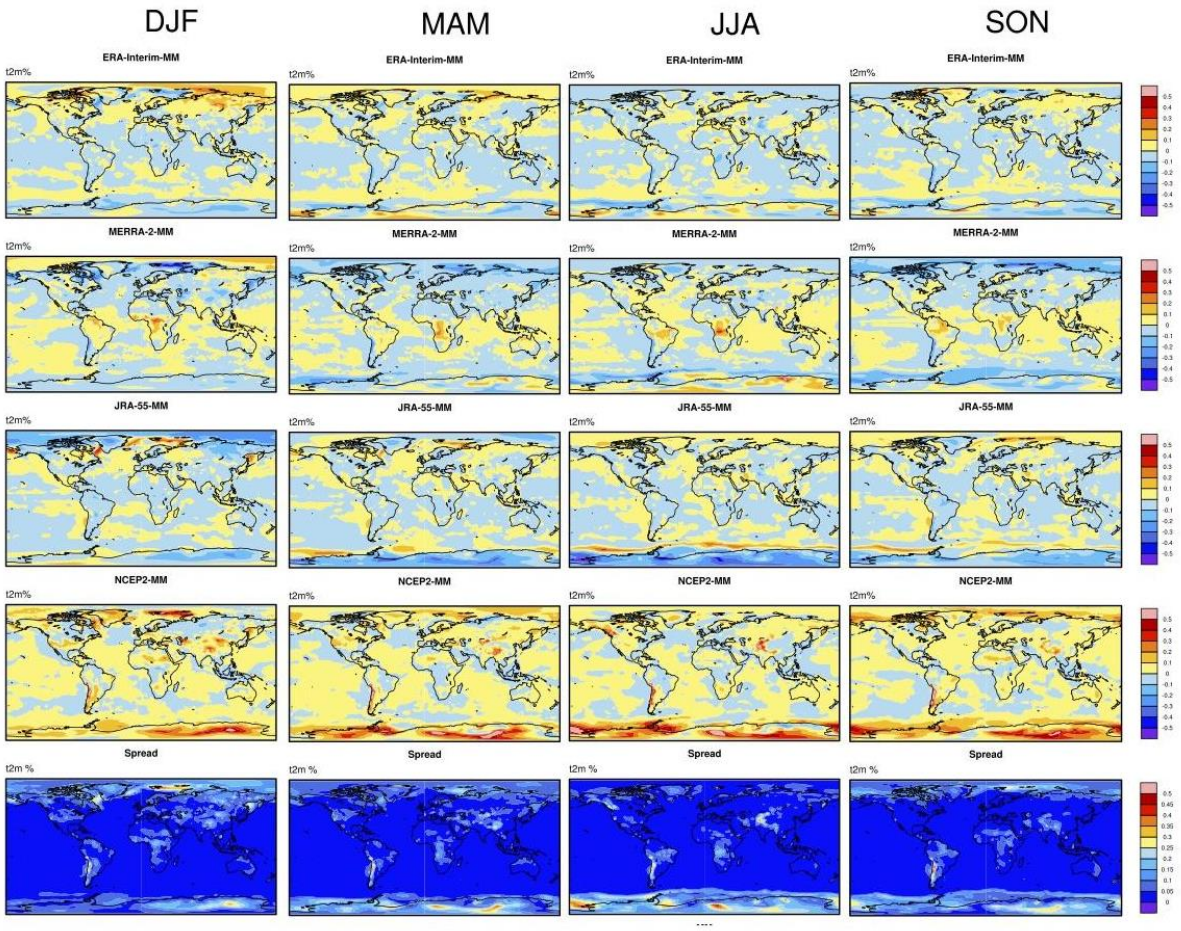

Figure 9: Differences of normalized interannual variability 2000-2017 2 m temperature between ERA5, ERA-Interim, MERRA-2, JRA-55, NCEP/DOE R2 and multi reanalysis mean. (Bottom) Multi reanalysis spread of interannual variability.

Intraseasonal variability

The intraseasonal variability is strongly related with season and hemisphere (Figure S7 and Figure S8). The multi reanalysis spread is larger at tropical latitudes (Figure 10).

ERA-Interim has an intraseasonal variability general lower than multi reanalysis mean especially in North Africa and in the Mediterranean region during JJA. MERRA-2 has a higher intraseasonal variability at mid and high latitudes and lower intraseasonal variability in tropical regions. JRA-55 has higher intraseasonal variability in North Africa. R2 largely exceed the intraseasonal variability of the multi reanalysis mean.

During the period 200-2017, ERA5 shows less intraseasonal variability in polar region respect to ERA-Interim and has a better agreement with the multi reanalysis mean than the others dataset (Figure 11).

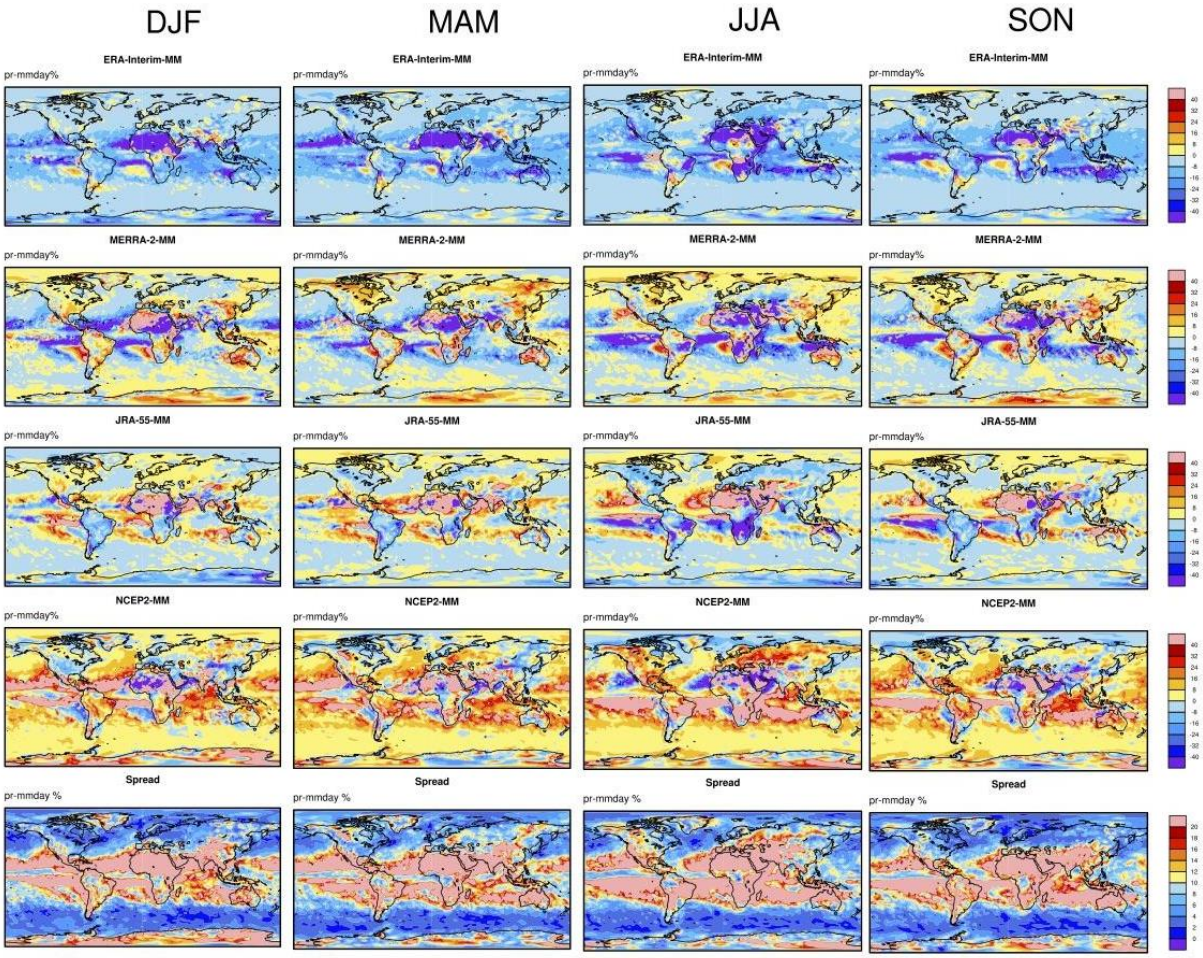

Figure 10: Differences of normalized intraseasonal variability 1980-2017 of monthly 2 m temperature between ERA-Interim, MERRA-2, JRA-55, NCEP/DOE R2 and multi reanalysis mean. (Bottom) Spread of the reanalysis ensemble.

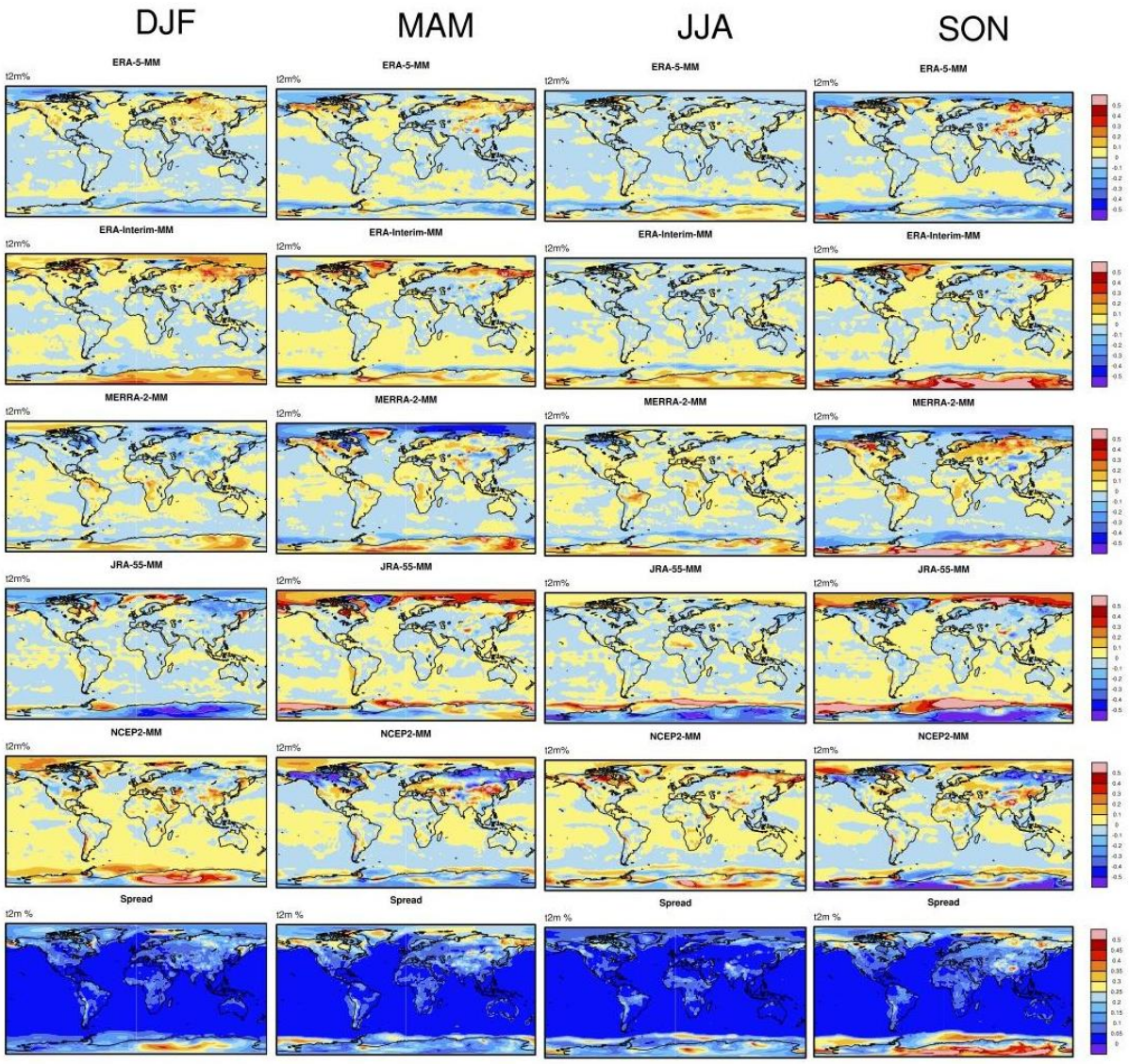

Figure 11: Differences of normalized intraseasonal variability 2000-2017 of monthly 2 m temperature between ERA5, ERA-Interim, MERRA-2, JRA-55, NCEP/DOE R2 and multi reanalysis mean. (Bottom) Multi reanalysis spread of intraseasonal variability.

3.1.3 Intercomparison of 2m temperature trends

Linear trend is calculated as Kelvin degrees per decade for the period from 1980-2017, ERA5 has been excluded in this analysis for having a too short period (Figure S9 and Figure 12). The geographical and seasonal features of the trend (Figure 12) are similarly reproduced by the reanalyses and values are comparable to the estimates values from observed measurement (Hartmann et al. 2013, AR5). All datasets points to a substantial warming of the Arctic over recent decades ('Arctic amplification'). MERRA-2 differs from ERA-Interim, JRA-55 and R2 in that it exhibits less warming. Simmons et al. 2015 shows that in situ data are much closer to that from ERA-Interim and JRA-55 than it is to that from MERRA-2. Only R2 presents a similar warming over Antarctic. Positive trend is always significant in Europe, except in DJF.

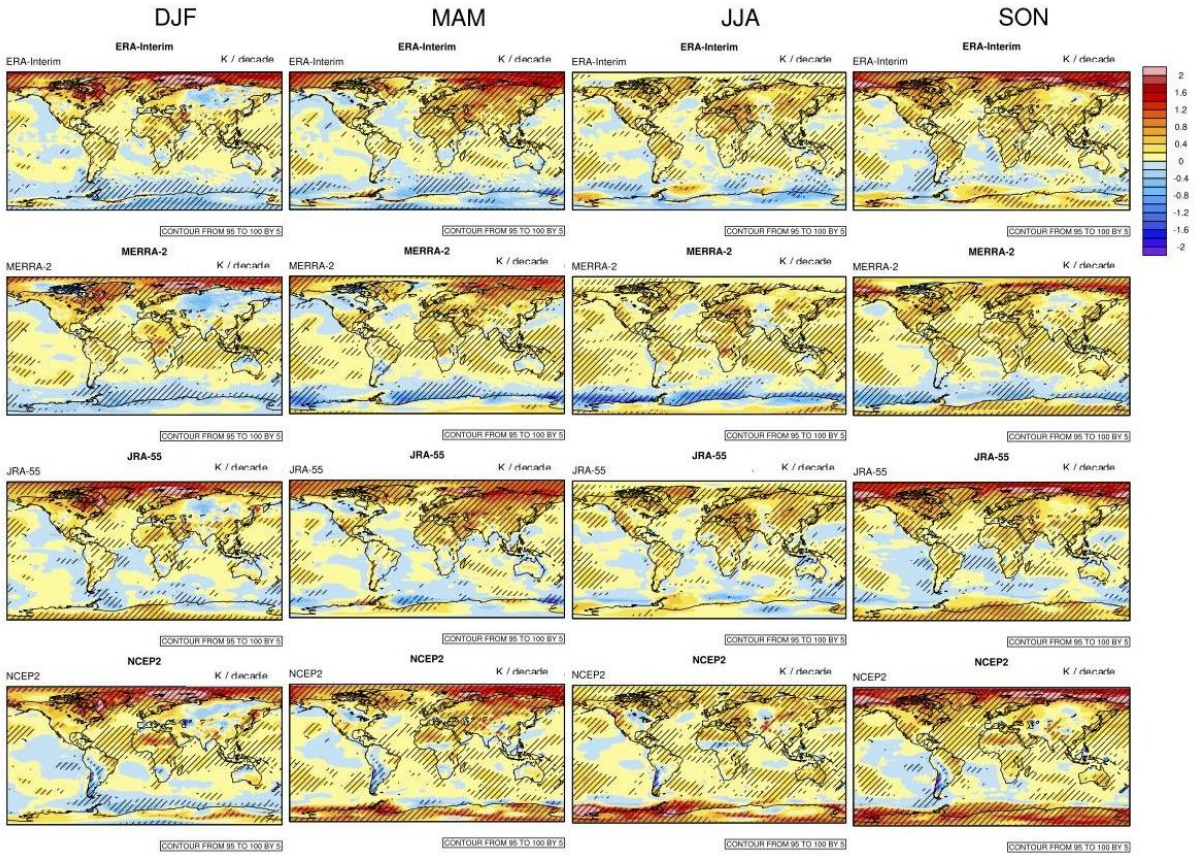

Figure 12: Trend 1980-2017 of seasonal 2 m temperature in ERA-Interim, MERRA-2, JRA-55, NCEP/DOE R2.

3.1.4 Verification of 2m temperature with E-OBS observations

Taylor diagrams provide a quantitative assessment of the spatial and temporal variability of the reanalysis. Gridded datasets are important for climate analysis, for monitoring climate change and for validation on climate models. E-OBS has significant advantages including high spatial resolution, long-term period, uncertainty estimation incorporation and a novel interpolation method (Haylock et al., 2008). E-OBS temperature has been already compared with reanalysis (van Der Schrier et al. 2013) and used in the energy sector (Jones et al 2017).

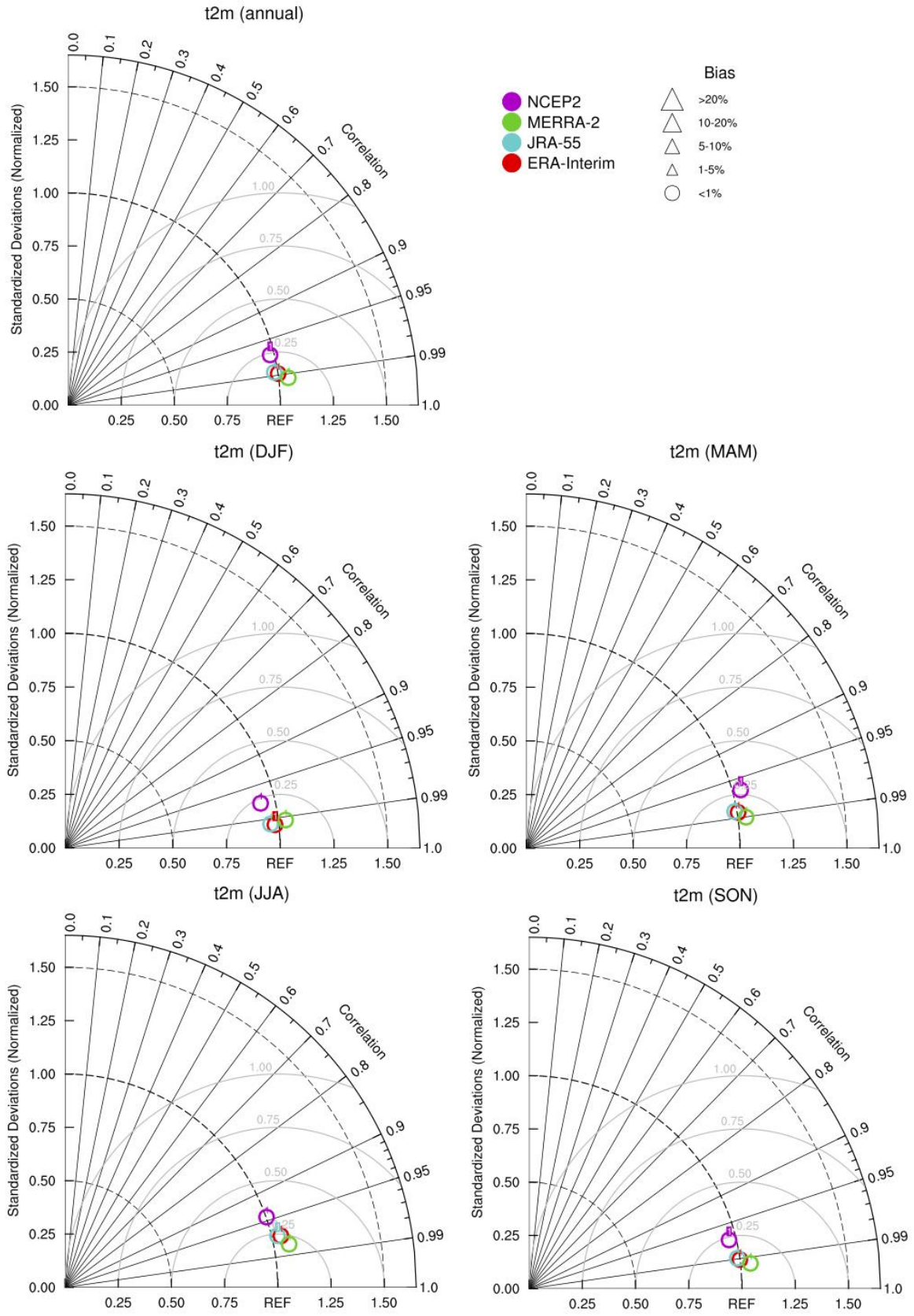

Figure 13: Taylor Diagram of climatological mean 1980-2017 of annual (Top) and seasonal (Center and Bottom) 2 m temperature in ERA-Interim, MERRA-2, JRA-55, NCEP/DOE R2 vs. E-OBS.

The spatial distribution of the climatological mean is evaluated in Figure 13 for annual and seasonal values respect to the E-OBS dataset. The domain validated is the E-OBS domain (Europe inland). There is good correlation between reanalysis and observation (up to 0.95 except R2 during JJA). Summer is the season when the spatial correlation is poorest. The bias is always below 1% (temperature values in Kelvin degrees has been considered).
ERA-Interim and JRA-55 show very good agreement in terms of variability (standard deviation ratio) and correlation. MERRA-2 variability is always higher than E-OBS and R2 has lower correlation in all the season especially JJA. Low values of R2 are related with the low resolution of this reanalysis. The spatial distribution of the climatological mean from 2000 to 2017 is shown in Figure 14. ERA5 is the reanalysis better correlated with E-OBS. Correlation is up to 0.99 for the annual climatological mean and seasonal DJF, MAM and SON mean and almost 0.99 for the JJA mean. As in ERA-Interim the variability is always close to the values of E-OBS. ERA-5 is dataset whit the lower bias in ANN, DJF and MAM.
The temporal and spatial distribution of the monthly mean is evaluated in Figure 15 for annual and seasonal values respect to the E-OBS dataset. Values of correlation are slightly lower than the values that take in account only spatial distribution (Figure 13). All the datasets show a higher variability than E-OBS, especially MERRA-2. JJA is the season when the correlation is lower in all the reanalysis. R2 is the dataset with the poorest correlation. In the analysis of the period 2000-2017 (Figure 16) ERA5 is in good agreement with ERA-Interim and MERRA-2 with correlation close to 0.95 and standard deviation ratio slightly greater than 1 (monthly values). ERA-5 is dataset whit the lower bias in ANN, MAM and SON.

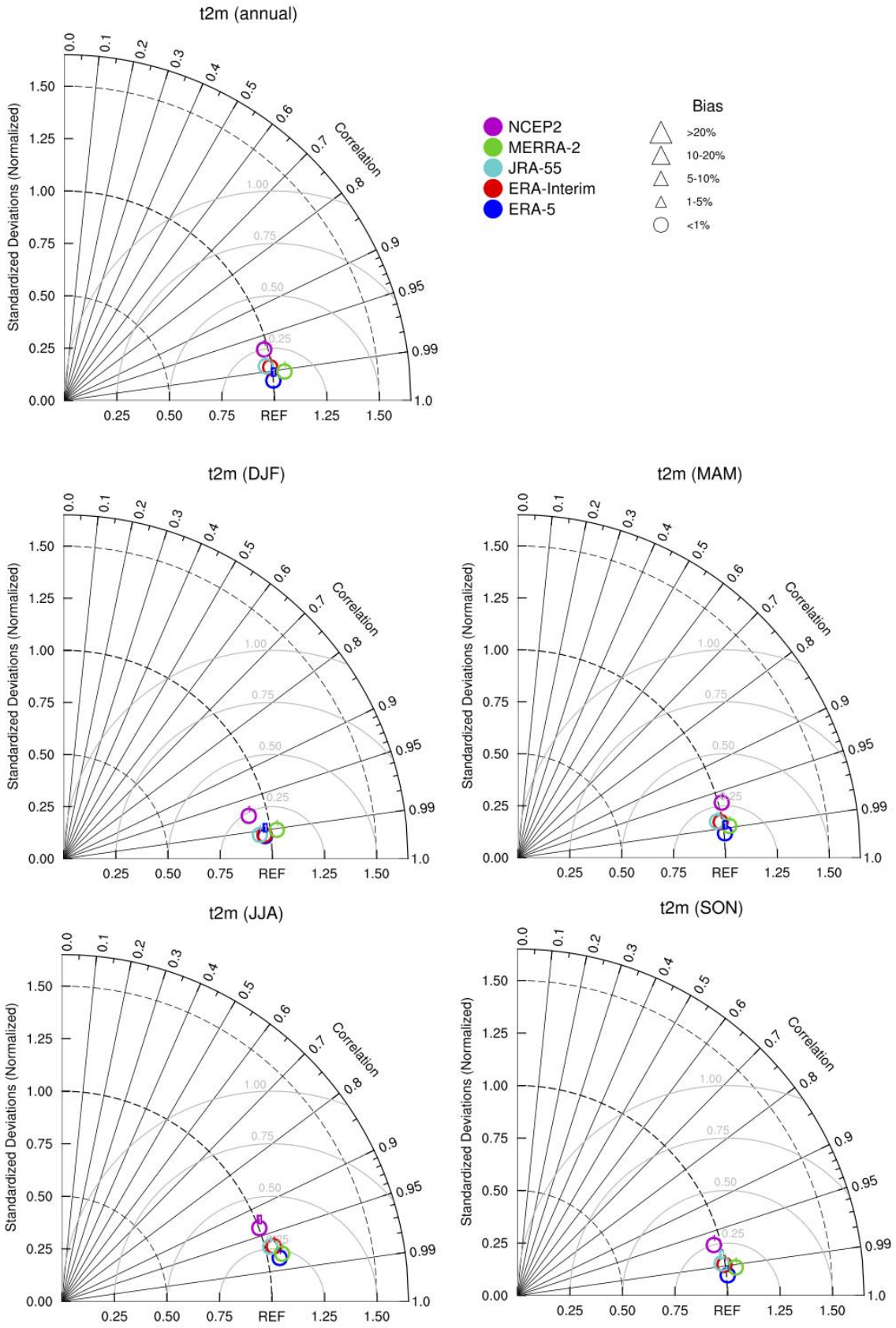

Figure 14: Taylor Diagram of climatological mean 2000-2017 of annual (Top) and seasonal (Center and Bottom) 2 m temperature in ERA5, ERA-Interim, MERRA-2, JRA-55, NCEP/DOE R2 vs. E-OBS.

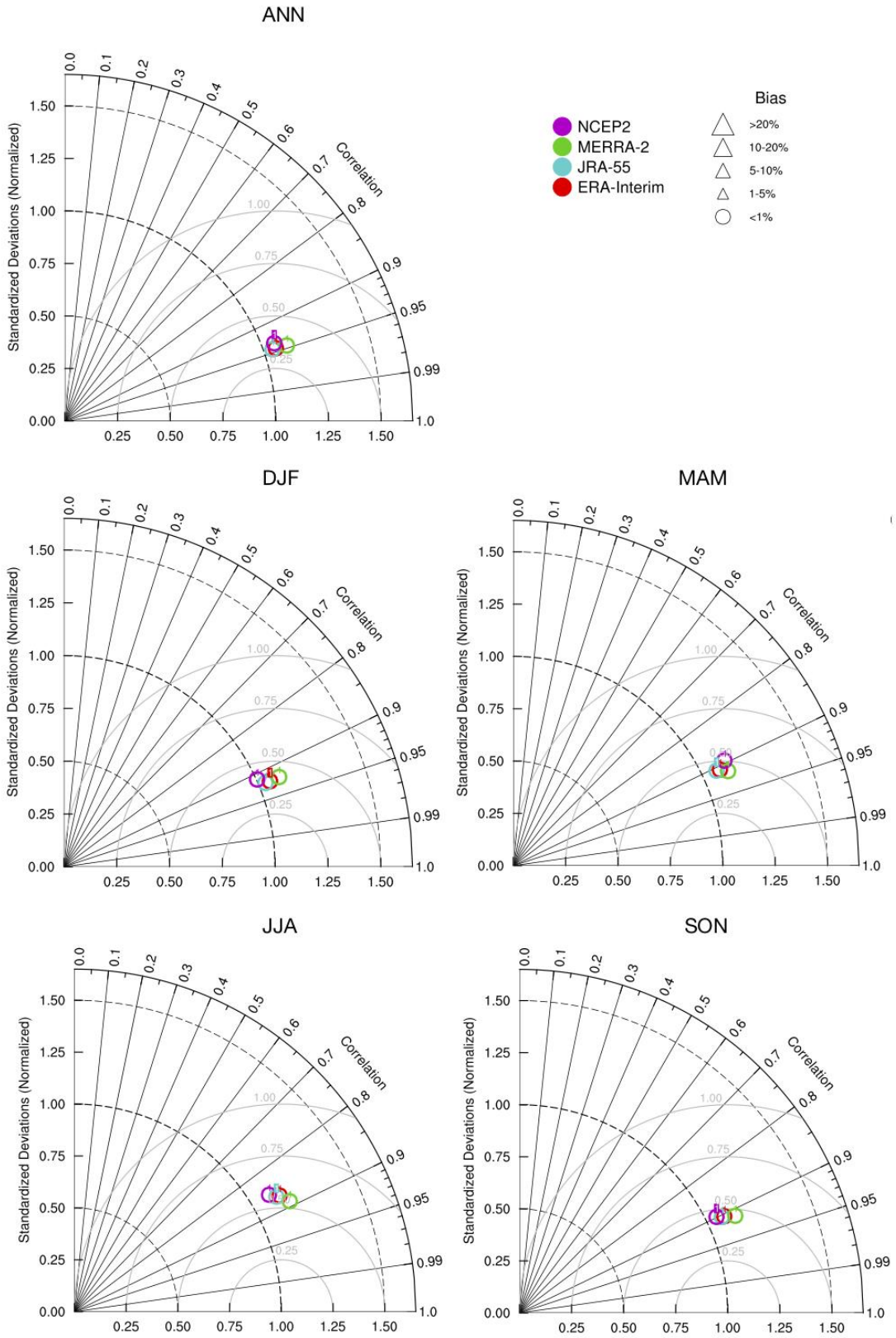

Figure 15: Taylor Diagram 1980-2017 of monthly (Top) and seasonal (Center and Bottom) 2 m temperature in ERA-Interim, MERRA-2, JRA-55, NCEP/DOE R2 vs. E-OBS.

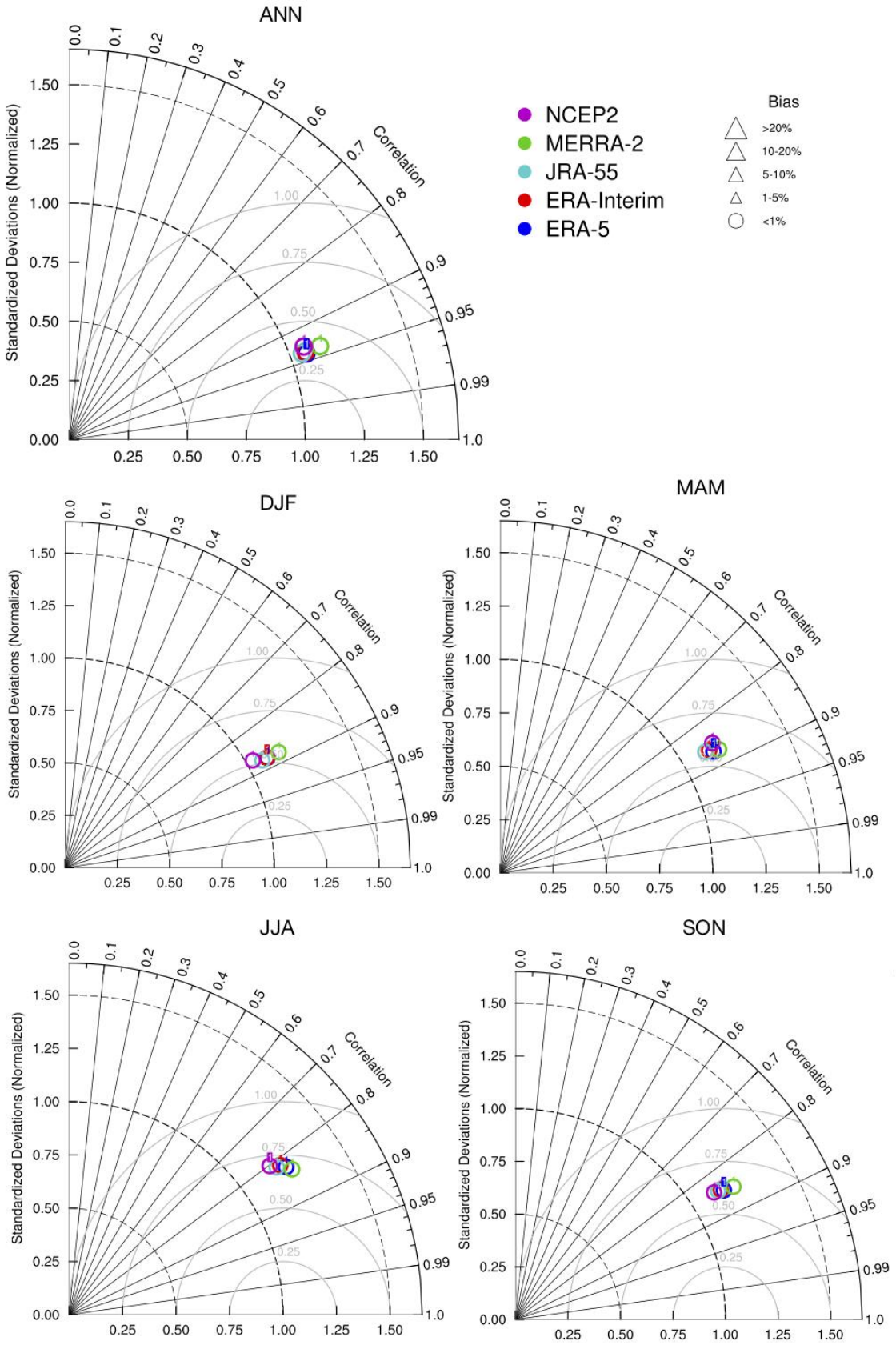

Figure 16: Taylor Diagram 2000-2017 of monthly 2 m temperature in ERA5, ERA-Interim, MERRA-2, JRA-55, NCEP/DOE R2 vs. E-OBS.

3.2 Validation results for solar radiation

The photovoltaic (PV) power output is primarily influenced by the solar irradiance. Atmospheric reanalysis produces long-term solar irradiance data with global coverage, intra-daily time resolutions and spatial resolutions around 30–80 km. Solar irradiance is not assimilated, but obtained with a Radiative Transfer Model (RTM) that simulates the attenuation of the irradiance from the top of the atmosphere to the ground. Its quality depends on the RTM used as well as on the elements that attenuate the irradiance (cloud, aerosol or water vapor data) that generally (see 1.1) aren't assimilated increasing the uncertainty around the surface irradiance estimates (You et al., 2013).

3.2.1 Intercomparison of solar radiation climatology

The latitudinal gradient of the annual (Figure S10) and seasonal (Figure S11) climatological mean of the downward radiation (RMSD) at the Earth's surface is primarily determined by the incoming solar flux at the top of the Atmosphere, while the patterns of longitudinal variation are mostly determined by cloud and surface properties. Therefore, large RMSD fluxes are found in polar regions during local summer. The values of reanalysis are equal to about 300–350 Wm−2 over Antarctica in DJF and 180– 260 Wm−2 over the Arctic in JJA. The hemispheric differences are largely due to differences in the incoming solar flux at the top of the Atmosphere. The latitudinal gradient of RMSD is mitigated during spring and autumn. Maximum values of RMSD are found over the regions associated with anticyclonic conditions and small cloud amounts, such as oceanic areas in low latitudes of the summer hemisphere, as well as over the polar areas of the summer hemisphere. Minimum values of RMSD are found over regions with large cloud amounts, such as the middle latitudes of the summer hemisphere. The strong anti-correlation between RMSD and cloud amount is a key to understand differences between reanalysis. Therefore, high values of multi reanalysis spread, computed as the standard deviation of the five climatologies, are found over the storm-track zone of the Southern hemisphere (50°S-70°S) during DJF and SON and in western coasts of South America and South Africa in JJA (Figure 17). There are relative high values of the spread over south-eastern Asia in JJA, where reanalyses simulate differently the large cloud cover associated with monsoons.

The maximum reanalysis spread over Arctic during JJA is largely due to the high values of RMSD produced by R2 and low values produced by ERA-Interim. MERRA-2 values are slightly lower than the multi reanalysis mean and JRA-55 slightly higher than the multi reanalysis mean. In south-eastern Asia during JJA over land, ERA-Interim and R2 underestimate the multi reanalysis mean, MERRA-2 and JRA-55 overestimate the multi reanalysis mean. R2 overestimates RMSD over Europe during MAM and JJA, largely contributing to increase the spread. Climatological values 2000-2017 of ERA5 are biased similar to ERA-Interim values (Figure 18).

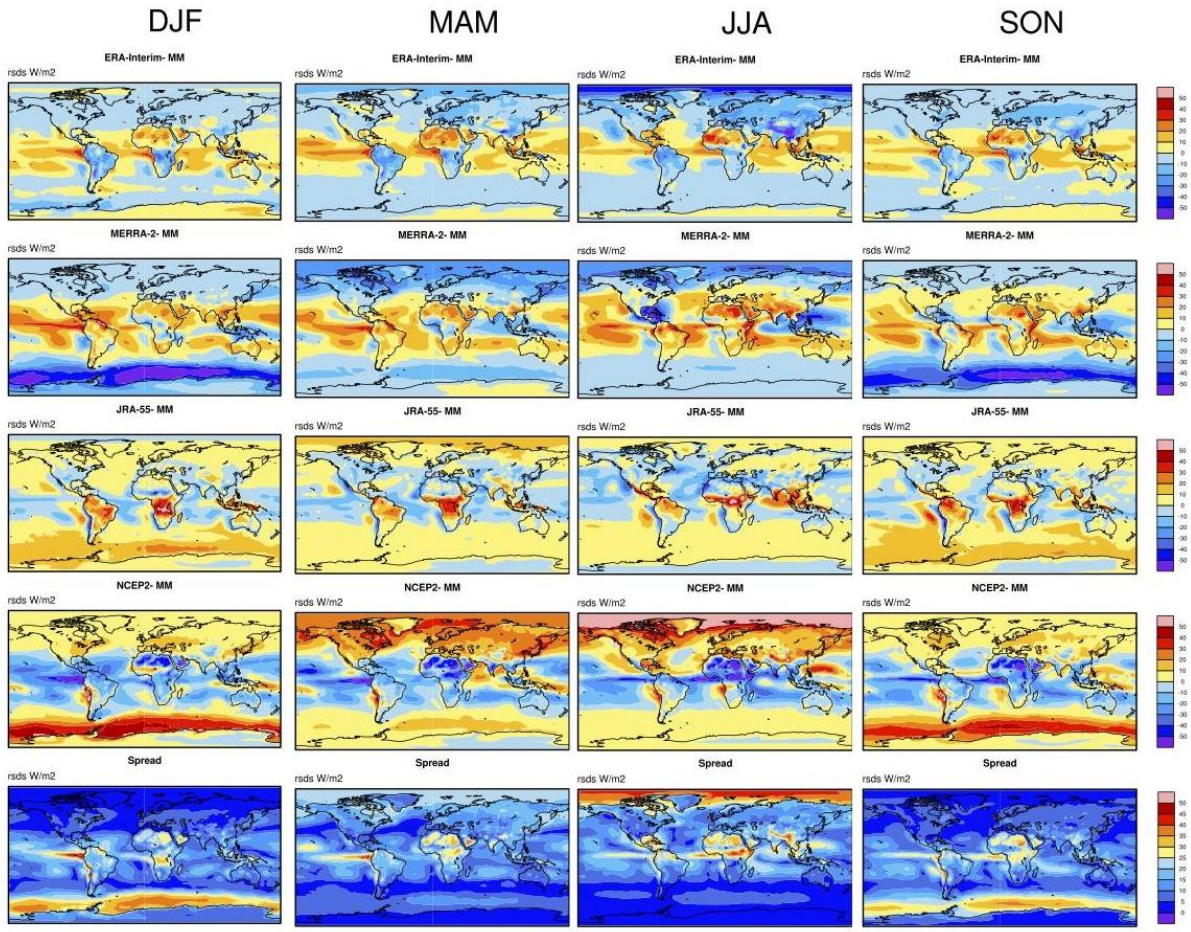

Figure 17: Differences of seasonal (DJF, MAM, JJA, SON) climatological mean 1980-2017 of solar radiation between ERA-Interim, MERRA-2, JRA-55, NCEP/DOE R2 and multi reanalysis mean. (Bottom) Spread of the reanalysis ensemble.

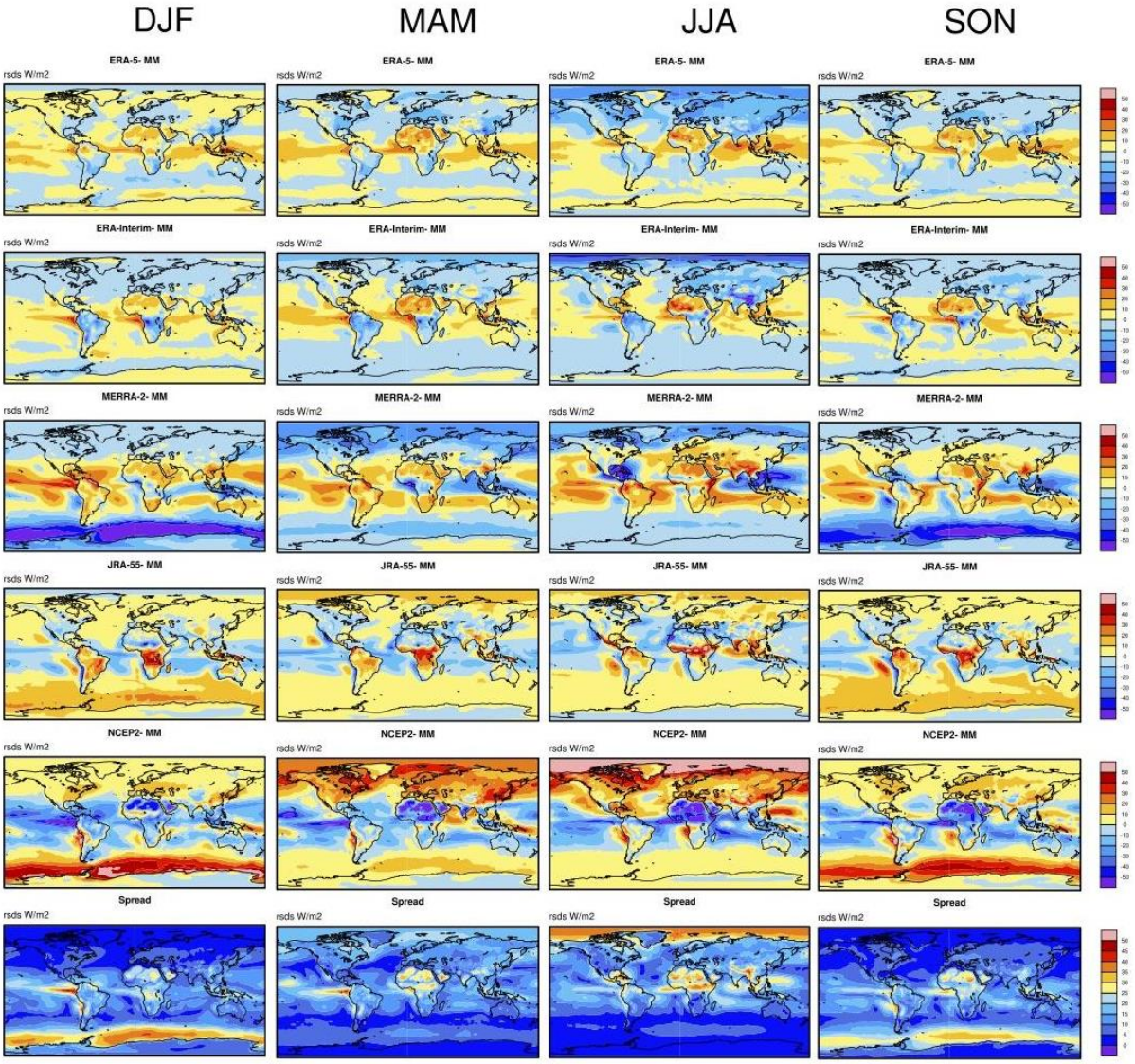

Figure 18: Differences of seasonal (DJF, MAM, JJA, SON) climatological mean 2000-2017 of solar radiation between ERA5, ERA-Interim, MERRA-2, JRA-55, NCEP/DOE R2 and multi reanalysis mean. (Bottom). Spread of the reanalysis ensemble.

3.2.2 Intercomparison of solar radiation variability

Interannual variability

Solar irradiance varies on time scales from seconds to years. The basic seasonal and diurnal variability depends on the motion of the earth, then cloudiness, water vapor and aerosols are the main factors of variability. In terms of interannual seasonal variability, tropical regions and Southern mid-latitudes present high values during all the seasons (Figure S12 and Figure S13). A major source of inter-annual climate variations in several parts of the globe is the El Nino Southern Oscillation (ENSO) and can explain a large part of the inter-annual rainfall variability closely associated with variation in cloudiness, which therefore impacts solar radiation.

The spread of the variability among the reanalysis (Figure 19) has relevant values in Western South America, South East Asia. High values in polar regions during winter are an artifact of the normalization. In Europe spread is almost always small, slightly increasing in DJF.
The ERA-Interim interannual variability in positively biased respect to the multi reanalysis mean in Eastern Australia and South America (ENSO related) and in Europe. MERRA-2 variability is higher than multi reanalysis mean over the oceans, mainly in central Pacific. JRA-55 has lower variability than the multi reanalysis mean in almost all the regions of the globe. R2 shows a variability higher than the multi reanalysis mean in the tropical regions.
During the period 2000-2017, values of ERA5 are in a better agreement with the multi reanalysis mean respect to ERA-Interim (Figure 20). Over most of the regions the variability of ERA5 is lower than the variability of ERA-Interim, in particular over tropical regions and high latitude of Northern Hemisphere during DJF and MAM.

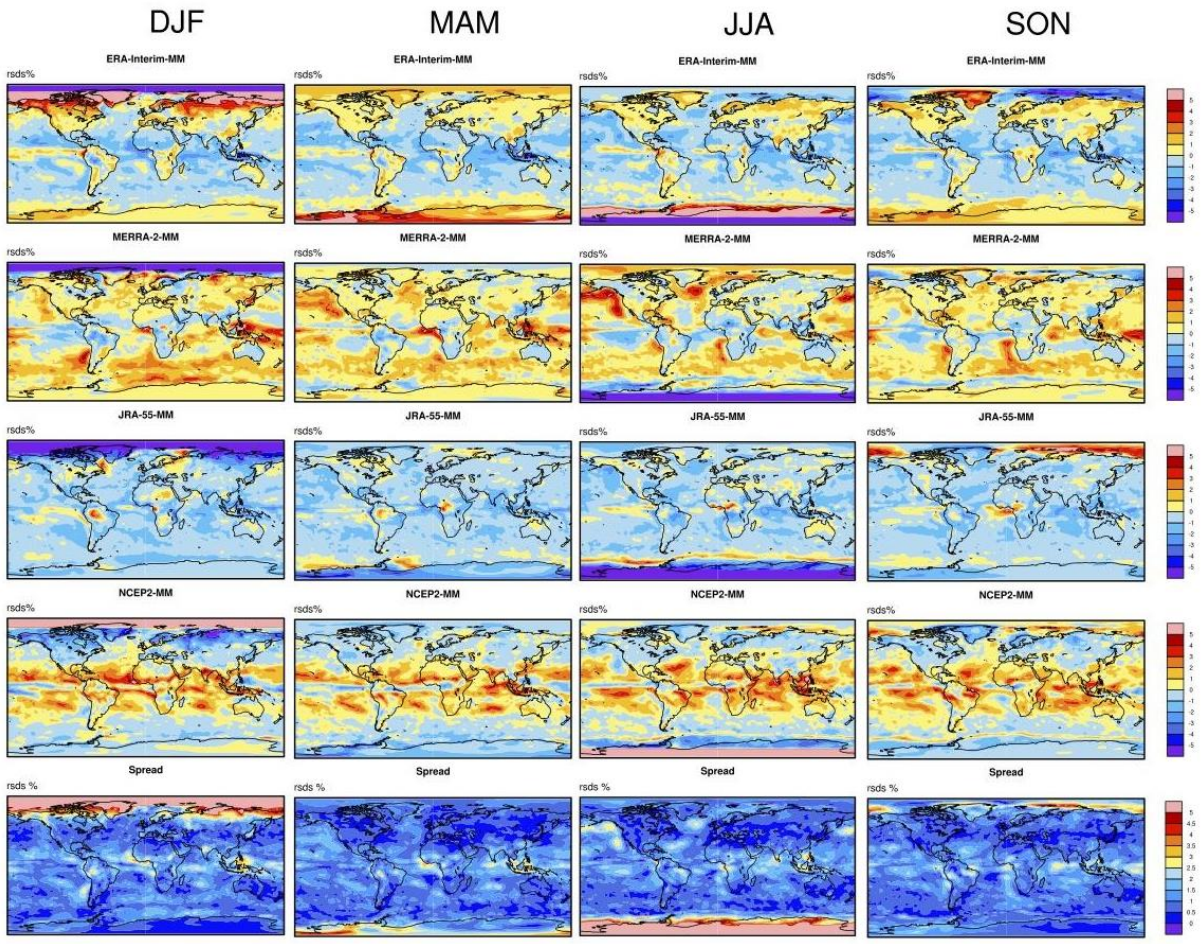

Figure 19: Differences of normalized interannual variability 1980-2017 of solar radiation between ERA-Interim, MERRA-2, JRA-55, NCEP/DOE R2 and multi reanalysis mean. (Bottom) Multi reanalysis spread of interannual variability.

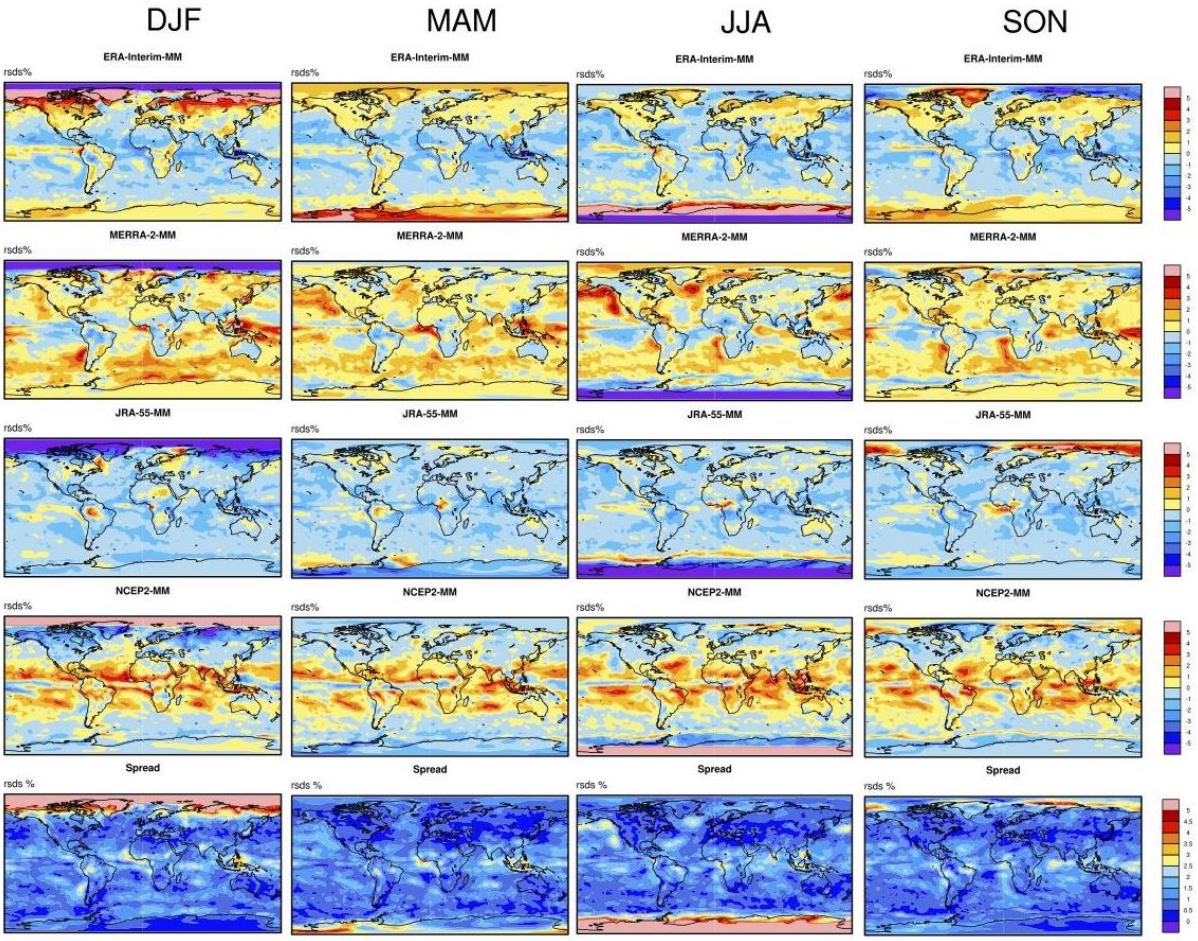

Figure 20: Differences of normalized interannual variability 2000-2017 of solar radiation between ERA5, ERA-Interim, MERRA-2, JRA-55, NCEP/DOE R2 and multi reanalysis mean. (Bottom) Multi reanalysis spread of interannual variability.

Intraseasonal variability

The latitudinal gradient strongly characterizes the intraseasonal variability since the month to month variability due to the earth motion is the main feature captured by this diagnostic (Figure S14 and Figure S15). Excluding spurious values over the polar regions due to the normalization, not negligible values of spread (Figure 21) are localized in almost the same regions where the interannual spread is higher (Figure 19). In this diagnostic R2 is the model that has the largest differences respect the multi reanalysis mean. ERA5 shows less intraseasonal variability than the multi reanalysis mean in almost all regions, except Southern high latitudes during MAM (Figure 22).

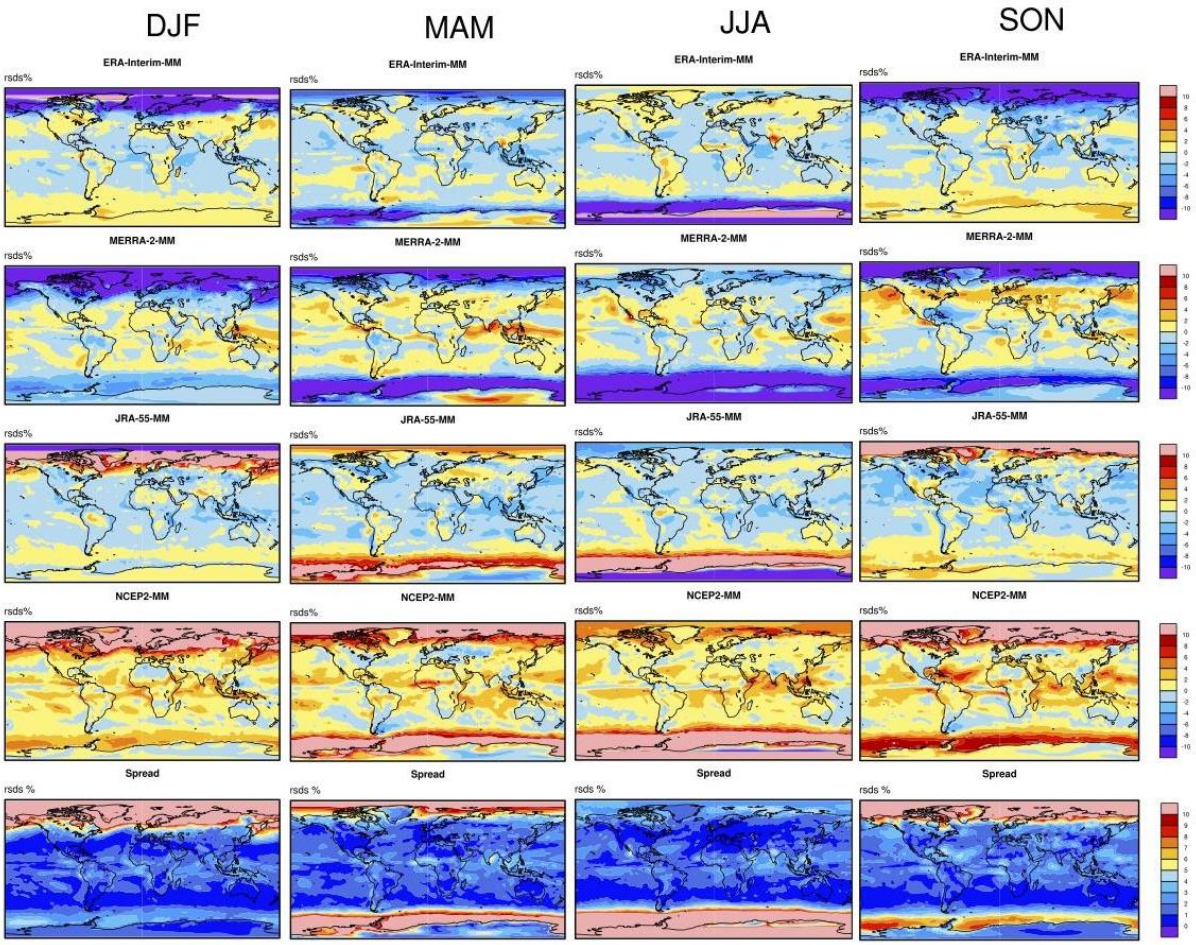

Figure 21: Differences of normalized intraseasonal variability 1980-2017 of monthly solar radiation between ERA-Interim, MERRA-2, JRA-55, NCEP/DOE R2 and multi reanalysis mean. (Bottom) Multi reanalysis spread of interannual variability.

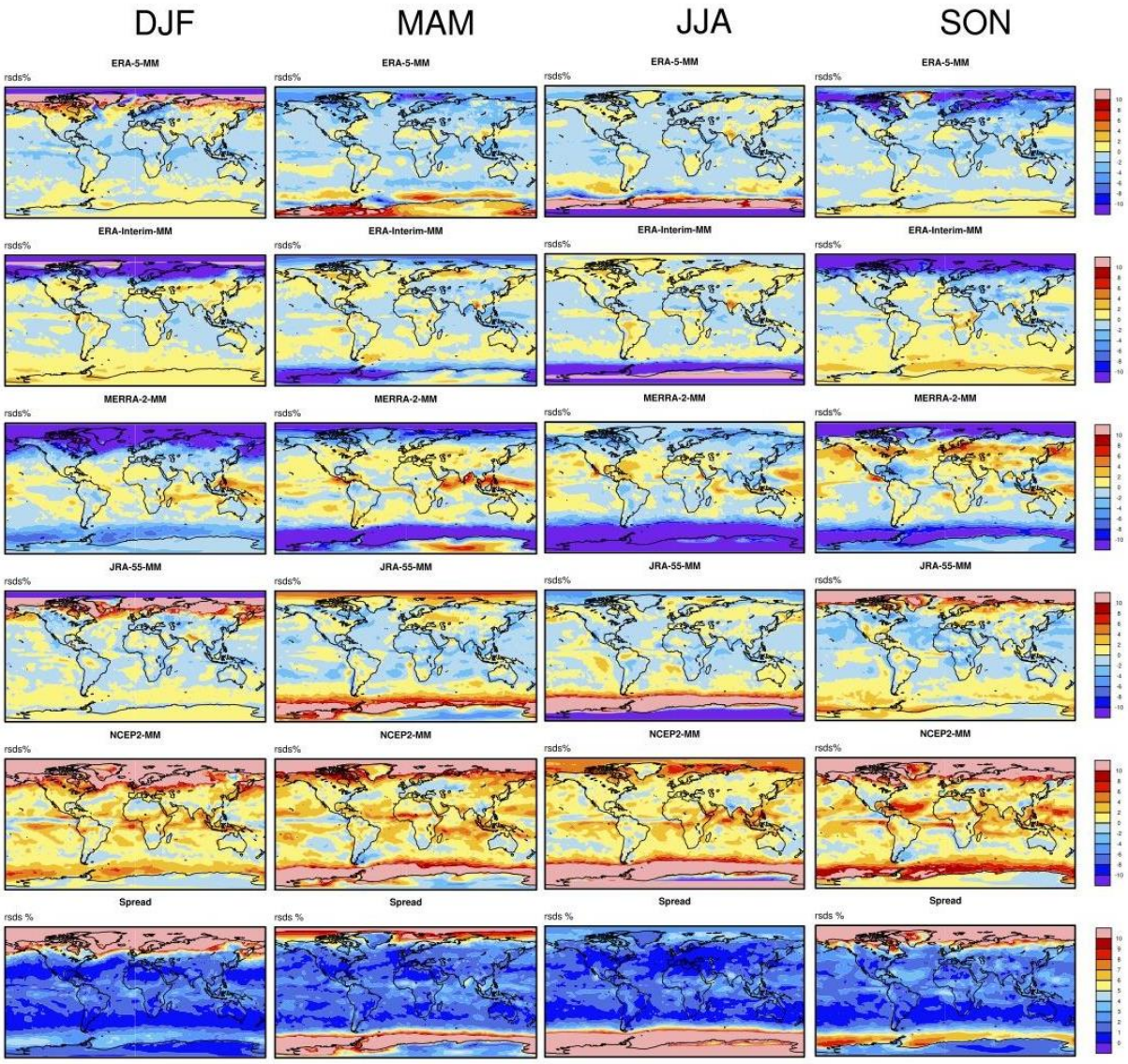

Figure 22: Differences of normalized intraseasonal variability 2000-2017 of monthly Solar Radiation between ERA5, ERA-Interim, MERRA-2, JRA-55, NCEP/DOE R2 and multi reanalysis mean. (Bottom) Multi reanalysis spread of interannual variability.

3.2.3 Intercomparison of solar radiation trends

Decadal variations in solar radiation incident at Earth's surface may profoundly influence surface temperature, evaporation, the hydrological cycle and ecosystem as well as the PV production. Traditionally, for the planning of the solar energy systems, the amount of solar radiation is assumed to remain constant over time. However, long-term radiation records demonstrated that surface radiation undergoes multidecadal variations. Observational measurements from 1950s to 1980s report a general decrease of sunlight over land surface, this period has been described as "dimming phase" (Stanhill and Cohen 2001). Observational data after the 1980s shows a trend reversal. The term "brightening period" (Wild et al. 2005) has been coined for the period after the 1980s to emphasize that the decline in RMSD no longer continued. The observed RMSD variations are not explained by changes of the solar radiation

at the top of the atmosphere and, therefore, have to originate from alterations in the transparency of the atmosphere, which depends on the presence of clouds, aerosols, and radiatively active gases. In particular, aerosols can directly attenuate RMSD by scattering and absorbing solar radiation (direct effect), or indirectly attenuate RMSD through their ability to act as cloud condensation nuclei, thereby increasing cloud reflectivity and lifetime (first and second indirect effects) (Lohmann and Feichter 2005). All these effects act towards reducing RMSD with increasing aerosol levels. In addition, long-range transports of aerosols can effectively modify cloud (and then alter RMSD) also in area far from pollution source (Rosenfeld et al. 2008). Large anthropogenic emissions of sulfur and black carbon has led to the past increase of aerosol levels. Implementation of air quality measures in industrialized countries has largely contributed to the decrease of aerosol burden after the 1980s (Wild 2012).
Trend analyzed in this study spans the years from 1980 to 2017 and correspond to the "brightening period" (Figure S16 and Figure 23). There is a general positive trend over land in the Northern Hemisphere. All the reanalysis present significant positive values over central Africa, continental North America, Eastern part of South America and a negative trend over South East Asia. In Europe, a large positive trend over central and eastern area during summer is represented in all the datasets. ERA-Interim, R2 and JRA also have a significant negative trend in eastern Mediterranean region during SON. MERRA-2 shows a significant negative trend over the ocean.

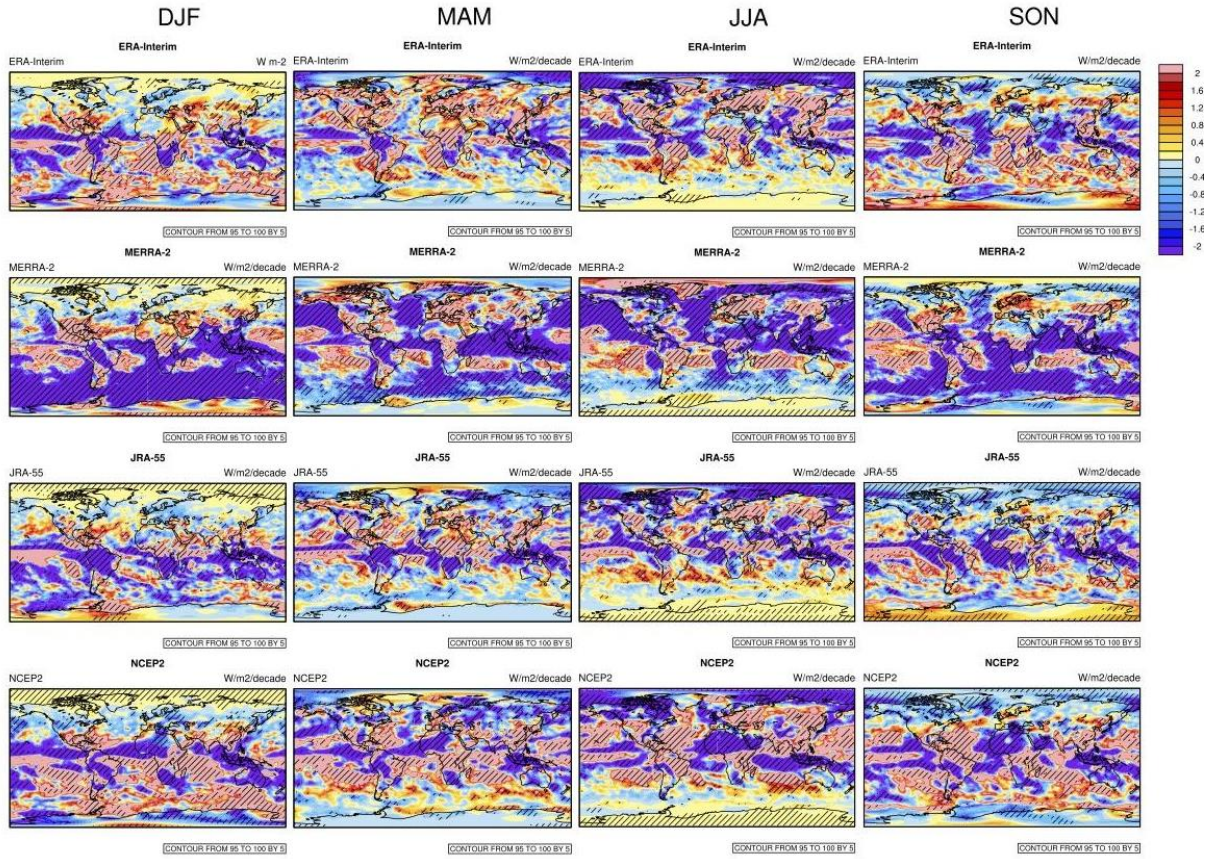

Figure 23: Trend 1980-2017 of seasonal solar radiation in ERA-Interim, MERRA-2, JRA-55, NCEP/DOE R2 and ensemble multi reanalysis mean.

3.2.4 Verification of solar radiation with CMSAF SARAH2 observations

Meteorological reanalyses can be an important data source to model solar energy. However, potential problems like model errors or insufficient spatial resolution make it necessary to validate reanalyses against measured data. Long-term measurements of RSDS exist only at selected terrestrial locations. Worldwide monitoring of RSDS from ground-based stations began in the late 1950s (AR5, Hartmann et al. 2013). Since the mid-1990s, sites of the Baseline Surface Radiation Network (BSRN) and the Atmospheric Radiation Measurement program (ARM) offer high-quality, but geographical limited, ground based data (Wild 2012). Satellite-based data records provide estimates of surface solar radiation with near-global and high frequency. In this study data from satellite observations as those provided by the EUMETSAT Satellite Application Facility on Climate Monitoring-CM SAF are used. Satellite-based data of RSDS from the CM SAF SARAH2 has been already validated by Urraca et al. 2017 using European station measurements from national and international databases. Sanchez-Lorenzo et al. 2017 and Pfeifroth et al. 2018 assess the accuracy and the ability of the CMSAF-SARAH2 to capture temporal and spatial variability of SSR in Europe. CMSAF-SARAH2 dataset covers Europe and Africa, therefore the reanalyses are validated over this domain (+/- 65°lat, +/- 65°lon).

While differences between the reanalysis are apparent in the previous figures, Taylor diagrams provide further quantitative assessment of the spatial variability of the RSDS compared with the observed dataset CMSAF-SARAH2. The Taylor diagram (Figure 24) compares normalized standard deviation ratio (variability), root mean square differences and correlation of the climatological field. All the reanalysis presents a spatial variability lower than the satellite observations in all the seasons. R2 is the dataset poorly correlated with the observations (particularly in MAM and JJA) and the variability is always lower than the observed. This performance can be related to the low spatial resolution of R2. JRA-55 has values of correlation up to 0.95 (except JJA). The normalized standard deviation ratio is always below one, revealing a spatial variability lower than observed. When compared with others reanalyses ERA-Interim is always a step closer to the observations (black dot).

ERA-Interim and MERRA-2 are always well correlated with observation especially during the winter and the autumn when also the variability is better reproduced.

The analysis from 2000-2014 shows that ERA5 is the dataset with better correlation in all the seasons (Figure 25). The standard deviation is largely improved respect to ERA-Interim, this can be related with the higher spatial resolution. The annual bias is below 5% for all the dataset except MERRA2 and NCEP2. The bias is below 1% for ERA5 and JRA-55 in JJA and ERA-Interim in SON

The spatial and temporal analysis of the datasets (Figure 26) show a good agreement with the observations during DJF and SON; variability is close to the variability of observed data and correlation is about 0.99 for all the dataset except R2. During MAM and JJA values are less correlated and the variability is always below the observations. MERRA-2 and ERA-Interim show the best agreement with the observation, instead R2 is far away from observation in terms of variability, root mean square difference and correlation. ERA5 (2000-2104) has values broadly similar to the ERA-Interim values with some improvements in the correlation and standard deviation during JJA (Figure 27). The dataset whit the lower bias are ERA-Interim, ERA5 and JRA-55.

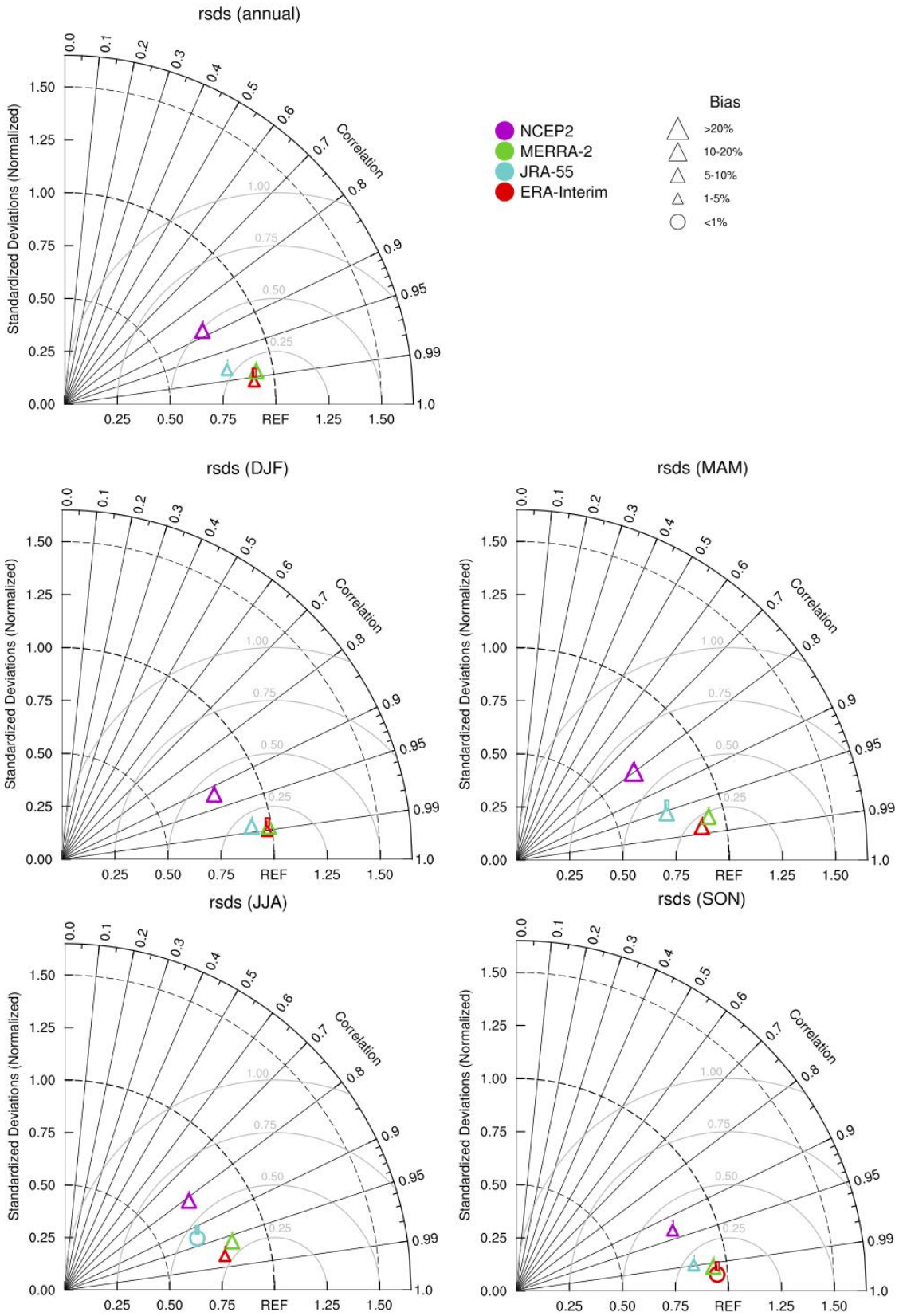

Figure 24: Taylor Diagram Climatological mean 1983-2014 of annual (Top) and seasonal (Center and Bottom) solar radiation in ERA-Interim, MERRA-2, JRA-55, NCEP/DOE R2 vs. CMSAF SARAH2.

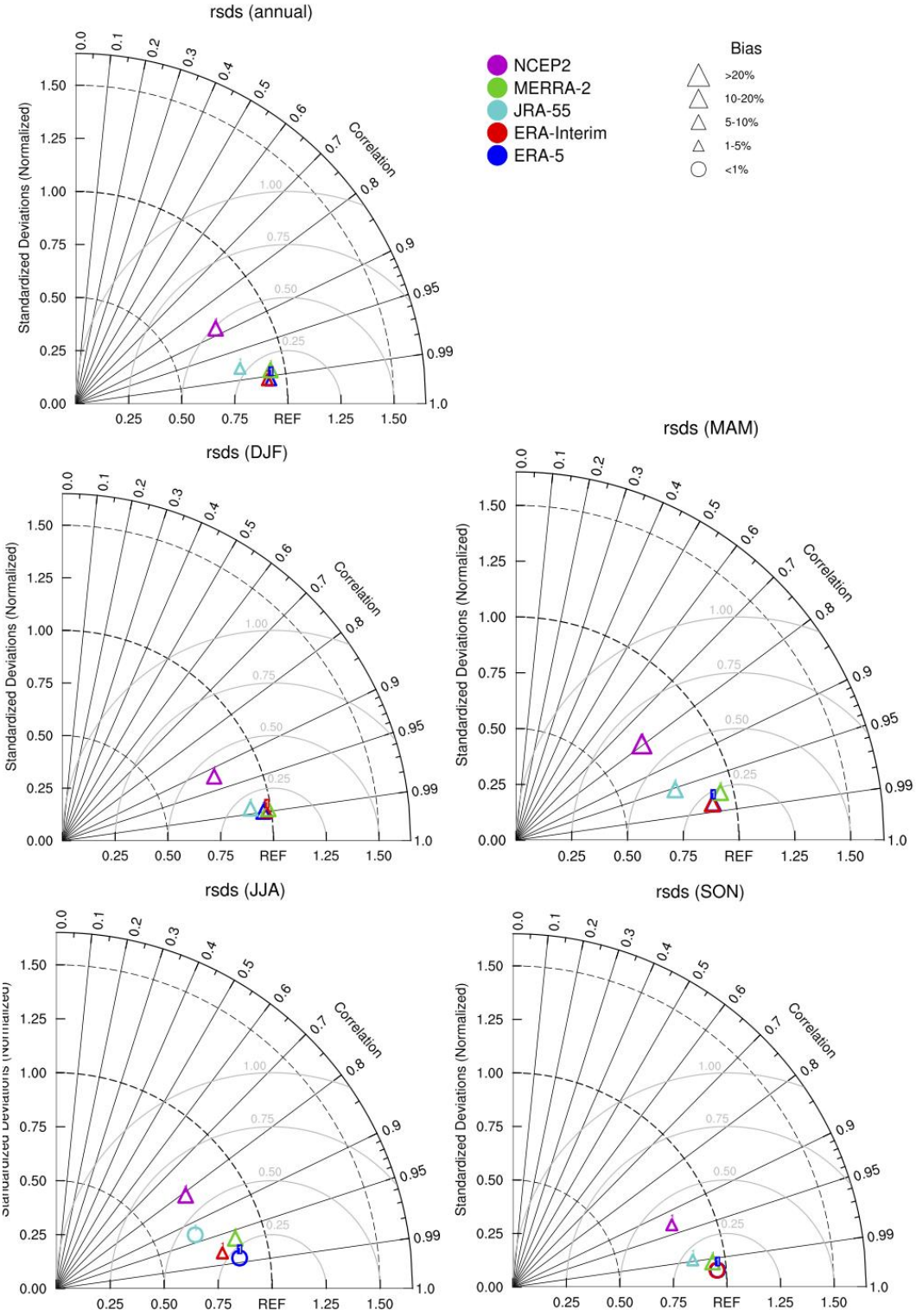

Figure 25: Taylor Diagram Climatological mean 2000-2014 of annual (Top) and seasonal (Center and Bottom) solar radiation in ERA5, ERA-Interim, MERRA-2, JRA-55, NCEP/DOE R2 vs. CMSAF SARAH2.

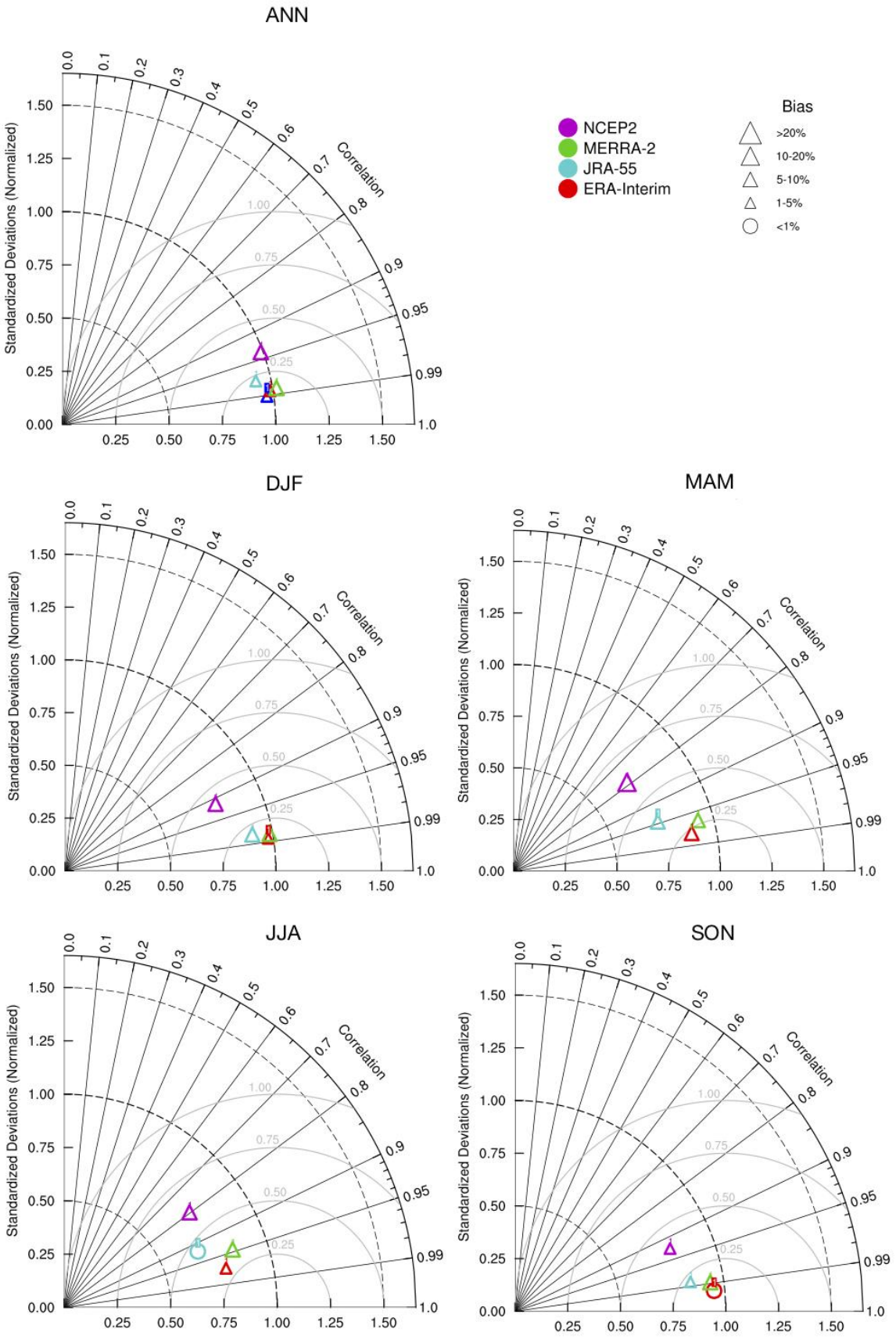

Figure 26: Taylor Diagram 1983-2014 of monthly (Top) and seasonal (Center and

Bottom) solar radiation in ERA-Interim, MERRA-2, JRA-55, NCEP/DOE R2 vs. CMSAF SARAH2.

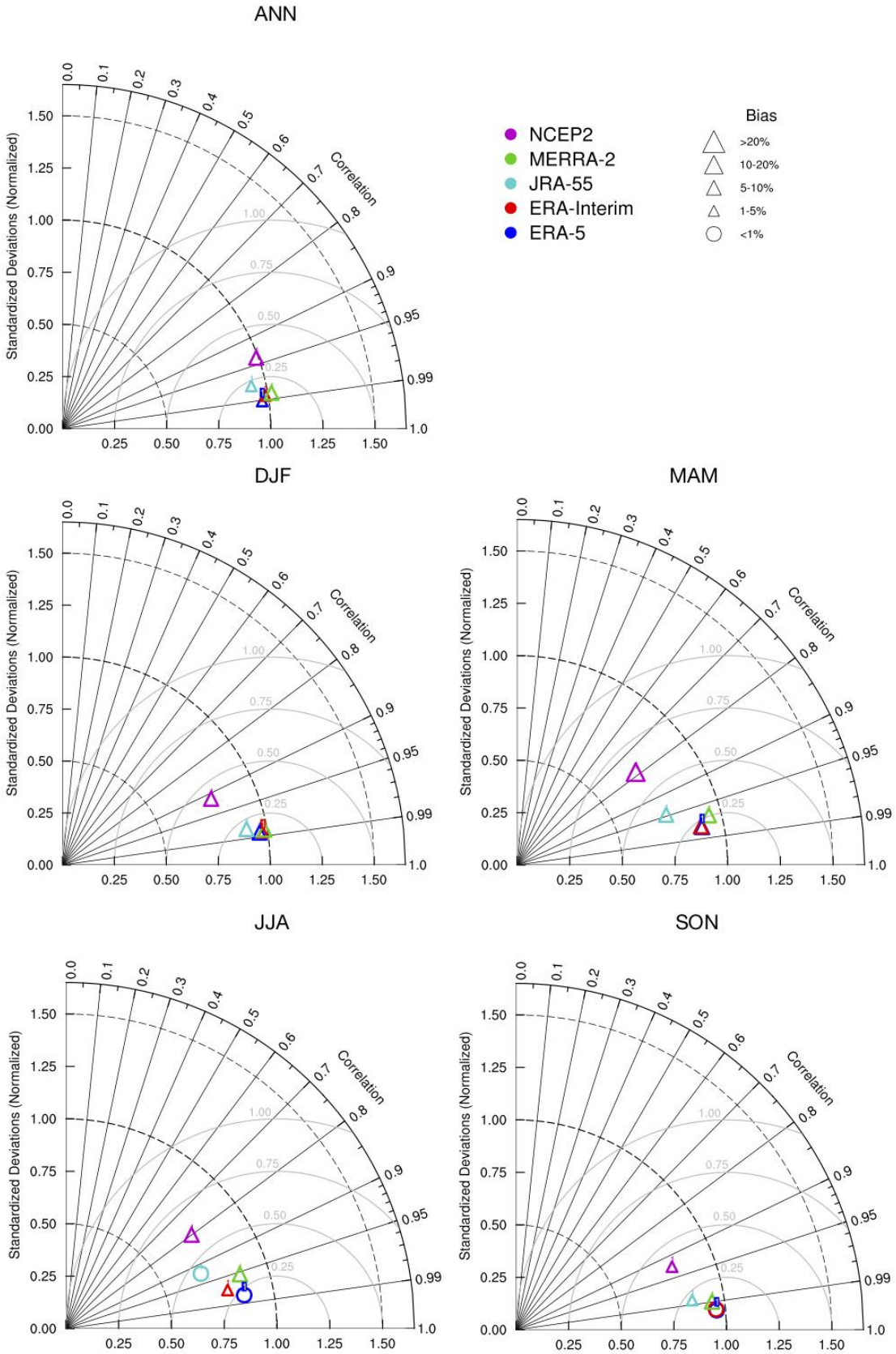
ANN
DJF
MAM
JJA
SON
Standardized Deviations (Normalized)
Correlation
NCEP2
MERRA-2
JRA-55
ERA-Interim
ERA-5
Bias
>20%
10-20%
5-10%
1-5%
<1%

Figure 27: Taylor Diagram 2000-2014 of monthly (Top) and seasonal (Center and Bottom) solar radiation in ERA5, ERA-Interim, MERRA-2, JRA-55, NCEP/DOE R2 vs. CMSAF SARAH2.

3.3 Validation results for surface wind

Wind power generation of a turbine depends mainly on wind speed at hub height. Modern turbines have hub heights in the range from 80 to 120 meters. However, most reanalysis datasets do not provide wind speed information at those levels, and for that reason near-surface (i.e. 10m) wind speed is typically used for the assessments. Indeed, 100m winds are only available for ERA5, while MERRA2 provides 50m winds. Those two fields have been verified in Ramon et al. 2019. Therefore, a comparison of surface winds among the selected reanalysis datasets has been carried out in order to establish the main differences amongst them. The newly released dataset ERA5 has been included in this intercomparison, but at the time of writing this document, only data from 2000 to present were available. Therefore, a common time period 2000-2017 has been selected to intercompare climatology and variability. Nevertheless, for long-term trends this period is deemed too short and we stick to 1980-2017 and discard ERA5. The 1980-2017 period has been also used for comparing reanalysis with tower observations, although most of the towers are relatively recent.
The characterization of the seasonal cycle is of importance within the Operations and Maintenance (O&M) activities in wind farms -to schedule activities during less windy periods- and for the preparation of monthly budgets. Quantifying the variability of wind speed between different years is also crucial. The seasons with more variability are the ones where seasonal forecasts will have more value, as power generation is more uncertain. The interannual variability (IAV) is also key to quantify project risks in terms of revenues. Finally, information on long-term trends is useful to evaluate the performance of wind farms during their lifetime (typically 20 to 30 years), and to estimate the return over investment.

3.3.1 Intercomparison of surface wind climatology

The multimodel 10-meter wind speed climatologies of ERA5, ERA-Interim, JRA-55, R1 and MERRA-2 reanalyses are shown in Figure 28 for each season. The maximum wind speeds occur over the ocean, particularly during winter (DJF for the northern hemisphere and JJA for the southern hemisphere). On the contrary, the lowest values (i.e. below 2.5 m/s) can be found inland along the equator. The multimodel spread, computed as the standard deviation of the five climatologies, highlights the areas where different reanalyses disagree on the climatological wind speeds. Discrepancies between reanalyses are found in several areas. Over land, the maximum values above 1 m/s are globally distributed over mountainous regions. Furthermore, high values are observed in some parts of the African continent, particularly along the tropics, as well as in Australia for all the target seasons. For DJF, the spread is considerable over many parts of Eurasia. It is noticeable that the highest spreads over the ocean are found in the eastern Pacific, where the El Niño/Southern Oscillation (ENSO) has an important effect in the wind speed.

The difference between each reanalysis climatology and the multimodel mean is also included in Figure 28 to understand discrepancies. The strongest wind speeds over elevated areas are

given by R1, especially for the Himalayas region. However, both R1 and JRA-55 tend to produce weaker wind speeds over continental areas -especially over Eurasia-, whilst ERA5, ERA-Interim and MERRA-2 show stronger winds in the same regions. Slight positive differences can be noted over polar ocean areas and Eastern Pacific for JRA-55 reanalysis. Similarly, ERA5 produces stronger wind speeds in the Eastern Pacific. In these regions, R1 gives the lowest wind speeds. MERRA-2 tends to show a uniform pattern of negative departures over the oceans. However, these differences are lower than the observed for R1. No significant biases with respect to multimodel mean are seen for ERA-Interim model over marine areas.

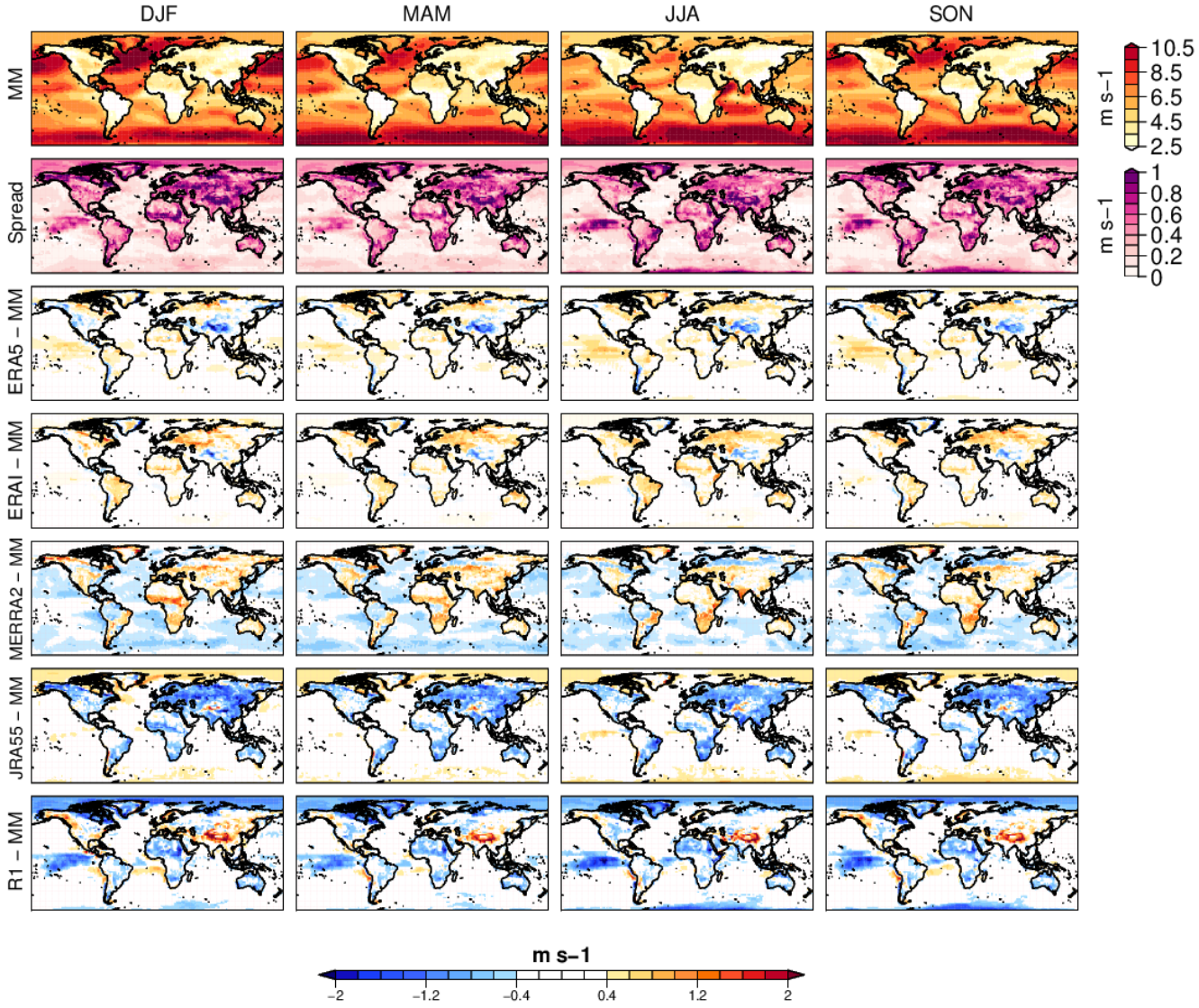

Figure 28: Analysis of 10-meter mean wind speeds for each season (columns) for the period 2000-2017. First row: multimodel mean (MM). Second row: multimodel spread (Spread). Third to seventh rows: differences between ERA5, ERA-Interim, MERRA-2, JRA-55 and R1 climatologies and the multimodel mean.

3.3.2 Intercomparison of surface wind variability

For wind speed, IAV and ISV parameters for each season have been normalized by the mean wind speed of the season. Hence, it is displayed as a percentage to highlight areas with high variations with respect to the mean. This is a common practice within the wind industry.
The normalized IAV derived from the five datasets is compared in Figure 29. Equatorial regions over both Pacific and Indian oceans show the highest relative values, with IAVs representing up to 20% of the mean wind speed. In general, lower values are observed inland. Nonetheless, for DJF an increase of IAV over Eurasia is noticeable. This result matches the patterns observed in Figure 28, where high spread was noticed in these regions for the boreal winter. Regarding the spread of the IAV, values up to 5% can be found spotted mainly in continental regions. However, an irregular pattern of high spread is also displayed over marine areas and it is remarkable for both JJA and SON seasons.
The normalized IAV departures from MM show several disagreements between the five datasets. On the one hand, both European datasets (i.e. ERA5 and ERA-Interim) tend to show the lowest values of IAV. Nevertheless, some spots of positive departures are found in some equatorial regions, especially for ERA-Interim. On the other hand, JRA-55 shows the highest IAV over continental areas. This evidence leads to conclude that the Japanese dataset is one of the main contributors to the high spread values observed inland. This increase is particularly remarkable over Eurasia, which disagrees with the patterns displayed by the other four reanalyses for the same region. As noticed by Torralba et al. (2017), JRA-55 uses observational data to correct the interpolation of wind speeds from the lowermost atmospheric level to the surface over areas with vegetation categorized as trees. These observations can present inhomogeneities that can lead to spurious changes in wind speed characteristics. A mixed pattern of positive and negative departures is observed for MERRA-2. In general, NASA's dataset tends to increase IAV over oceanic regions while decreases this parameter inland along the equator. A complementary pattern is displayed by R1.
Regarding ISV, similar results are observed in Figure 30. Values representing more than the 20% of the climatology are displayed over large equatorial zones in the Indian and Pacific oceans. Remarkable large areas of high ISVs are found in MAM and SON, expanding to the north over the Atlantic. Both seasons correspond to transition periods of the climatological cycle. Thus, they are expected to concentrate a high variability between the constituent months. The computed standard deviation of the ISVs shows an analogue pattern to the described in the IAV, but systematically stronger. Values up to 3-5% are observed in several areas mainly located within the continents. The departures from MM are also similar to the IAV's. Yet again, the European datasets show the lowest ISVs. JRA-55 is displaying the most uniform pattern of positive differences over continental areas. The mixed pattern observed for MERRA-2 in Figure 29 is also noticed in Figure 30: big amounts of ISV are found spotted worldwide in except of the equatorial regions. The complementarity of this behavior with R1 is noted again. The NCEP/NCAR reanalysis displays the highest values of ISV under the equator.

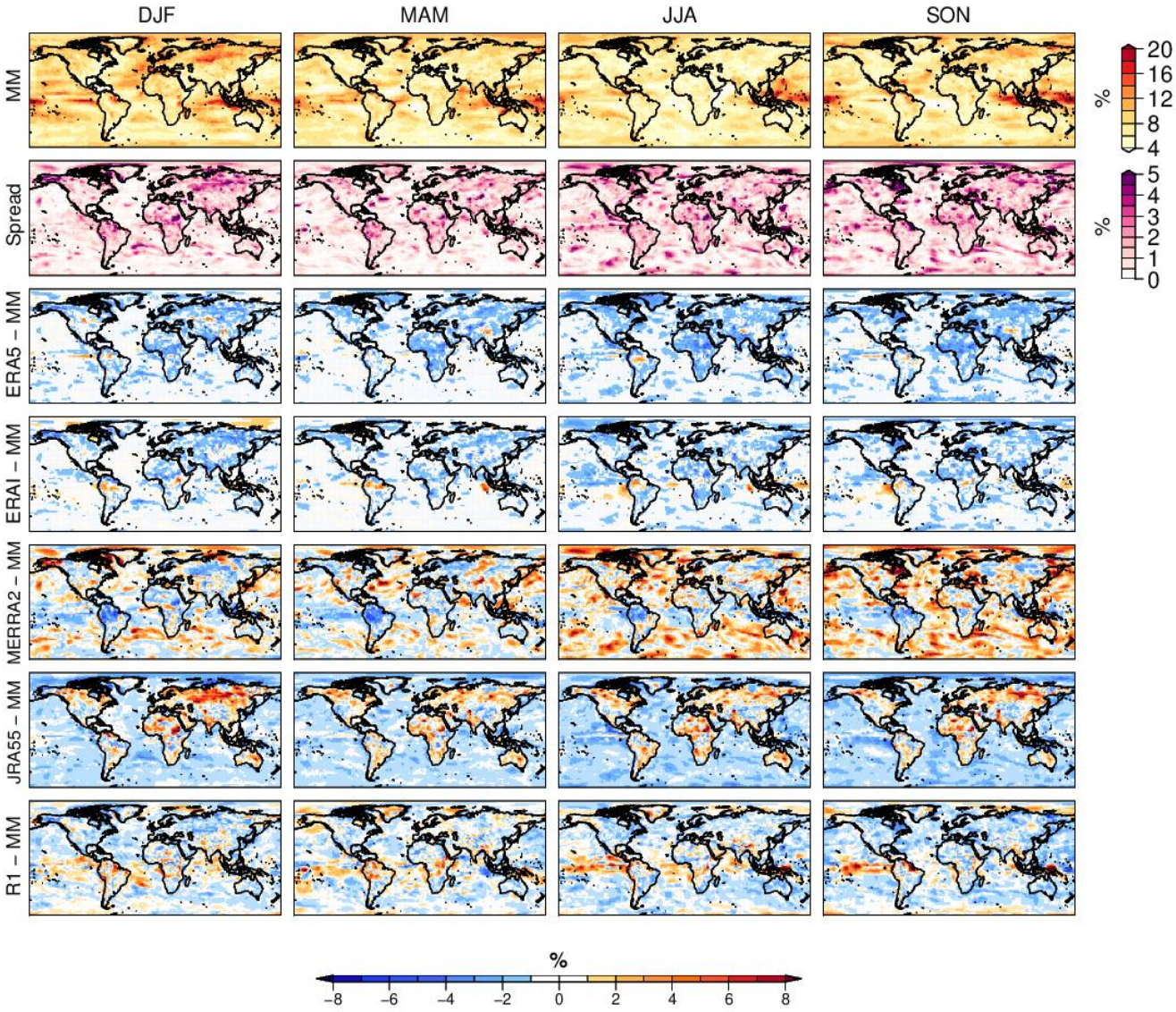

Figure 29: Analysis of normalized IAV by the multimodel climatologies of 10-meter wind speeds for each season (columns) for the period 2000-2017. First row: multimodel mean IAV (MM). Second row: multimodel spread (Spread). Third to seventh rows: differences between ERA5, ERA-Interim, MERRA-2, JRA-55 and R1 IAVs and the multimodel mean IAV.

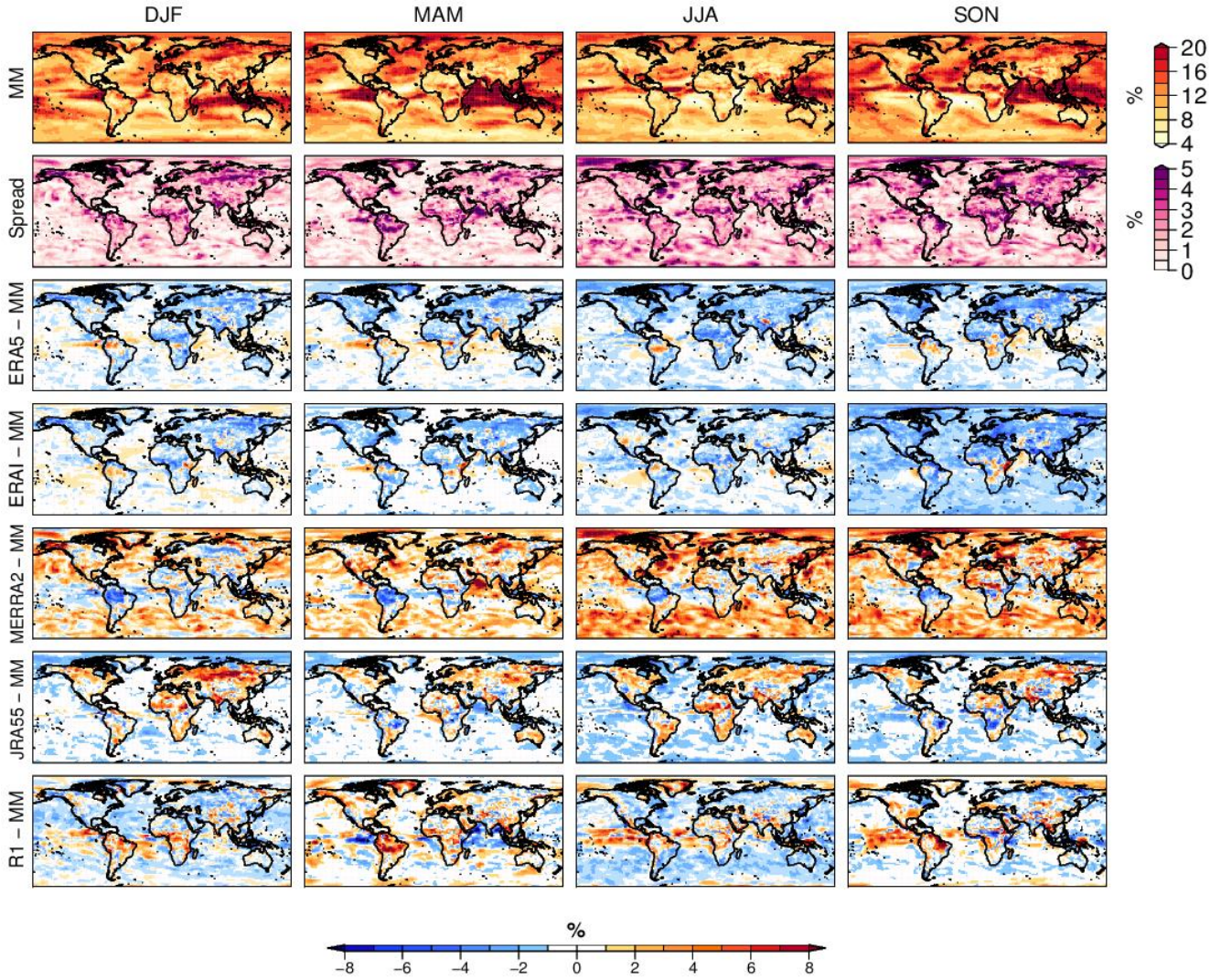

Figure 30: Analysis of normalized ISV by the multimodel climatologies of 10-meter wind speeds for each season (columns) for the period 2000-2017. First row: multimodel mean ISV (MM). Second row: multimodel spread (Spread). Third to seventh rows: differences between ERA5, ERA-Interim, MERRA-2, JRA-55 and R1 ISV and the multimodel mean ISV.

3.3.3 Intercomparison of surface wind trends

Linear trends are presented as the rate of change of the wind speed over the considered period 1980-2017 for four reanalysis products: ERA-Interim, JRA-55, MERRA-2 and R1. As argued before, ERA5 has been discarded in this analysis for having a too short period. Following Torralba et al. (2017), linear trends have been normalized by the climatology and shown in percentage per decade (Figure 31). Results are similar to those obtained by the previously mentioned article, although R1 has been included here. In general, wind speed trends are positive over the oceans and negative within the continents. All datasets agree on showing negative trends over Eurasia for all the target seasons. This decrease of wind speeds over time could be linked to the wind stilling effect. Indeed, several studies have reported evidence of a slight reduction of wind speeds in some continental regions, especially in Eurasia attributed to an increase in surface roughness (Vautard et al. 2010, Bichet et al. 2012). The most pronounced

negative trends are displayed by JRA-55, reaching up to -9% per decade. All datasets reproduce the highest positive trends over oceans along the equator. This was explained by Torralba et al. (2017) referring to the strengthening of the Walker circulation as a consequence of climate change. Notwithstanding, the same authors attributed the disagreement between JRA-55 on the one side, and ERA-Interim and MERRA-2 on the other, alluding to deficiencies in deriving wind speed in areas where the vegetation type is categorized as trees. A decrease in wind speeds over South Africa is also worth to note, especially for DJF.

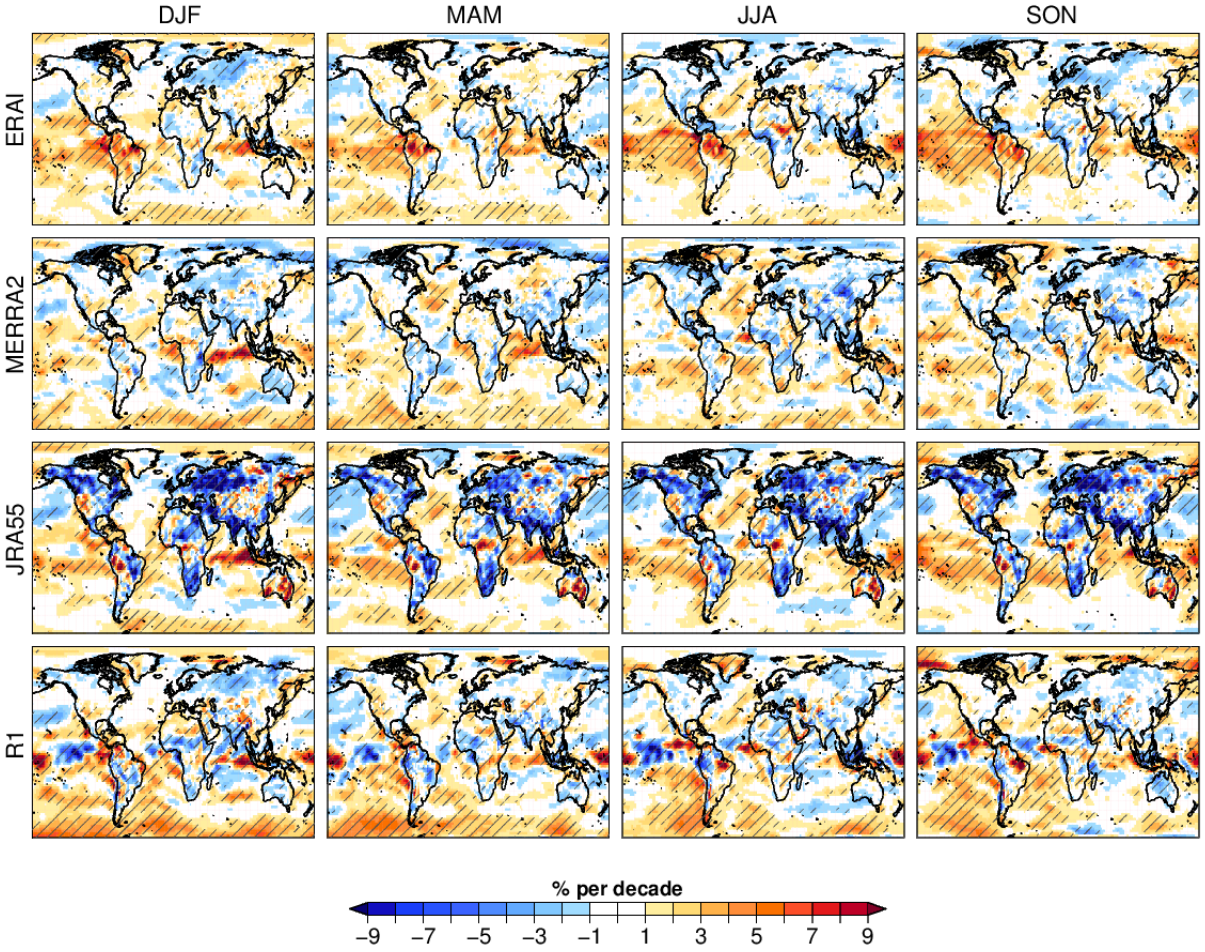

Figure 31: Normalized linear trend (% per decade) calculated as the linear trend of 10 m wind speed divided by the seasonal climatology of 10-meter wind speeds for each season over the period 1980-2017. Hatched regions indicate where the trends are significant at the 95% of confidence level (adapted from Torralba et al. 2017).

As mentioned before, data are assimilated by the different atmospheric analysis systems using different techniques. Moreover, these variables ingested into the datasets usually do not cover the same periods of time (Fujiwara et al. 2017). That could lead to the generation of fictitious trends and, therefore, to spurious correlations (Dee et al. 2011, Thorne and Vose 2010). To help reduce the uncertainty derived from these discontinuities, the use of more than one reanalysis is strongly recommended. Figure 32 shows a comparison of agreements and discrepancies between the four reanalyses (i.e. ERA-Interim, MERRA-2, JRA-55 and R1) when computing the linear trends. Positive trends at 95% of confidence level are displayed by the four datasets over large oceanic areas in the southern hemisphere for the four seasons. These positive trends

over oceanic areas could be linked to changes in the Walker circulation (L'Heureux et al. 2013, England et al. 2014). On the contrary, the four datasets display negative significant trends over some scattered continental regions. Some of these areas are located in Eurasia and North America, where the wind stilling was identified as the main driver of the decreasing of wind speeds.

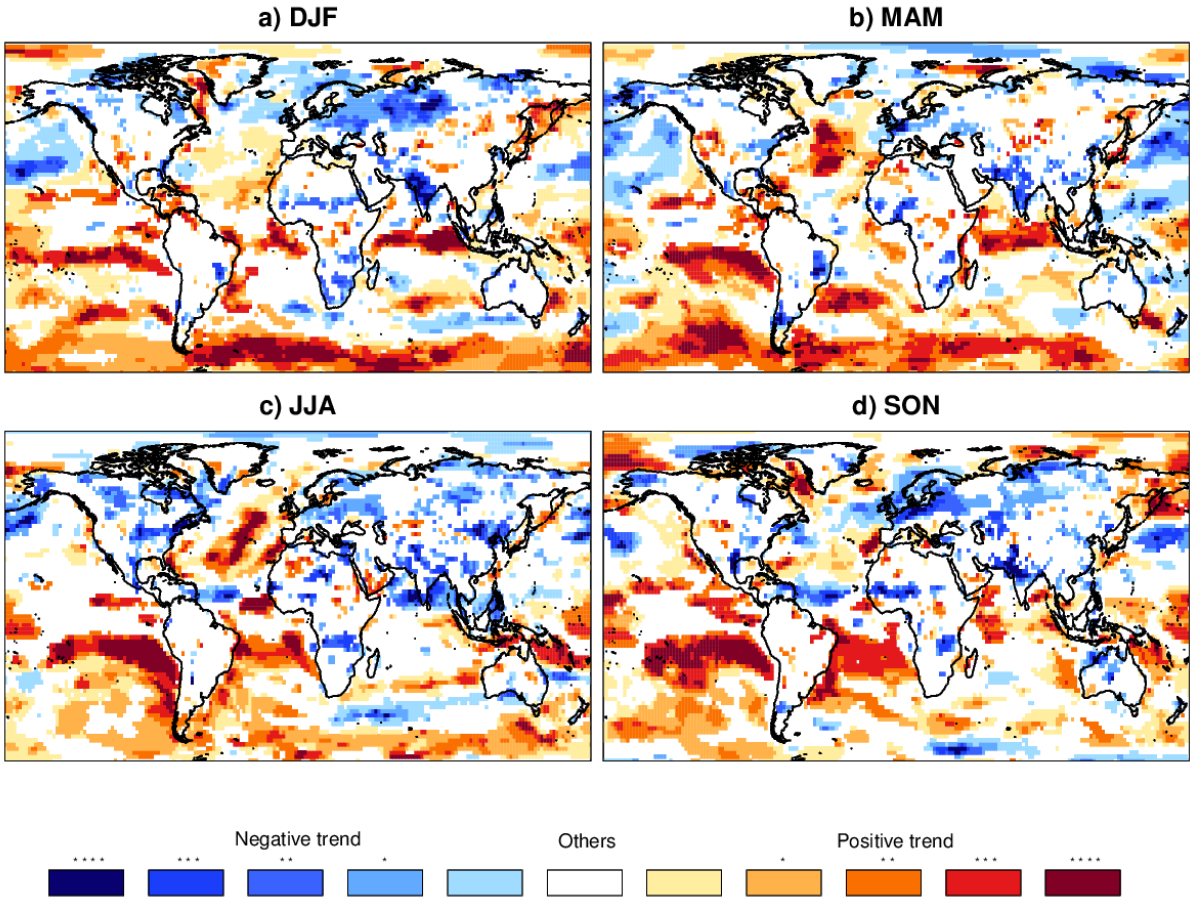

Figure 32: Comparison of the 10 m wind speed trends produced by ERA-Interim, JRA-55, MERRA-2 and R1 reanalyses. Blues (Reds) indicate agreement between the four reanalyses on the negative (positive) trends of 10 m wind speed for (a) DJF, (b) MAM, (c) JJA and (d) SON in the period of 1980–2017. Asterisks indicate that the trends are significant at the 95% confidence level: no asterisk indicates that the trends are not significant, (*) indicates that only one of the reanalysis has significant trends, (**) informs that two reanalyses have significant trends, (***) indicates that three reanalyses have significant trends and (****) means that the four reanalyses have significant trends (adapted from Torralba et al. 2017).

3.3.4 Verification of surface wind with Tall Tower observations

In the previous sections an overview of the differences between the selected reanalyses has been presented. By means of the tall tower observations more robust conclusions can be extracted.

Tall tower observations record wind speed at heights above 10 meters. Therefore, an extrapolation of surface wind from reanalyses to the tower measurement level is needed before computing scores. Surface wind speeds have been extrapolated using a power law with shearing exponent of 0.11 for offshore sites and 0.143 for onshore sites:

$wind_h = wind_{10m} * (h/10)^{alpha}$

This correction has an inherent uncertainty. To reduce the impact of this error on the results, most of the metrics have been normalized by mean wind speed and presented as relative values. The use of power law has been preferred to the possibility of employing a logarithmic profile because the latest method requires knowledge of atmospheric stability parameters such as Monin-Obukov length, which are harshly available in modelled datasets and need to be estimated. Also, this expression is more accurate than the power law when using it on a sub-daily time resolution (i.e. allowing for changes in stability), but employing a monthly mean stability parameter for the site will not deliver better estimates than a power law.

As an overview of overall quality, Figure 33 presents the correlation, standard deviation and centered RMSE (CRMSE) metrics for each reanalysis in a Taylor diagram. Both spatial and temporal variability are verified together in this analysis (Jolliffe and Stephenson 2012, section 6.3.1, equation ii). Different interpolation methodologies to extract model values at the tall tower sites have been compared: bilinear (*bil*), nearest neighbor (*nea*) and nine-point (*9pt*) average (see section 1.3 for details). Daily and monthly means have been distinguished and verified. These two diagrams are very similar, although monthly correlations are slightly lower than daily. MERRA-2 is the model that performs better in terms of variability, correlation and CRMSE. ERA5 follows closely, although it has more variability than observations. JRA-55 also tend to overestimate variability, while ERA-Interim adjusts to the observed variability. R1 has the poorest correlation with observations. Regarding interpolation methods, bilinear and nine-point averages have less variability than nearest neighbor. This makes sense, since bilinear and nine-point are averages over several grid points and therefore the values are smoother. Bilinear interpolations show a modest increase in correlation, and it is especially noticeable for MERRA-2.

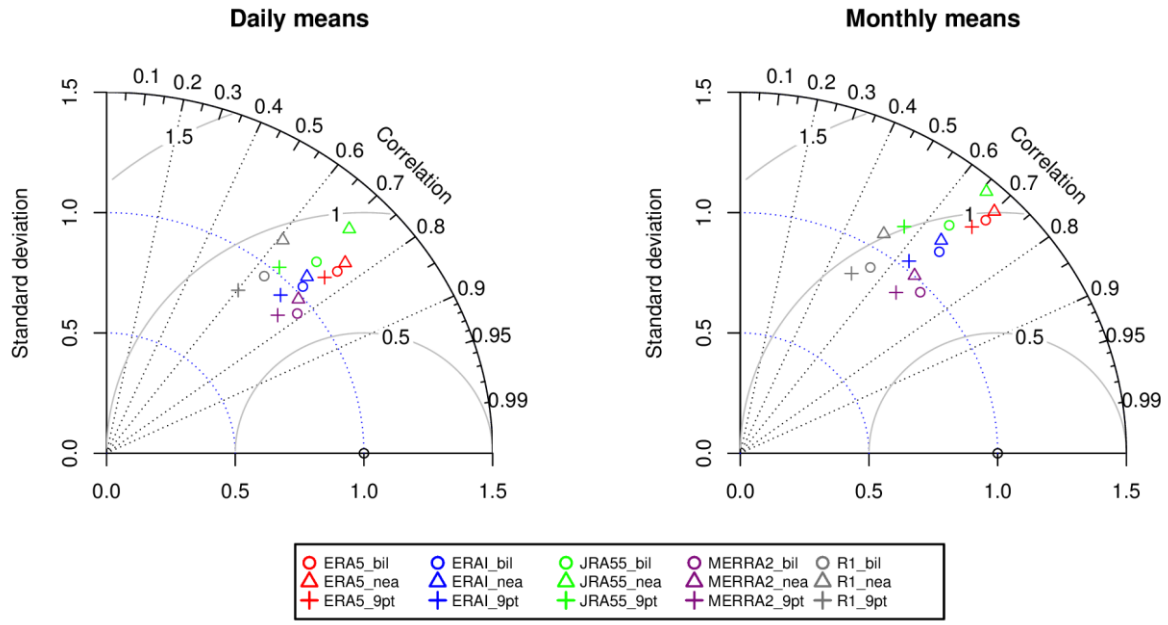

Figure 33: Taylor diagrams summarizing verification metrics of daily and monthly means for the five reanalyses and three interpolation methods with the tall tower observations.

Climatological values are difficult to compare with tall tower wind measurements due to the fact that observations are not taken at surface level. As mentioned before, using the power law as a vertical interpolation method introduces uncertainty. Figure 34 summarizes the differences in climatology between observations (*obs*) and reanalyses (*mod*). In general, reanalyses produce weaker winds than observations, although there are sites with the opposite behaviour. MERRA-2 is generally the reanalysis with the lowest biases.

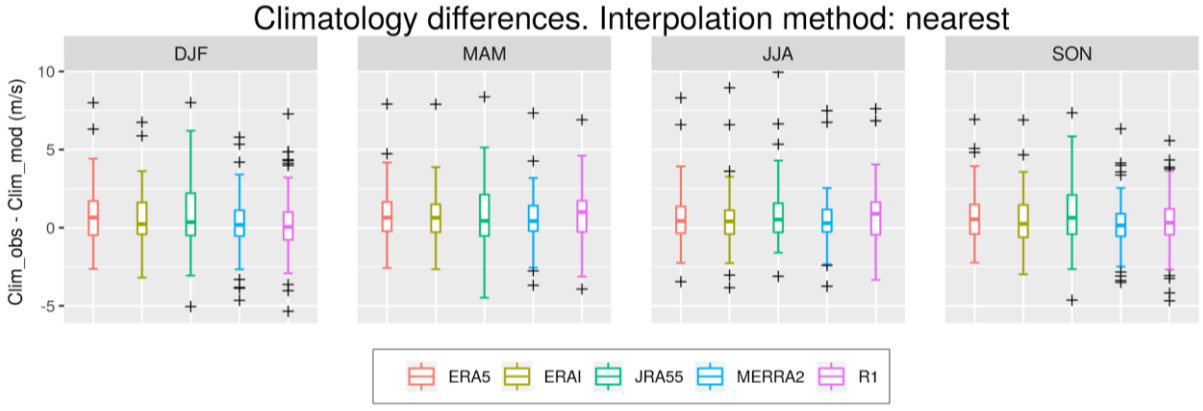

Figure 34: Boxplot of the differences between observed (obs) and reanalysis (mod) seasonal mean wind speeds. Surface wind speeds from reanalyses have been extrapolated to observation height using the power law approximation. Only towers with more than two years of period of record have been included.

Interannual variability (IAV) for each season has been compared with observations (see Figure 35). Although some outliers are found for MAM, JJA and SON, the biggest discrepancies are noted in DJF. In this season, all models produce less variability than observed. This is probably a consequence of comparing punctual site observations to grid point values representing an average over a wider area. ERA5 performs very well in this metric, with a narrow range in all seasons.

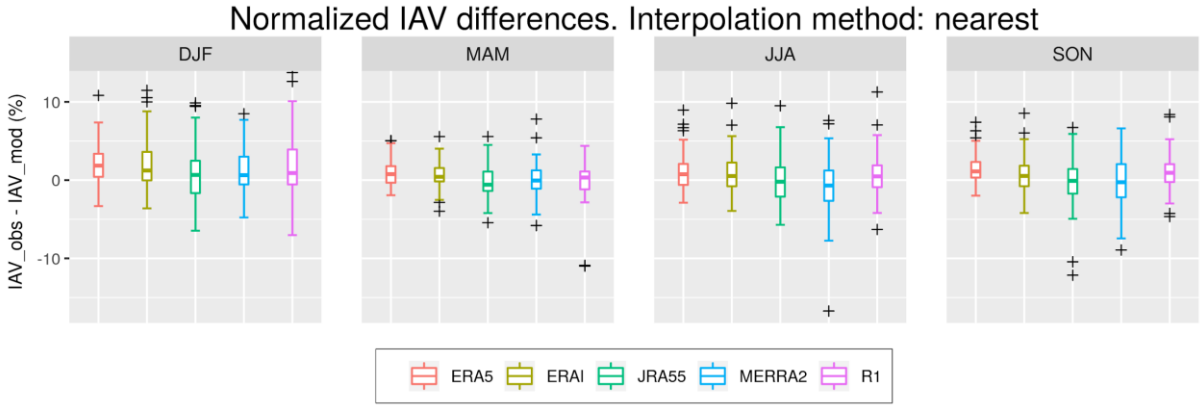

Figure 35: Boxplot of the differences between observed (obs) and reanalysis (mod) IAVs. Only towers with more than five years of period of record have been included.

Long-term trends computed from reanalysis data have also been compared with observations. Figure 36 shows the differences between observed and modeled trends. These differences have similar magnitude to the observed trends (Figure 31). Moreover, for the considered sites in this verification there is not agreement between model trends (Figure 37), and from this we conclude that the trends from the reanalyses models cannot be trusted for the sites considered here. Looking at Figure 37 we also see that there is not a good relationship between observed and modeled trends for any of the five reanalyses.

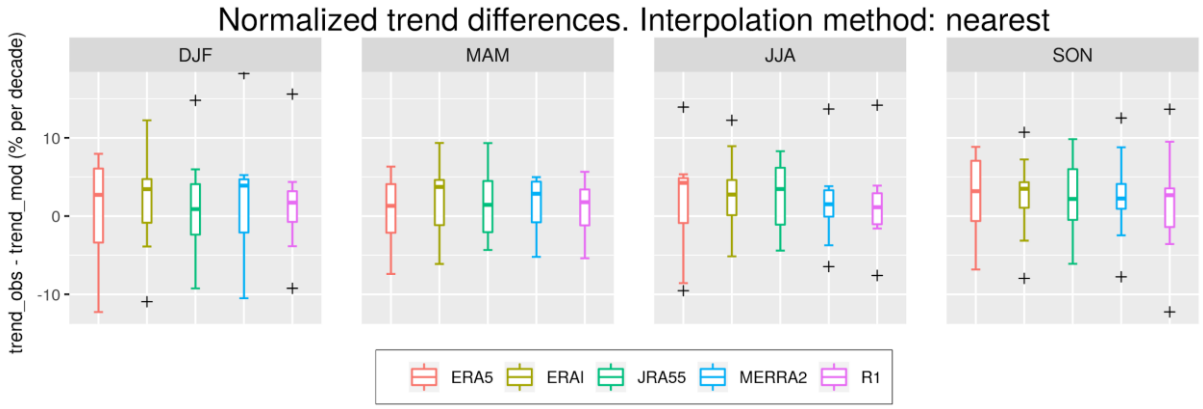

Figure 36: Boxplot of the differences between observed (obs) and reanalysis (mod) long-term trends. Only towers with more than twenty years of period of record have been included.

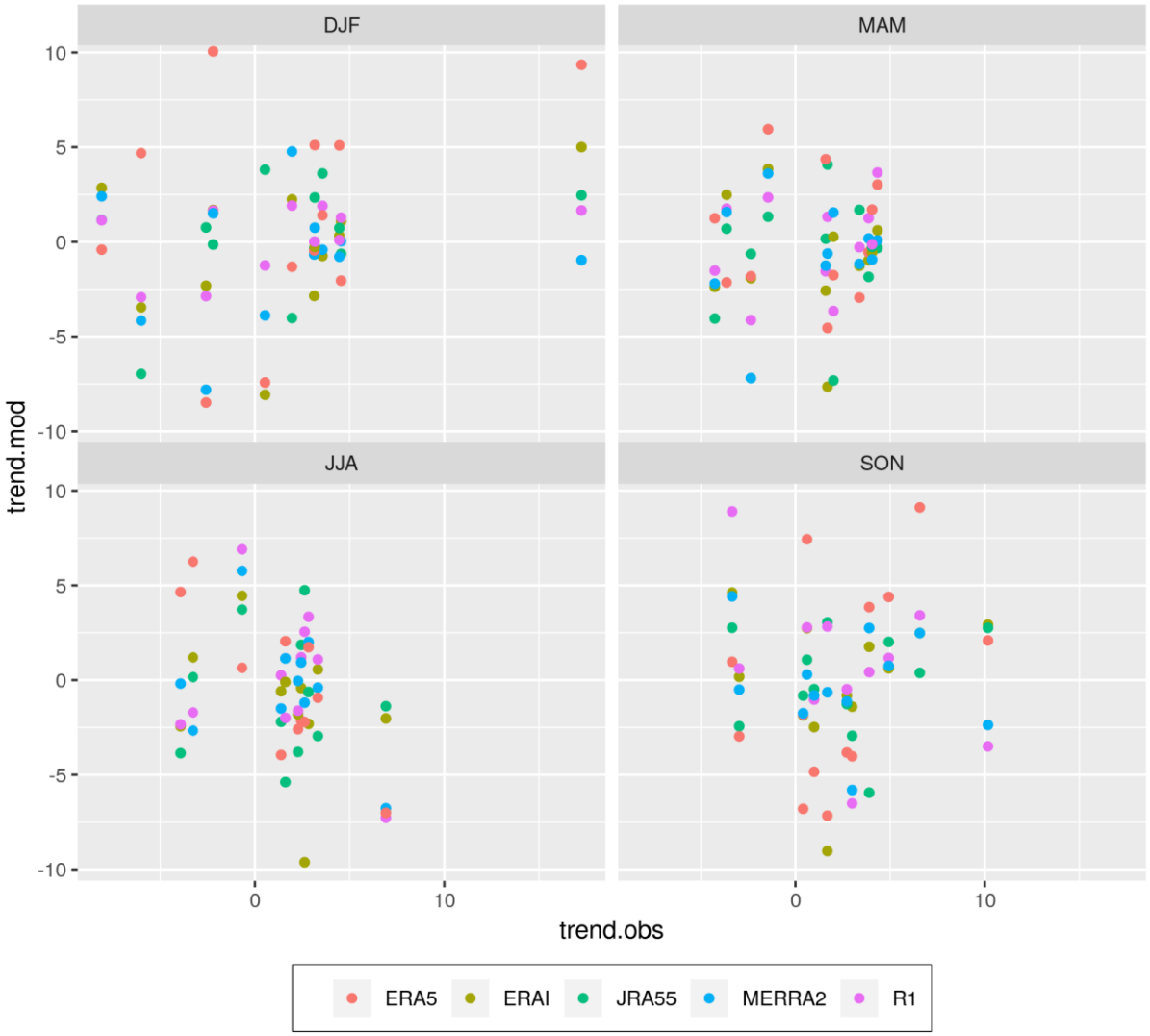

Figure 37: Scatter plot of observed (obs) and reanalysis (mod) trends. Only towers with more than twenty years of period of record have been included.

In order to produce a deeper analysis, towers have been grouped according to their location and the characteristics of the surrounding terrain. Hence, three groups have been distinguished: offshore towers, complex terrain towers and relatively flat terrain towers (hereafter referred as 'simple terrain towers'). Daily mean correlations for those groups are plotted in Figure 38 and monthly mean correlations in Figure 39.

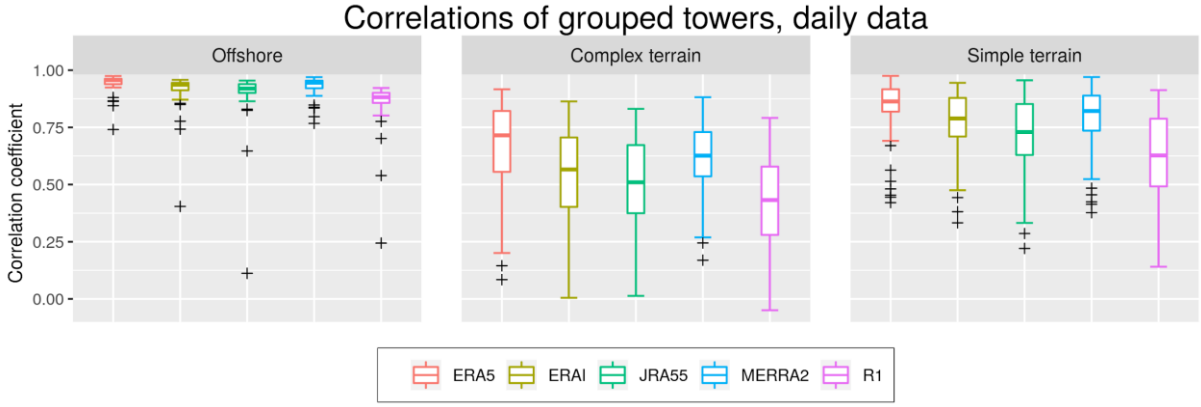

Figure 38: Boxplot of the correlation values between observed and reanalysis daily means. Only towers with more than one year of period of record have been included.

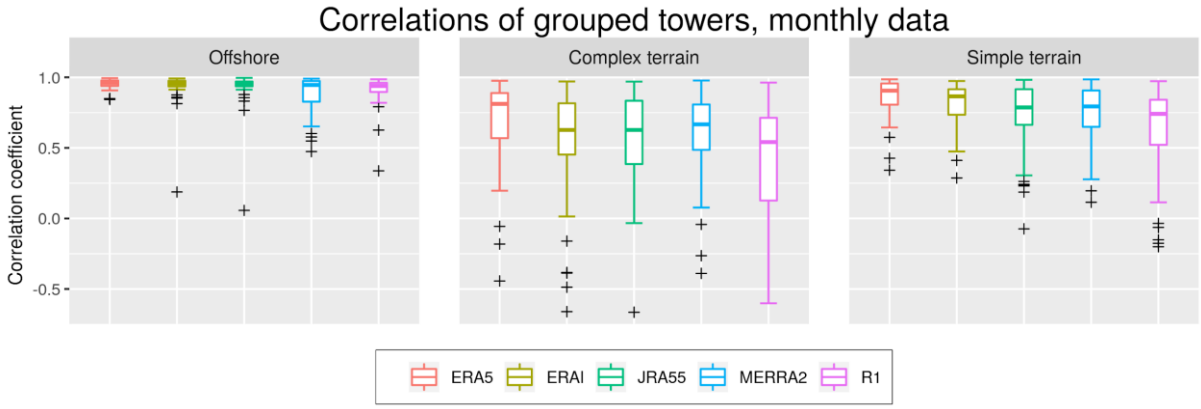

Figure 39: Boxplot of the correlation values between observed and reanalysis monthly means for offshore towers, complex terrain sites and simple terrain sites. Only towers with more than one year of period of record have been included.

Results observed in both Figure 38 and Figure 39 lead to conclude that ERA5 performs the best among the 5 selected datasets for all the considered groups whilst R1 shows the widest range of correlation values. It is also worth to note the good performance of all the datasets over oceanic areas. Most of the towers show correlations close to 1, indicating a good agreement between observational and reanalysis data. The lowest performance of the reanalyses is observed in complex terrain regions. Yet again, those reanalyses with higher resolution (i.e. ERA5 and MERRA-2) tend to produce better results, as they are able to incorporate more terrain features.

3.4 Validation results for precipitation

The weather parameter that most affects the hydroelectric power generation is the rainfall. Precipitation varies from year to year and over decades, and changes in amount, intensity, frequency, and type affect the environment and society. Electricity generated by hydropower is the most widely used form of renewable energy, and as such, its vulnerability to precipitation changes is of great interest. The amount of precipitation that drains into rivers and streams in a

geographic area determines the amount of water available for producing hydropower. Seasonal variations in precipitation and long-term changes in precipitation patterns, such as droughts, have a big impact on hydropower production (Lehner et al. 2005).
Observed global dataset of precipitation are based on various algorithms applied to satellite data because of the scarcity of the ground-based measurements over the globe. These datasets, such as the GPCP (Huffman et al. 2009) and the CMAP (Xie and Arkin 1997), reveal large discrepancies.
Precipitation from reanalysis is one of the critical components of the water and energy cycles, but is also largely related to modeled physical parameterizations. Reanalyses assimilate a wide variety of observations, but in general not precipitation measurements or analyses. Precipitation is a model product, influenced by observations through data assimilation, and inherits the systematic errors of the global circulation models used to provide the forecast background. The advantage to reanalyses is that all variables are dynamically consistent to some extent. However, as precipitation data are not typically constrained by the analysis procedure, reanalyzed precipitation is highly model dependent.

3.4.1 Intercomparison of precipitation climatology

Although the climatologies (Figure S17 a Figure S18) for the period 1980-2017 are generally similar, there are significative differences on estimating the amplitude and extension of the tropical rainband, especially in the area of the intertropical convergence zone (ITCZ). Global averaged values are included between 2.9 and 3.3 mm/day for the annual, 2.9-3.2 mm/day during DJF, 2.9-3.3 mm/day MAM, 2.9-3.4 JJA and 2.9-3.2 mm/day SON.
The spread of the dataset (Figure 40) is larger over the ITCZ. MERRA-2 underestimates the multi reanalysis mean in tropical area during all the seasons and slightly overestimates the multi reanalysis mean over the dry ocean zone of meridional Pacific and Atlantic. ERA-Interim has a similar behavior with values slightly lower. Instead, JRA-55 and R2 show a wetter tropical rainband. The high bias of the R2 reanalysis with respect to the Tropical Rainfall Measuring Mission (TRMM) satellite precipitation has been largely discussed by Roads et al. (2003). High values of spread are found in western coasts of South America JJA and over south-eastern Asia in JJA (monsoon area) in good agreement with the spread of the climatological RMSD (Figure 18). Other regions with large differences in the means are continental areas in the summer hemisphere and the western boundary ocean current regions. Large differences occur in central Africa in MERRA-2 in JJA. They were first identified by Bosilovich et al. (2011) as due to erroneous radiosonde station not rejected by the quality control. Europe has large spread in the regions of Alps. In Europe, North America and Asia the spread is higher during boreal summer. In these regions ERA-Interim is drier than the multi reanalysis mean and R2 wetter than the multi reanalysis mean. The large spread in tropics and over continents during the summer, when convective precipitation dominates, is mostly related with the parametrization of the numerical weather prediction models underlying the reanalysis. ERA5 (2000-2017) has generally higher values of precipitation over oceans. Values over continents are higher in the Northern Hemisphere and lower in the Southern Hemisphere (Figure 41). ITCZ is dryer than the multi reanalysis mean and dryer than ERA-Interim.

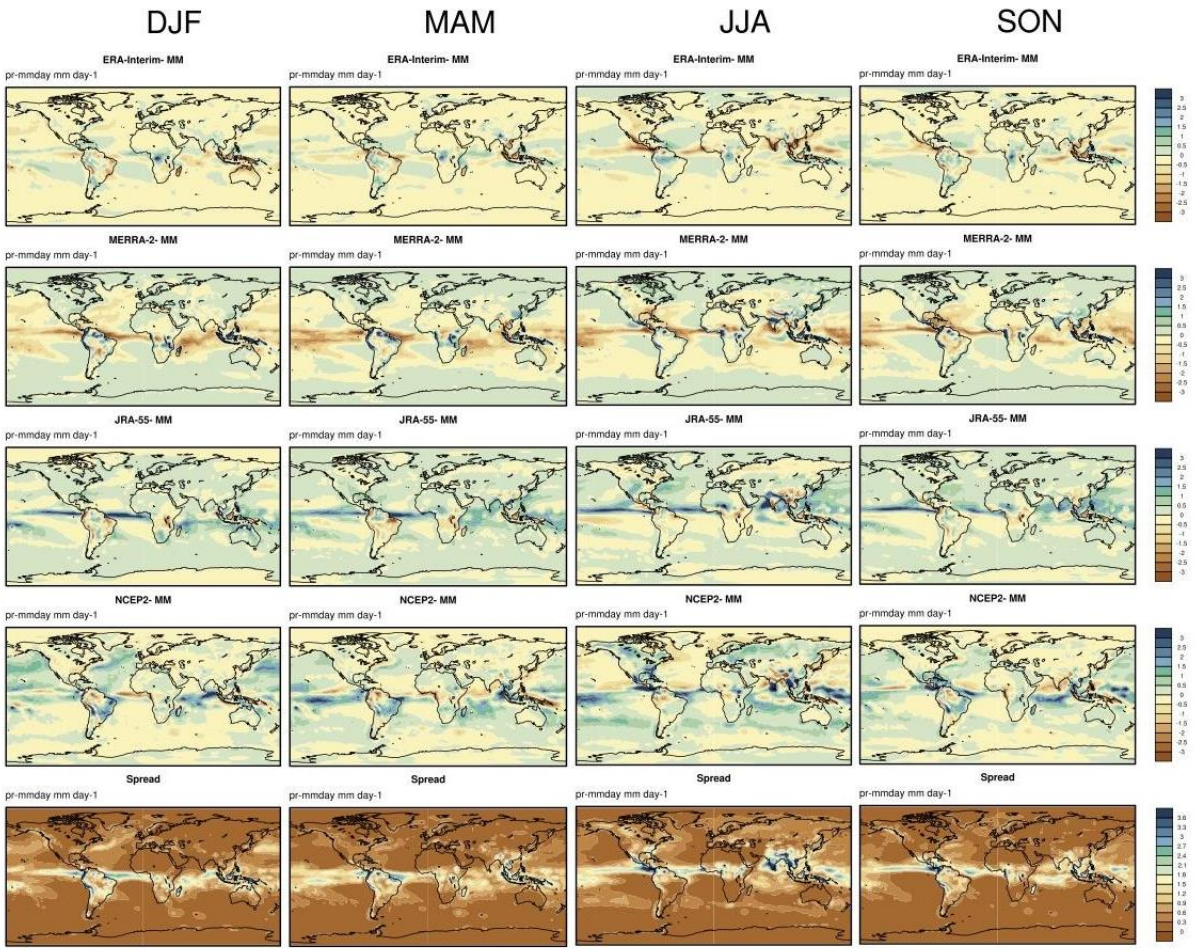

Figure 40: Differences of seasonal (DJF, MAM, JJA, SON) climatological mean of precipitation 1980-2017 between ERA-Interim, MERRA-2, JRA-55, NCEP/DOE R2 and multi reanalysis mean. (Bottom) Multi reanalysis spread.

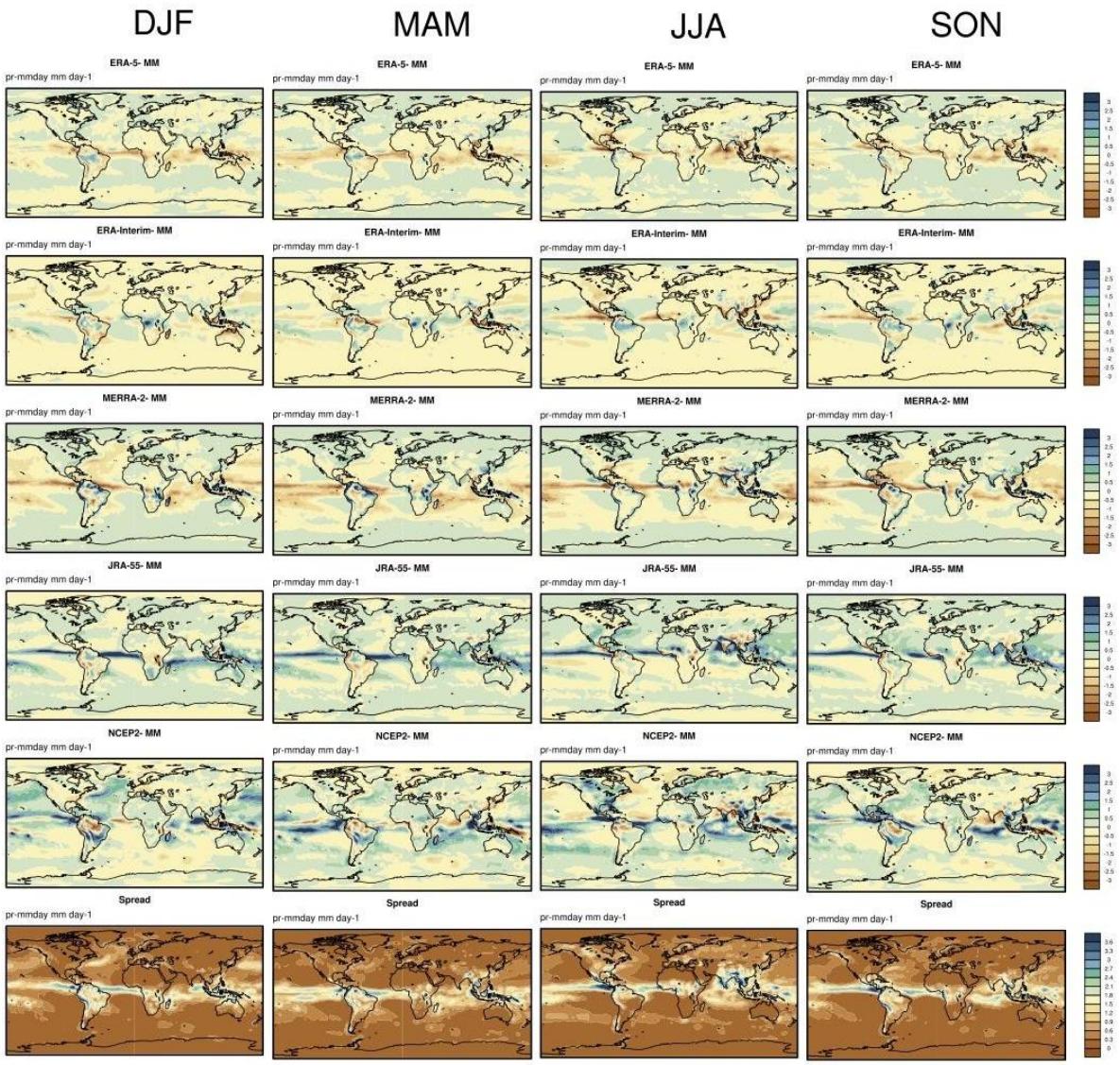

Figure 41: Differences of seasonal (DJF, MAM, JJA, SON) climatological mean of precipitation 2000-2017 between ERA5, ERA-Interim, MERRA-2, JRA-55, NCEP/DOE R2 and multi reanalysis mean. (Bottom) Multi reanalysis spread.

3.4.2 Intercomparison of precipitation variability

Interannual Variability

Inter annual daily precipitation variance is large where mean precipitation is large (Figure S19 and Figure S20). The largest variances are in areas with highly variable convective precipitation such as the ITCZ, the Indian Ocean, and the Indian monsoon region. The spread (Figure 42) among the estimated variability is high not only in the ITCZ, but also in dry area such as North Africa, Middle East, oceanic regions of South Pacific and South Atlantic. The spread is large over continents at mid latitudes during boreal summer. ERA-Interim variability is generally lower than the multi reanalysis mean especially in dry area of Africa and Australia. MERRA-2 variability is low biased in Eastern part of Sahara and high biased in the western part of Sahara. JRA-55 estimates higher variability than the multi reanalysis mean in the dry regions of Africa

and Asia. R2 overestimates the variability of the multi reanalysis mean over most of the oceanic regions, over tropics and over Europe and Asia in JJA. One of the main driver of the interannual variability of precipitation is ENSO. As documented by Trenberth et al. (2011) the main variations in the global mean precipitation occur in the tropics, where the precipitable water is largest, in association with ENSO events. ERA5 (2000-2017) has an increased variability respect ERA-Interim in better agreement with the other reanalyses (Figure 43). During most of the seasons over Europe there is larger variability of precipitation than the multi reanalysis mean.

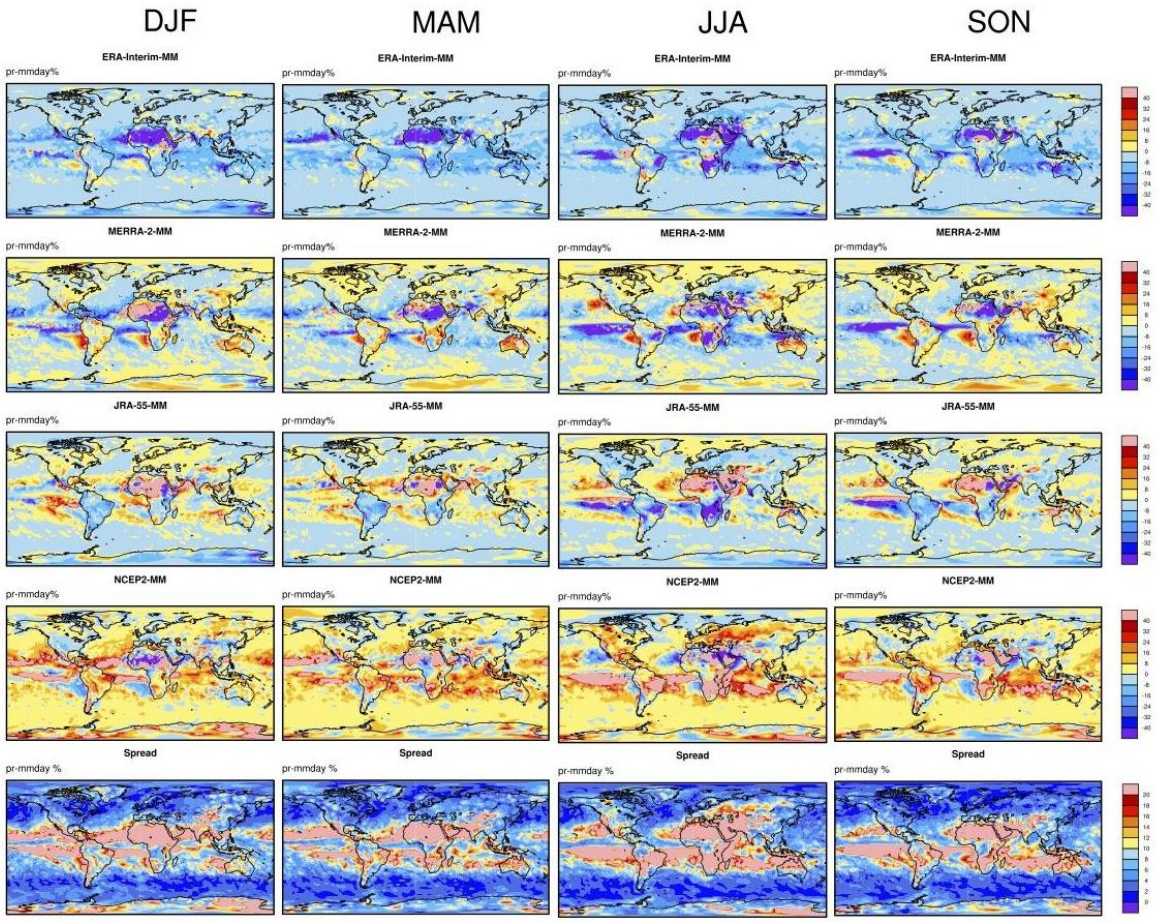

Figure 42: Differences of normalized interannual variability 1980-2017 of precipitation between ERA-Interim, MERRA-2, JRA-55, NCEP/DOE R2 and multi reanalysis mean. (Bottom) Multi reanalysis spread of the interannual variability.

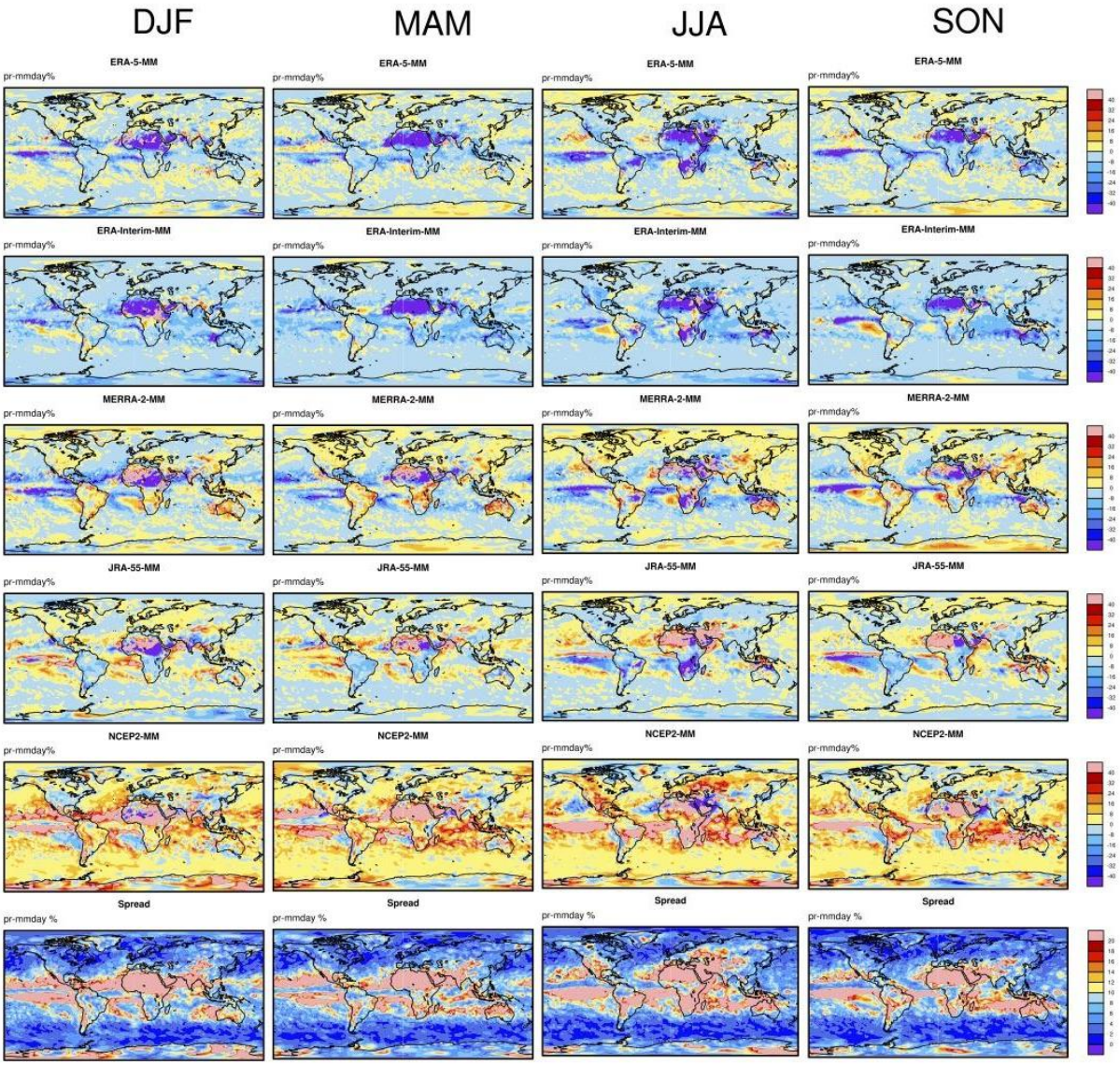

Figure 43: Differences of normalized interannual variability 2000-2017 of precipitation between ERA5, ERA-Interim, MERRA-2, JRA-55, NCEP/DOE R2 and multi reanalysis mean. (Bottom) Multi reanalysis spread of interannual variability.

Intraseasonal Variability

The intraseasonal variability is higher over the ITCZ (Figure S21 and Figure S22). There are relative high values of intraseasonal variability at mid latitudes in summer.

The spread (Figure 44) has large values over areas where the intraseasonal variability is large, such as ITCZ and JJA Northern mid-latitude and DJF Southern mid latitude, but also in dry regions since the normalization increases the percentage of variance. ERA-Interim is lower biased than the multi reanalysis mean, R2 generally high biased. In all the datasets intraseasonal variability has similar behavior than the interannual variability. Figure 45 shows the intraseasonal variability from 2000 to 2017 and includes ERA5. ERA5 is less negative biased than ERA-Interim and presents values of intraseasonal variability broadly comparable with the values of the others reanalyses.

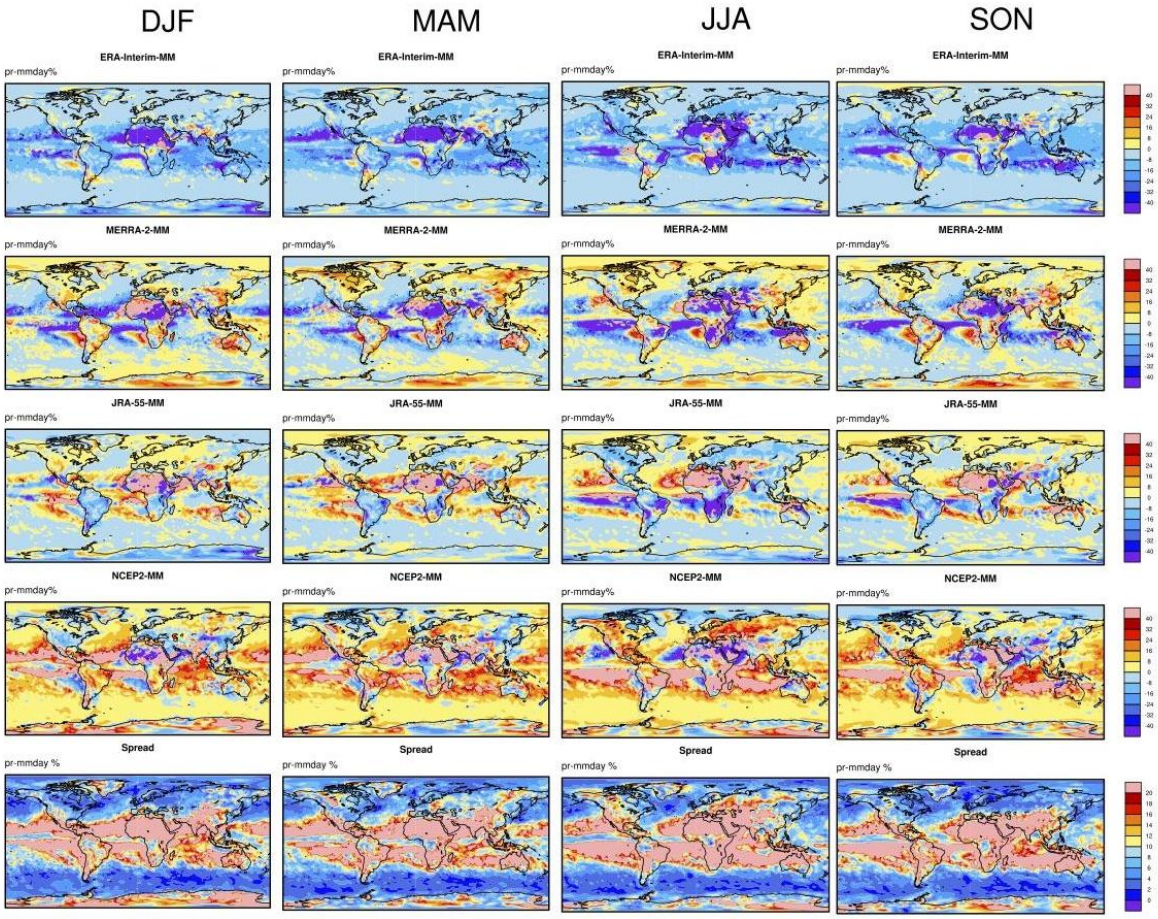

Figure 44: Differences of normalized intraseasonal variability 1980-2017 of monthly precipitation between ERA-Interim, MERRA-2, JRA-55, NCEP/DOE R2 and multi reanalysis mean. (Bottom) Multi reanalysis spread of intraseasonal variability.

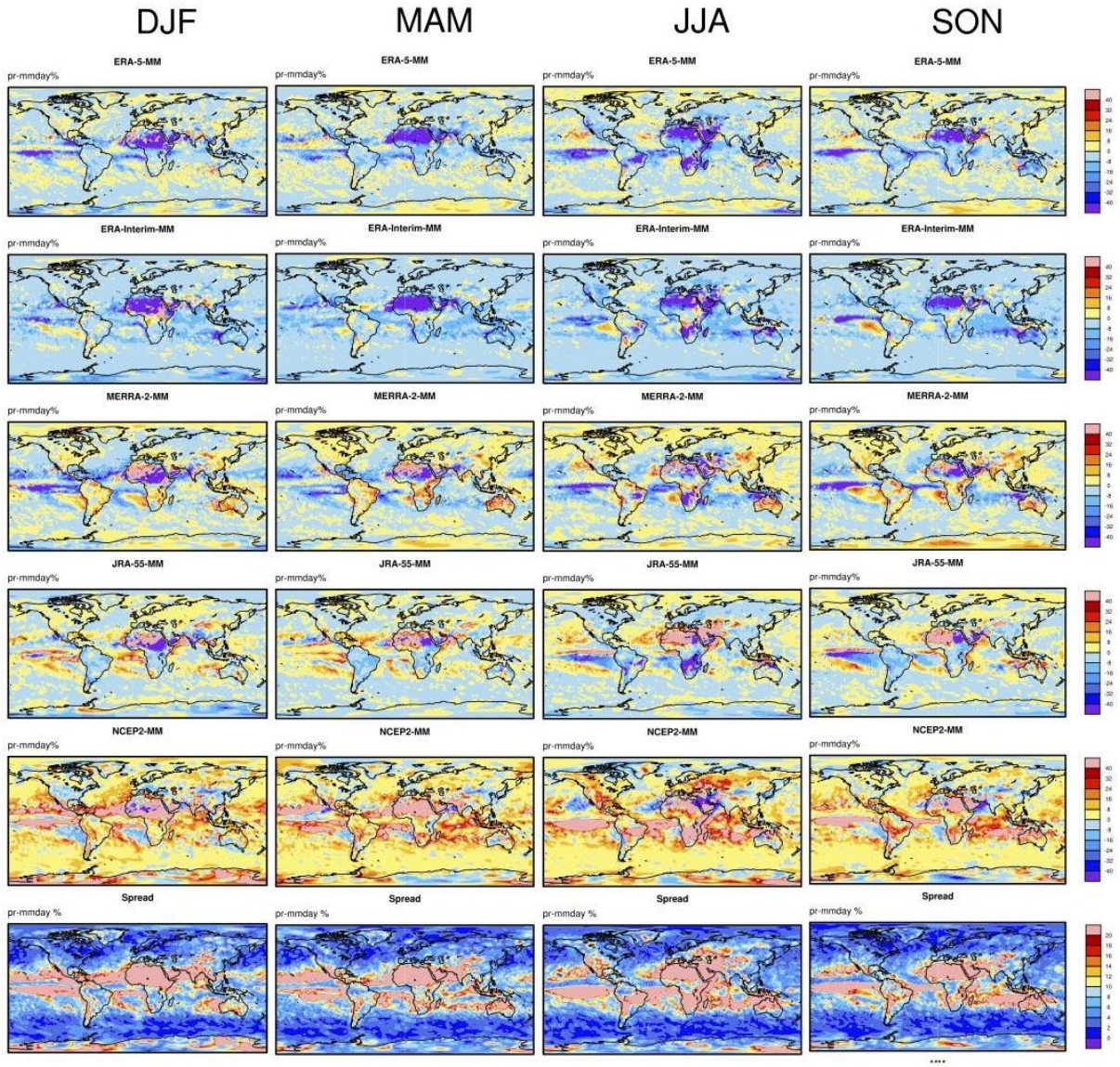

Figure 45: Differences of normalized intraseasonal variability 2000-2017 of monthly precipitation between ERA5, ERA-Interim, MERRA-2, JRA-55, NCEP/DOE R2 and multi reanalysis mean. (bottom) Multi reanalysis spread of intraseasonal variability.

3.4.3 Intercomparison of precipitation trends

According to Hartmann et al. (2013), there is still a large uncertainty about past observed global change of precipitation. Gu et al. (2007) and Huffman et al. (2009) documented global and tropical rainfall changes using the Global Precipitation Climatology Project (GPCP), and found near zero global changes, but with large variability and changes over land that are largely compensated for by opposite changes over the oceans. Wentz et al. 2007 found a significant positive trend from 1987 to 2006, but that result depended critically on the time period and the dataset used.

Reanalyses are often evaluated unable to characterize long-term trends in precipitation (Trenberth et al., 2011). Indeed, there are several spurious trends in reanalysis precipitation

arising from transitions of observation system (Bosilovich et al. 2011) of assimilated variables (i.e. radiance).
Annual and seasonal trends in precipitation are represented in Figure S23 and Figure 46. ERA-interim and MERRA-2 have lower and less significant values of trend respect to JRA-55 and R2. In all the datasets, the precipitation over tropical land areas (30°S to 30°N) has increased over the last decades. In observed datasets (Hartmann et al. 2013) the mid-latitudes of the NH (30°N to 60°N) show an overall increase in precipitation that is not in the reanalysis. Seasonal trends in Europe are only significant for R2.

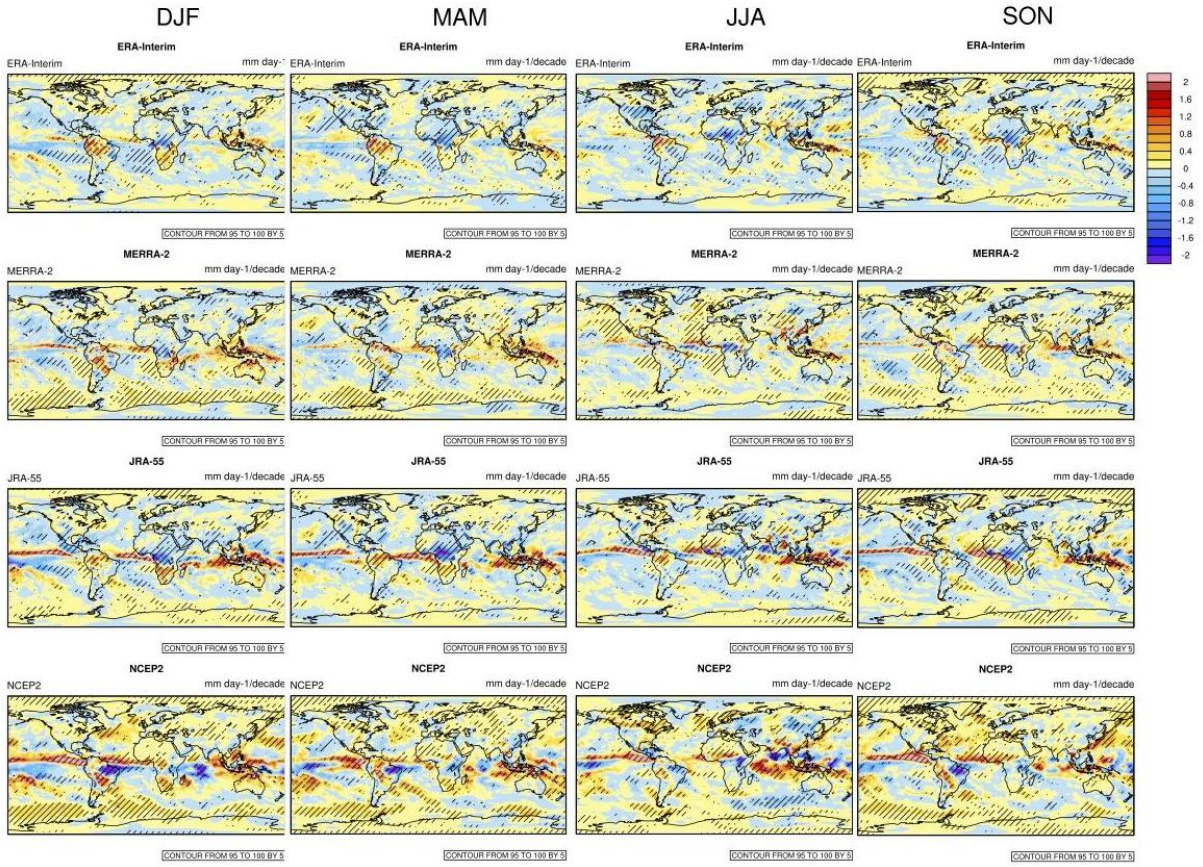

Figure 46: Trend 1980-2017 of precipitation in ERA-Interim, MERRA-2, JRA-55, NCEP/DOE R2.

3.4.4 Verification of precipitation with E-OBS observations

The spatial correlation of the annual and seasonal climatology over the E-OBS domain is shown in Figure 47. In the case of the annual climatology all reanalysis (except R2) have values of correlation close to 0.9. MERRA-2 overestimates the observed spatial variability. All the reanalysis has lower correlation in DJF and MAM. JRA-55 and ERA-Interim have values of standard deviation similar to the observation. Variability of precipitation is overestimated in summer by all reanalysis, especially R2. The performance of ERA5 is broadly different from ERA-Interim during the 2000-2017 period (Figure 48). Despite some improvements noted in the correlation, the variability is overall larger than the observed variability. The bias is generally positive and included between 5%and 1-10 % except for NCEP2 that has negative bias in DJF and SON.

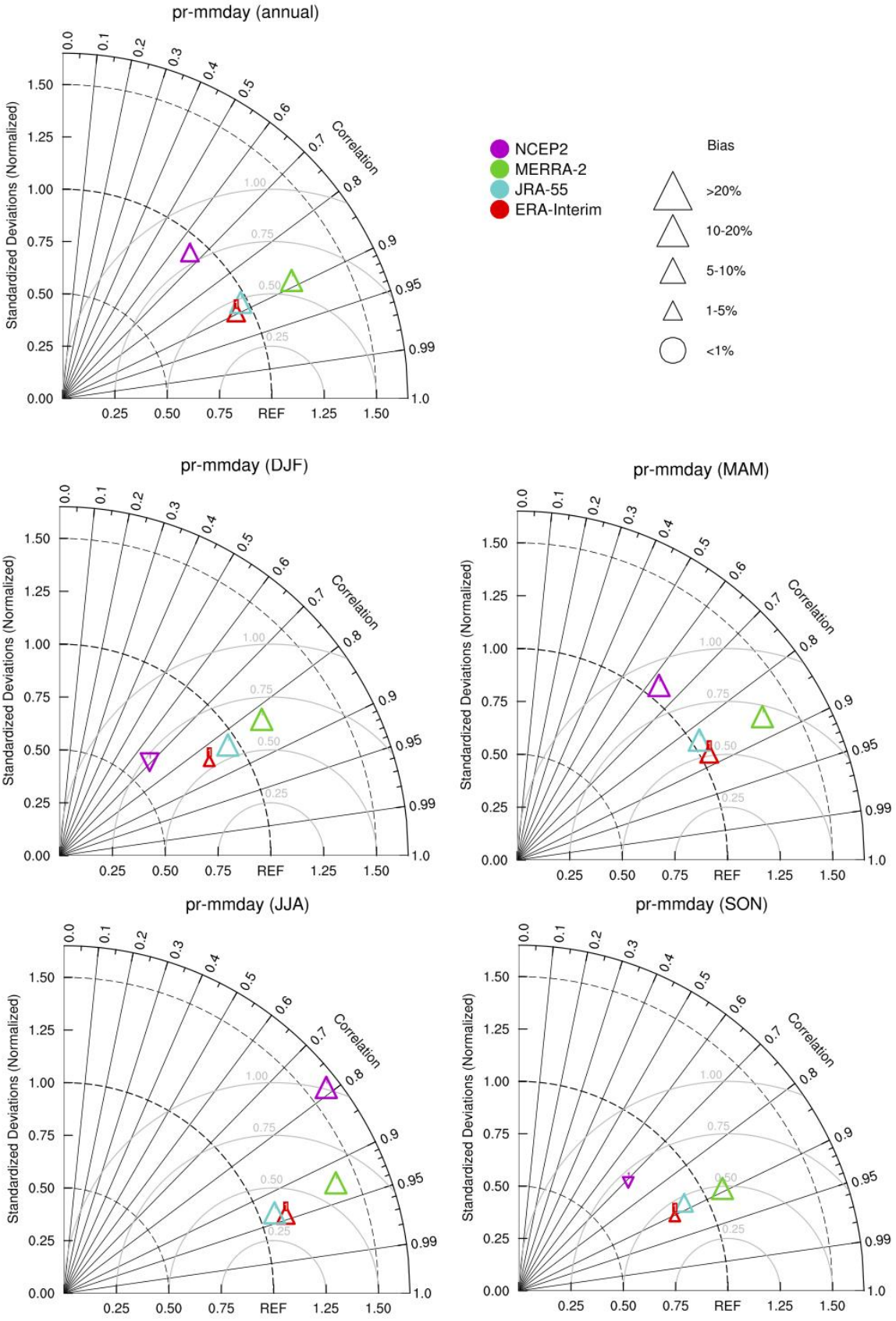
pr-mmday (annual)
pr-mmday (DJF)
pr-mmday (MAM)
pr-mmday (JJA)
pr-mmday (SON)
Standardized Deviations (Normalized)
Correlation
REF
NCEP2
MERRA-2
JRA-55
ERA-Interim
Bias
>20%
10-20%
5-10%
1-5%
<1%

Figure 47: Taylor Diagram Climatological mean 1980-2017 of annual (Top) and seasonal (Center and Bottom) precipitation in ERA-Interim, MERRA-2, JRA-55, NCEP/DOE R2 vs. E-OBS.

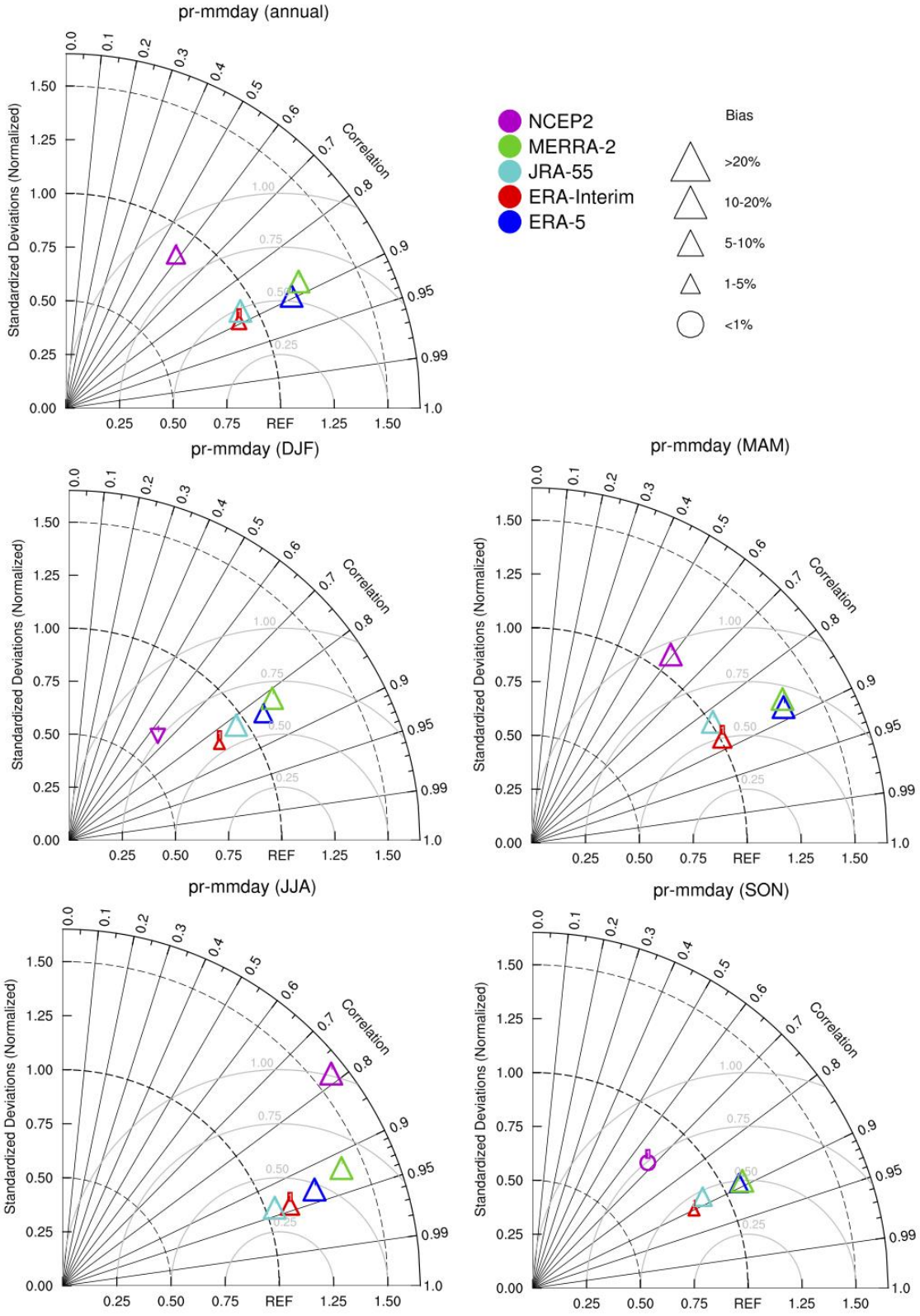

Figure 48 Taylor Diagram Climatological mean 2000-2017 of annual (Top) and seasonal (Center and Bottom) precipitation in ERA5, ERA-Interim, MERRA-2, JRA-55, NCEP/DOE R2 vs. E-OBS.

Values of correlation based on spatial and temporal variability (Figure 49) are always below 0.8 and for R2 close to 0.6. MERRA-2 overestimates the variability of E-OBS. Others reanalysis show lower values of variability respect to the observational dataset in MAM and JJA and higher values in DJF and SON. The correlation of ERA5 for the period 2000-2017 is broadly similar to the correlation of ERA-Interim (Figure 50), although the variability is higher. Era-Interim is generally the dataset with lower bias.

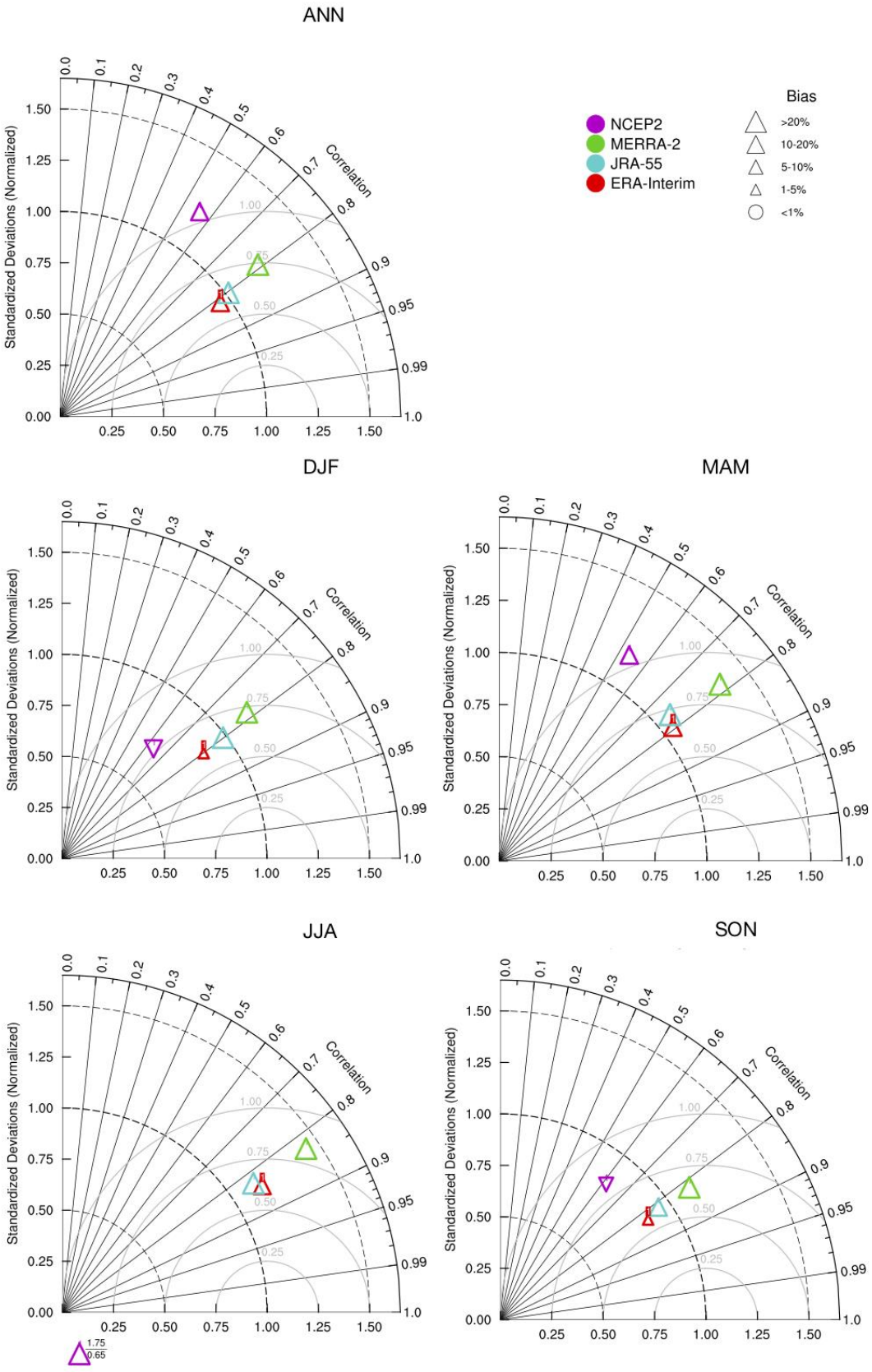

Figure 49: Taylor Diagram 1980-2017 of monthly (Top) and seasonal (Center and Bottom) precipitation in ERA-Interim, MERRA-2, JRA-55, NCEP/DOE R2 vs. E-OBS.

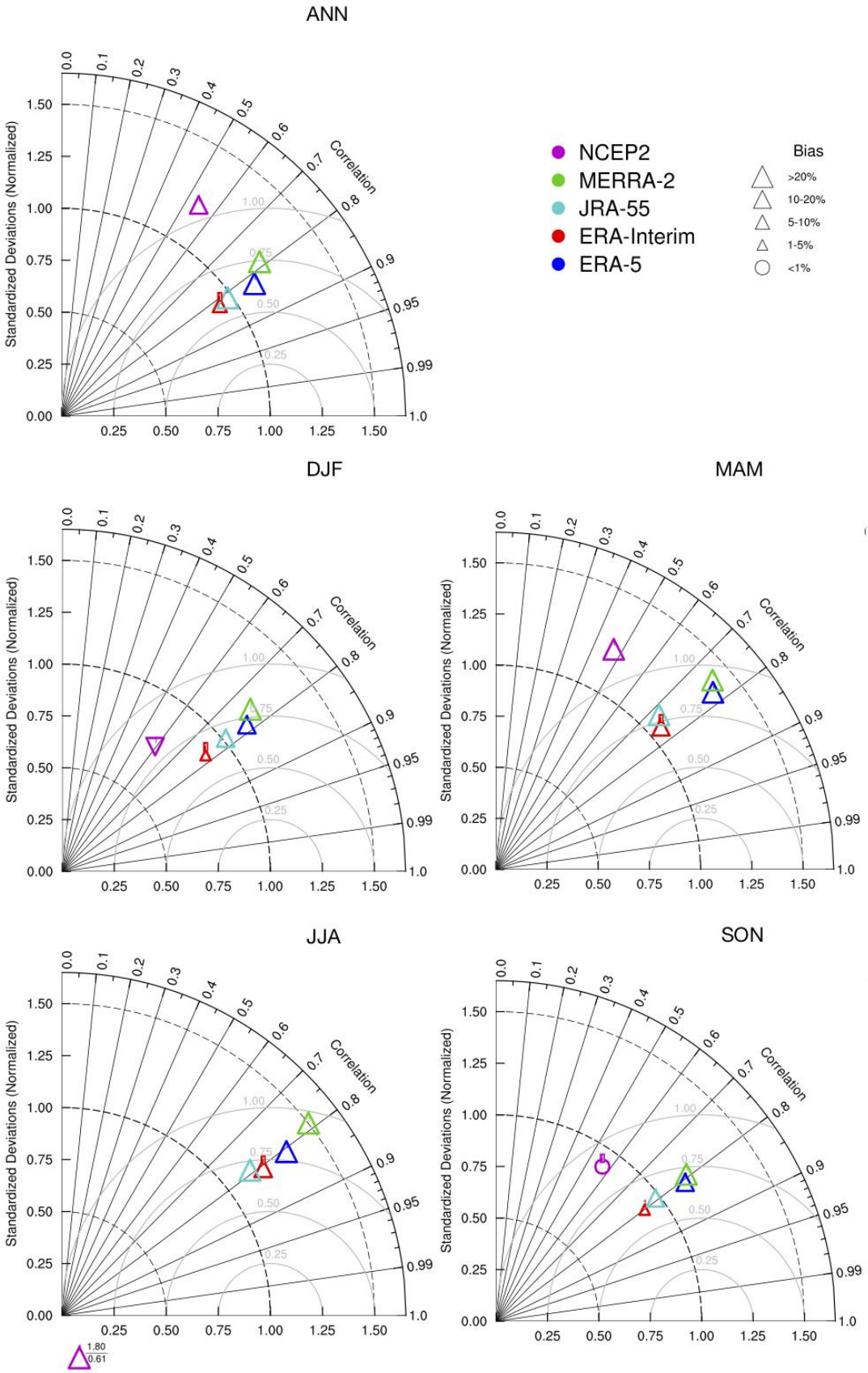

Figure 50: Taylor Diagram 2000-2017 of monthly precipitation in ERA5 ERA-Interim, MERRA-2, JRA-55, NCEP/DOE R2 vs. E-OBS.

Conclusions

Main conclusions of reanalysis intercomparison and evaluation are summarized in Tables 6-9. For each reanalysis and for each ECV, the more relevant results about the explored diagnostics (climatology, variability, trends) are reported, as well as some considerations about the evaluation against observed datasets. The tables allow cross-referencing the performance of the single reanalysis over the different ECVs.

		ERA5	MERRA-2	JRA-55	ERA-Interim	R1 or R2
Temperature	Climatology	-Generally low biased	-Negative bias in North Europe, North America and North Asia in DJF and SON	-Positive biased in East Antarctica	-Warmer winter bias in Arctic	-Large bias in Africa
		The spread among the reanalysis is higher in locations with fewer assimilated data (i.e. Africa and Poles). High correlation in Europe with observed data.				
	IAV	-Variability comparable to the MM	-High variability in central Africa and Amazonia	-Small Variability in Antarctica	-High variability in North Europe and Asia	-Too large variability in Africa and polar regions
		Larger spread of variability where the climatology is biased due to scarcity of data assimilated. Spatio-temporal correlation and variability well performed respect to observed data.				
	Trends	Trend estimates and significance are broadly similar.				

Table 6: Summary of reanalysis performance for 2m temperature

		ERA5	MERRA-2	JRA-55	ERA-Interim	R1 or R2
Precipit	Climatol	-Negative bias in ITCZ	-Negative bias in ITCZ.	-Positive bias in ITCZ	-Generally negative bias over sea	-Large negative bias over ITCZ

		Large spread over the ITCZ and in Summer at mid latitude over land. In Europe, spatial correlation and variability respect to observed data are not always good.				
	IAV	-Too small variability over dry areas	-Mixed pattern of variability over dry areas	-Mixed pattern of variability over dry areas	-Generally too low variability	Generally too large variability
		High spread of variability over ITCZ. Spatio-temporal correlation and variability not always well performed respect to observed data.				
	Trends	Positive trend over tropical areas. Low significance over continental area of the Northern Hemisphere.				

Table 7: Summary of reanalysis performance for precipitation

		ERA5	MERRA-2	JRA-55	ERA-Interim	R1 or R2
Surface wind	Climatology	Generally low biased. Negative biases only for elevated areas	Positive bias inland. Slight negative departures in oceanic areas	Low bias inland	Similar to ERA5	Negative bias for polar and tropical regions
		Discrepancies observed for continental regions				
	IAV	Low variability inland	Mixed pattern. Low variability in Amazonia	High variability within continents. Low IAV offshore	Similar to ERA5	Generally low variability. High IAVs only between tropics
		Important disagreements between reanalyses for both oceans and continents				
	Trends	Not considered	Strong positive trends along the equator	Systematically large and negative trends inland. Spurious correlations	In agreement with MERRA2	Strong trends over the tropics
		Strong discrepancies among models in most regions. No coincidence with obs for the available sites.				

Table 8: Summary of reanalysis performance for surface wind

		ERA5	MERRA-2	JRA-55	ERA-Interim	R1 or R2
Solar Radiation	Climatology	-Less biased dataset	-Positive bias over south-eastern Asia during JJA	-High positive bias over storm-track zone of the Southern hemisphere and inland tropical area	-Similar to ERA5 but with stronger bias over Africa (positive) and South-East Asia (negative)	-Generally high positive bias
		Important disagreement between reanalysis over tropical regions and mid latitudes in Summer. Good correlation with satellite data over Europe and Africa.				
	IAV	High spread among reanalyses where the interannual variability is higher. Underestimated observed variability over Europe and Africa.				
	Trends		Significative negative trend over oceans	Mixed pattern of positive and negative trend over continents	Strong positive trend in North America and Europe during Summer	-Strong positive trend
		Broadly common positive trend in the Northern Hemisphere inland.				

Table 9: Summary of reanalysis performance for solar radiation

Bibliography

IEA. (2017). *World Energy Outlook*. IEA, Paris. https://www.iea.org/weo2017/

Brayshaw, D. J., Troccoli, A., Fordham, R., and Methven, J.: The impact of large scale atmospheric circulation patterns on wind power generation and its potential predictability (2011). A case study over the UK. *Renewable Energy*, 36, 2087–2096, DOI: 10.1016/j.renene.2011.01.025

Bengtsson, L., Haines, K., Hodges, K. I., Arkin, P., Berrisford, P., Bougeault, P., Kallberg, P., Simmons, A. J., Uppala, S., Folland, C. K., Gordon, C., Rayner, N., Thorne, P. W., Jones, P., Stammer, D., and Vose, R. S. (2007). The need for a dynamical climate reanalysis, *Bulletin of the American Meteorological Society*, 88, 495–501, https://doi.org/10.1175/bams-88-4-495.

GCOS. (2010): Implementation plan for the global observing system for climate in support of the UNFCCC (2010 update). *GCOS Rep*. 138, 186 pp. www.wmo.int/pages/prog/gcos/Publications/gcos-138.pdf.

Gregow, H., Jylhä, K., Mäkelä, H. M., Aalto, J., Manninen, T., Karlsson, P., Kaiser-weiss, A.K., Kaspar, F., Poli, P., Tan, D. G. H., Obregon, A., and Su, Z. (2016). Worldwide survey of awareness and needs concerning reanalyses and respondents views on climate services, *Bulletin of the American Meteorological Society*, 97(8), 1461–1474, doi:10.1175/BAMS-D-14-00271.1.

Compo, G. P., Whitaker, J. S., Sardeshmukh, P. D., Matsui, N., Allan, R. J., Yin, X., Gleason, B. E., Vose, R. S., Rutledge, G., Bessemoulin, P., Brönnimann, S., Brunet, M., Crouthamel, R. I., Grant, A. N., Groisman, P. Y., Jones, P. D., Kruk, M. C., Kruger, A. C., Marshall, G. J., Maugeri, M., Mok, H. Y., Nordli, Ø., Ross, T. F., Trigo, R. M., Wang, X. L., Woodruff, S. D., and Worley, S. J.(2011). The twentieth century reanalysis project, *Quarterly Journal of the Royal Meteorological* Society, 137, 1–28, https://doi.org/10.1002/qj.776.

Dee, D. P., Uppala, S. M., Simmons, A. J., Berrisford, P., Poli, P., Kobayashi, S., Andrae, U., Balmaseda, M. A., Balsamo, G., Bauer, P., Bechtold, P., Beljaars, A. C. M., van de Berg, L., Bid- lot, J., Bormann, N., Delsol, C., Dragani, R., Fuentes, M., Geer, A. J., Haimberger, L., Healy, S. B., Hersbach, H., Hólm, E. V., Isaksen, L., Kållberg, P., Köhler, M., Matricardi, M., McNally, A. P., Monge-Sanz, B. M., Morcrette, J. J., Park, B. K., Peubey, C., de Rosnay, P., Tavolato, C., Thépaut, J. N., and Vitart, F. (2011). The ERA-Interim reanalysis: configuration and performance of the data assimilation system, *Quarterly Journal of the Royal Meteorological*, 137, 553– 597, https://doi.org/10.1002/qj.828.

Fujiwara, M., Wright, J. S., Manney, G. L., Gray, L. J., Anstey, J., Birner, T., Davis, S., Gerber, E. P., Harvey, V. L., Hegglin, M. I., Homeyer, C. R., Knox, J. A., Kruger, K., Lambert, A., Long, C. S., Martineau, P., Molod, A., Monge-Sanz, B. M., San- tee, M. L., Tegtmeier, S., Chabrillat, S., Tan, D. G. H., Jack- son, D. R., Polavarapu, S., Compo, G. P., Dragani, R., Ebisuzaki, W., Harada, Y., Kobayashi, C., McCarty, W., Onogi, K., Paw- son, S., Simmons, A., Wargan, K., Whitaker, J. S., and Zou, C.-Z. (2017). Introduction to the SPARC reanalysis intercomparison project (S-RIP) and overview of the reanalysis systems, *Atmospheric Chemistry and Physics*, 17, 1417–1452, https://doi.org/10.5194/acp- 17-1417-2017.

Saha, S., Moorthi, S., Pan, H. L., Wu, X. R., Wang, J. D., Nadiga, S., Tripp, P., Kistler, R., Woollen, J., Behringer, D., Liu, H. X., Stokes, D., Grumbine, R., Gayno, G., Wang, J., Hou, Y. T., Chuang, H. Y., Juang, H. M. H., Sela, J., Iredell, M., Treadon, R., Kleist, D., Van Delst, P., Keyser, D., Derber, J., Ek, M., Meng, J., Wei, H. L., Yang, R. Q., Lord, S., Van den Dool, H., Kumar, A., Wang, W. Q., Long, C., Chelliah, M., Xue, Y., Huang, B. Y., Schemm, J. K., Ebisuzaki, W., Lin, R., Xie, P. P., Chen, M. Y., Zhou, S. T., Higgins, W., Zou, C. Z., Liu, Q. H., Chen, Y., Han, Y., Cucurull, L., Reynolds, R. W., Rutledge, G., and Goldberg, M.(2010). The NCEP climate forecast system reanalysis, *Bulletin of the American Meteorological Society*, 91, 1015–1057, https://doi.org/10.1175/2010BAMS3001.1.

Bett, P.E., Thornton, H.E. (2016). The climatological relationships between wind and solar energy supply in britain. *Renewable Energy* 87, 96-110.

Jones, P.D., Harpham, C., Troccoli, A., Gschwind, B., Ranchin, T., Wald, L., Goodess, C.M., Dorling, S. (2017). Using ERA-Interim Reanalysis output for creating datasets of energy- relevant climate variables. *Earth System Science Data*, 9, 471–495. doi:10.5194/essd-2016-67.

Kobayashi, S., Ota, Y., Harada, Y., Ebita, A., Moriya, M., Onoda, H., Onogi, K., Kamahori, H., Kobayashi, C., Endo, H., Miyaoka, K., and Takahashi, K. (2015). The JRA-55 reanalysis: general specifica- tions and basic characteristics, *Journal of the Meteorological Society of Japan*, 93, 5–48, https://doi.org/10.2151/jmsj.2015-001.

Gelaro, R., McCarty, W., Suárez, M.J., Todling, R., Molod, A., Takacs, L., Randles, C.A., Darmenov, A., Bosilovich, M.G., Reichle, R., Wargan, K., Coy, L., Cullather, R., Draper, C., Akella, S., Buchard, V., Conaty, A., da Silva, A.M. , Gu, W. , Kim, G. , Koster, R. ,Lucchesi, R., Merkova, D., Nielsen, J.E. , Partyka, G., Pawson, S., Putman, W., Rienecker, M., Schubert, S. D., Sienkiewicz, M., and Zhao, B. (2017).The Modern-Era Retrospective Analysis for Research and Applications, Version 2 (MERRA-2). *Journal of Climate*, 30, 5419–5454, doi:10.1175/JCLI-D-16-0758.1

Molod, A., Takacs, L., Suarez, M., and Bacmeister, J. (2015). Development of the GEOS-5 atmospheric general circulation model: Evolution from MERRA to MERRA2. *Geoscientific Model Development*, 8, 1339–1356, doi:10.5194/gmd-8-1339-2015.

Rienecker, M. M., Suarez, M. J., Gelaro, R., Todling, R., Bacmeis- ter, J., Liu, E., Bosilovich, M. G., Schubert, S. D., Takacs, L., Kim, G.-K., Bloom, S., Chen, J., Collins, D., Conaty, A., da Silva, A., Gu, W., Joiner, J., Koster, R. D., Lucchesi, R., Molod, A., Owens, T., Pawson, S., Pegion, P., Redder, C. R., Reichle, R., Robertson, F. R., Ruddick, A. G., Sienkiewicz, M., and Woollen, J.(2011). MERRA: NASA's Modern-Era Retrospective Analysis for Research and Applications, *Journal of Climate*, 24, 3624–3648, https://doi.org/10.1175/JCLI-D-11-00015.1.

Kalnay, E., Kanamitsu, M., Kistler, R., Collins, W., Deaven, D., Gandin, L., Iredell, M., Saha, S., White, G., and Woollen, J. (1996). The NCEP/NCAR 40-year reanalysis project, *Bulletin of the American Meteorological Society*, 77, 437–471, *https://doi.org/10.1175/1520-0477(1996)077<0437:TNYRP>2.0.CO;2*

Kanamitsu, M., Ebisuzaki, W., Woollen, J., Yang, S.-K., Hnilo, J. J., Fiorino, M., and Potter, G. L. (2002). NCEP–DOE AMIP- II Reanalysis (R-2), *Bulletin of the American Meteorological Society*, 83, 1631–1643, https://doi.org/10.1175/BAMS-83-11-1631.

Haylock, M.R., Hofstra, N., Klein Tank, A.M.G., Klok, E.J., Jones, P.D., New, M.. (2008). A European daily high-resolution gridded dataset of surface temperature and precipitation. *Journal of Geophysical Research (Atmospheres)*, 113, D20119, doi:10.1029/2008JD1020.

Van der Linden, P. and Mitchell, J.F.B. (2009). *ENSEMBLES: Climate Change and Its Impact: Summary of Research and the Results from the ENSEMBLES Project*. Met Office Hadley Centre, Exeter.

Müller, R., Pfeifroth, U., Träger-Chatterjee, C., Cremer, R., Trentmann, J., Hollmann, R. (2015). *Surface solar radiation data set – Heliosat (SARAH) – Edition 1. Satellite Application Facility on Climate Monitoring (CM SAF)*, doi:10.3390/rs71114445.

Pfeifroth, U., Kothe, S., Müller, R., Trentmann, J., Hollmann, R., Fuchs, P., Werscheck, M. (2017). *Surface Radiation Data Set – Heliosat (SARAH) – Edition 2. Satellite Application Facility on Climate Monitoring (CM SAF)*. doi: 10.5676/EUM_SAF_CM/SARAH/V002

McGinnis S. A., Mearns, L.O. and McDaniel L. (2010). Effects of Spatial Interpolation Algorithm Choice on Regional Climate Model Data Analysis. *AGU Fall Meeting Abstracts*.

Taylor, K. E. (2001). Summarizing multiple aspects of model performance in a single diagram. *Journal of Geophysical Research*, 106, 7183– 7192.

Thornton H. E., Hoskins, B. J. and Scaife, A. A. (2016). The role of temperature in the variability and extremes of electricity and gas demand in Great Britain. *Environmental Research Letters*, 11 (2016) 114015.

Hahn, H., Meyer-Nieberg, S. and Pickl, S. (2009). Electric load forecasting methods: tools for decision making *European Journal of Operational Research*, 199 902–7.

De Felice M., Alessandri A. and Ruti P. M. (2013). Electricity demand forecasting over Italy: potential benefits using numericalweather prediction models *Electric Power Systems Research*, 104 71–9.

Auger, S.B., Maasch, K. A., Mayewski, P. A., and Schuenemann, K. C. (2018). An Ensemble Mean and Evaluation of Third Generation Global Climate Reanalysis Models. *Atmosphere,* 2018, 9(6), 236; https://doi.org/10.3390/atmos9060236.

Simmons, A. J., Berrisford, P., Dee, D. P., Hersbach, H., Hirahara, S., and Thépaut, J.-N.: A reassessment of temperature vari- ations and trends from global reanalyses and monthly surface climatological datasets, *Quarterly Journal of the Royal Meteorological* Society, 143: 101–119, https://doi.org/10.1002/qj.2949, 2017.

Hartmann, D.L., Klein Tank, A.M.G., Rusticucci, M., Alexander, L.V., Brönnimann, S., Charabi, Y., Dentener, F.J., Dlugokencky, E.J., Easterling, D.R., Kaplan, A., Soden, B.J., Thorne, P.W., Wild, M. and Zhai, P. M. (2013): Observations: Atmosphere and Surface. In: *Climate Change 2013: The Physical Science Basis. Contribution of Working Group I to the Fifth Assessment Report of the Intergovernmental Panel on Climate Change* [Stocker, T.F., Qin, D., Plattner, G.-K., Tignor, M., Allen, S.K., Boschung, J., Nauels, A., Xia, Y., Bex, V. and Midgley, P.M. (eds.)]. Cambridge University Press, Cambridge, United Kingdom and New York, NY, USA.

van der Schrier, G., Barichivich, J., Briffa, K. R. and Jones, P. D. (2013). A scPDSI-based global data set of dry and wet spells for 1901–2009, *Journal of Geophysical Research Atmosphere*, 118, 4025–4048, doi:10.1002/jgrd.50355.

You, Q., Sanchez-Lorenzo, A., Wild, M., Folini, D., Fraedrich, K., Ren, G., Shichang, K. (2013). Decadal variation of surface solar radiation in the Tibetean Plateau from observations, reanalysis and model simulations. *Climate Dynamics*, 40 (7–8), 2073–2086. doi:10.1007/s00382-012-1383-3.

Stanhill, G., & Cohen, S. (2001). Global Dimming: A review of the evidence for a widespread and significant reduction in global radiation with discussion of its probable causes and possible agricultural consequences. *Agricultural and Forest Meteorology*, 107, 255–278. https://doi.org/10.1016/S0168-1923(00)00241-0.

Wild, M., Gilgen, H., Roesch, A., Ohmura, A., Long, C. N., Dutton, E. G., Forgan B., Kallis A., Russak V., Tsvetkov, A. (2005). From dimming to brightening: Decadal changes in solar radiation at Earth's surface. *Science*, *308*, 847–850. https://doi.org/10.1126/science.1103215.

Lohmann, U., and Feichter, J. (2005). Global indirect aero- sol effects: A review. *Atmospheric Chemistry and Physics*, 5, 715–737.

Rosenfeld D., Lohmann U., Raga G.B., O'Dowd C.D., Kulmala M., Fuzzi S., Reissell A., Andreae M.O. (2008). Flood or drought: How do aerosols affect precipitation? *Science,* **321,** 1309–1313.

Wild, M. (2012). Enlightening global dimming and brightening. *Bulletin of the American Meteorological Society*, 93(1), 27–37. https://doi.org/10.1175/BAMS-D-11-00074.1

Urraca R., Huld, T., Gracia-Amillo, A., Martinez-de-Pison, F.J., Kaspar, F., Sanz-Garcia, A. (2018). Evaluation of global horizontal irradiance estimates from ERA5 and COSMO-REA6 reanalyses using ground and satellite-based data. *Solar Energy*, 164 (2018) 339-354.

Pfeifroth, U., Sanchez-Lorenzo, A., Manara, V., Trentmann, J., & Hollmann R. (2018). Trends and variability of surface solar radiation in Europe based on surface- and satellite-based data records. *Journal of Geophysical Research: Atmospheres*, 123, 1735–1754. https://doi.org/10.1002/2017JD027418.

Ramon J.,Lledò L, Torralba V., Soret A.,Doblas-Rees FJ. What global reanalysis best represents near-surface winds?. Q J R Meteorol. –soc. 2019;1-16. https://doi.org/10.1002/qj.3616

Torralba, V., F. J. Doblas-Reyes, and Gonzalez-Reviriego, N. (2017). Uncertainty in recent near-surface wind speed trends: a global reanalysis intercomparison. *Environmental Research Letters*, 12, 114019, doi:10.1088/1748-9326/aa8a58.

Vautard, R., Cattiaux, J., Yiou, P., Thépaut, J. N. and Ciais, P. (2010). Northern Hemisphere atmospheric stilling partly attributed to an increase in surface roughness. *Nature Geoscience*, 3, 756–761, doi:10.1038/ngeo979. http://dx.doi.org/10.1038/ngeo979.

Bichet, A., Wild, M., Folini, D., Schar, C. (2012). Causes for decadal variations of wind speed over land: sensitivity studies with a global climate model. *Geophysical Research Letters*, 39(11) L11701, doi:10.1029/2012GL051685.

Fujiwara, M., Wright, J. S., Manney, G. L., Gray, L. J., Anstey, J., Birner, T., Davis, S., Gerber, E. P., Harvey, V. L., Hegglin, M. I., Homeyer, C. R., Knox, J. A., Kruger, K., Lambert, A., Long, C. S., Martineau, P., Molod, A., Monge-Sanz, B. M., San- tee, M. L., Tegtmeier, S., Chabrillat, S., Tan, D. G. H., Jack- son, D. R., Polavarapu, S., Compo, G. P., Dragani, R., Ebisuzaki, W., Harada, Y., Kobayashi, C., McCarty, W., Onogi, K., Paw- son, S., Simmons, A., Wargan, K., Whitaker, J. S., and Zou, C.-Z. (2017). Introduction to the SPARC reanalysis intercomparison project (S-RIP) and overview of the reanalysis systems, *Atmospheric Chemistry and Physics*, 17, 1417–1452, https://doi.org/10.5194/acp- 17-1417-2017.

Thorne, P.W. and Vose, R.S. (2010). Reanalyses Suitable for Characterizing Long-Term Trends. *Bulletin of the American Meteorological Society*, 91, 353–362, doi:10.1175/2009BAMS2858.1.

L'Heureux, M. L., Lee, S., and Lyon, B. (2013). Recent multidecadal strengthening of the Walker circulation across the tropical Pacific. *Nature Climate Change*, 3, 571–576, doi:10.1038/nclimate1840.

England, M. H., McGregor, S., Spence, P., Meehl, G., Timmerman, A., Cai, W., Sen Gupta, A., McPhaden, M., Purich, A., Santoso, A. (2014). Recent intensification of wind-driven circulation in the Pacific and the ongoing warming hiatus. *Nature Climate Change*, 4, 222–227, doi:10.1038/nclimate2106.

Jolliffe, I. T., and Stephenson, D. B. (editors). (2003). *Forecast Verification: A Practitioner's Guide in Atmospheric Science, 2nd edition*. Wiley-Blackwell. ISBN: 978-0-470-66071-3.

Lehner, B., Czisch, G., Vassolo, S. (2005). The impact of global change on the hydropower potential of Europe: a model-based analysis. *Energy Policy* 33:839–855.

Huffman G. J., Adler, R. F., Bolvin, D. T. and Gu, G. (2009). Improving the global precipitation record: GPCP version 2.1. *Geophysical Research Letters*, 36, L17808, doi:10.1029/2009GL040000.

Xie, P., and Arkin, P.A. (1997). Global precipitation: A 17-year monthly analysis based on gauge observations, satellite estimates, and numerical model outputs. *Bulletin of the American Meteorological Society*, 78, 2539–2558, doi:10.1175/1520-0477(1997)078,2539: GPAYMA.2.0.CO;2.

Roads, J. (2003). The NCEP/NCAR, NCEP/DOE and TRMM tropical atmosphere hydrologic cycles, *Journal of Hydrometeorology*, 4, 826–840.

Bosilovich, M. G., Robertson, F. R. and Chen, J. (2011): Global energy and water budgets in MERRA. *Journal of Climate*, 24, 5721-5739.

Trenberth, K. E., Fasullo, J. T. and Mackaro, J. (2011). Atmospheric moisture transports from ocean to land and global energy ows in reanalyses. *Journal of Climate*, 24, 4907– 4924.

Gu, G., Adler, R. F., Huffman, G. and Curtis, S. (2007). Tropical rainfall variability on interannual-to-interdecadal/longer-time scales derived from the GPCP monthly product. *Journal of Climate*, 20, 4033–4046.

Wentz, F. J., Ricciardulli, L., Hilburn, K. and Mears, C. (2007). How much more rain will global warming bring? *Science*, **317**, 233–235.

ANNEX A- Supplementary Figures

This supplement contains:

- Figures in support to the section "1.3 Regridding methodologies": S1, S2
- Figures to support the discussion of the ECVs verification in the document. S3-S23

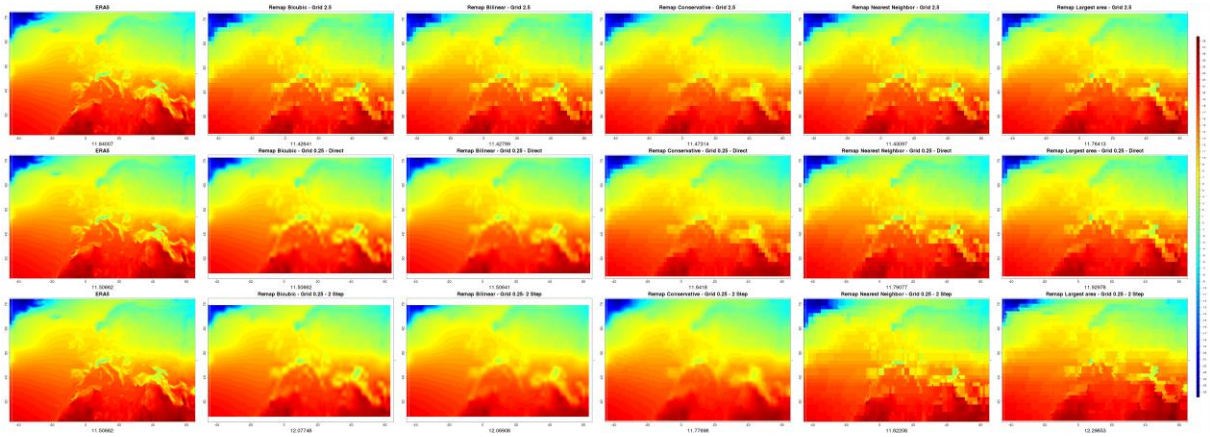

Figure S1: The figure shows the doubleback interpolation for the 2.5°grid. All fields are averaged over the period. First column is the original ERA5 field, the four others are for the different remapping methods. First line is the direct remapping on the targeted grid. The second line is the direct "backwards" interpolation to the original grid, and the third one is again the backwards interpolation but with 2 steps (single and three steps not shown because not significantly different).

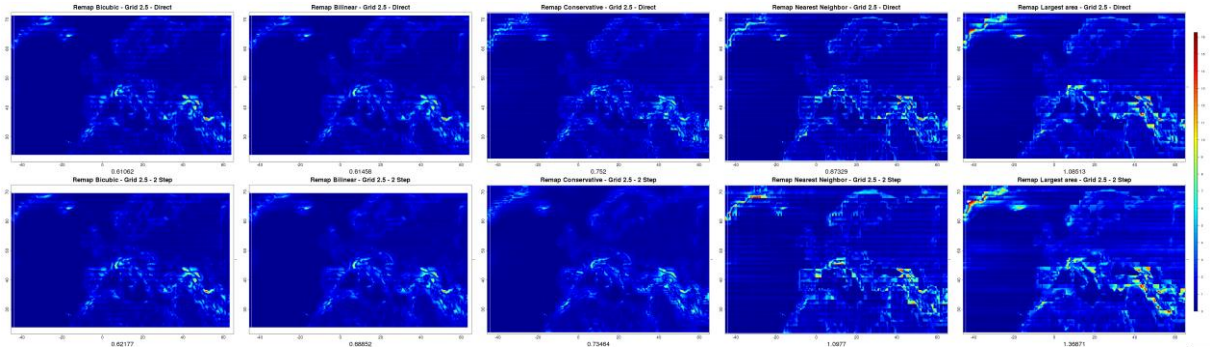

Figure S2: The figure shows the error fields from doubleback interpolation for the 2.5° grid. All fields are averaged over the period. Columns are the interpolation methods and lines the direct and two step approach (single and three steps not shown because not significantly different).

Temperature

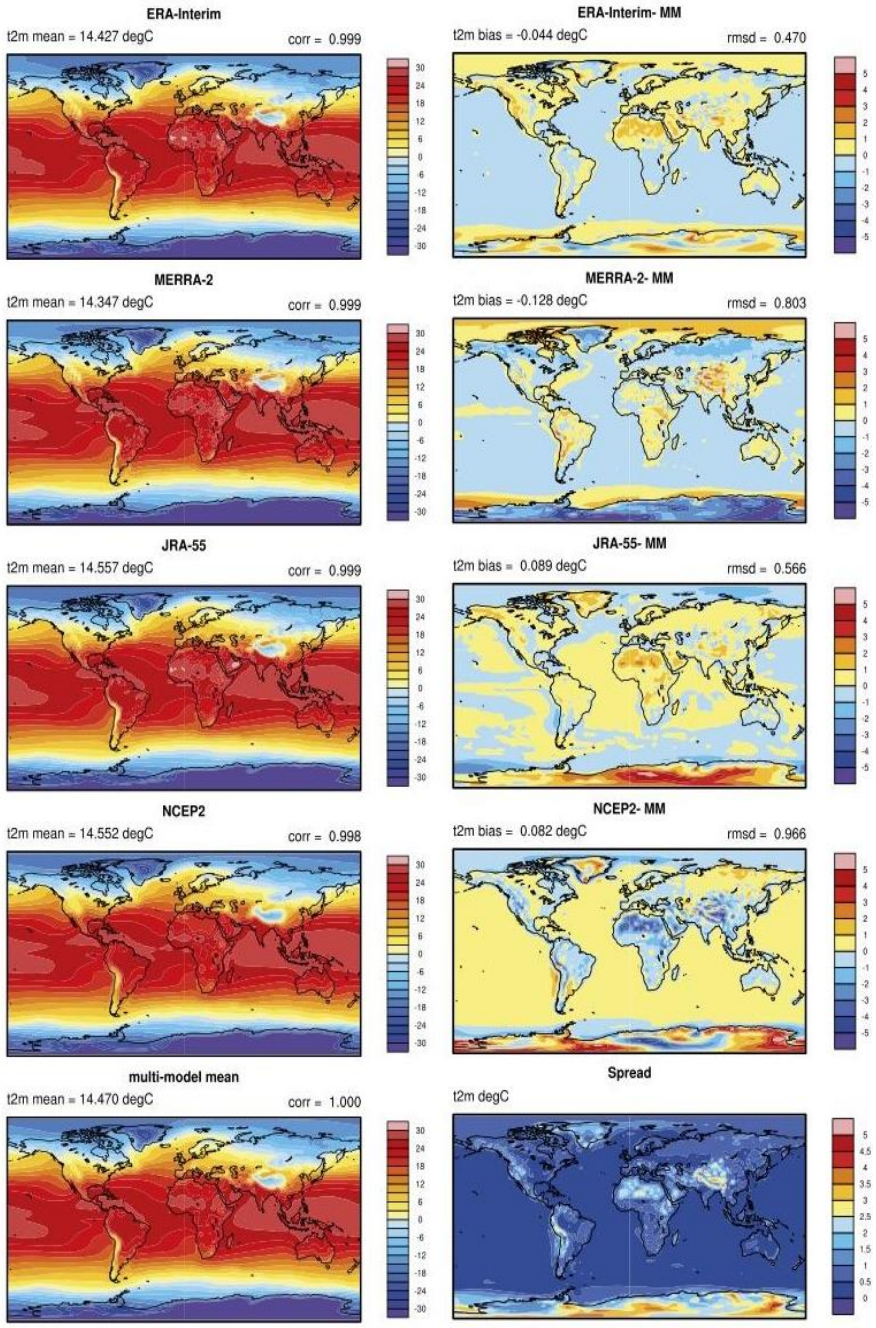

Figure S3: Climatological Mean 1980-2017 (Left) of 2 m temperature in ERA-Interim, MERRA-2, JRA-55, NCEP2 and ensemble multi reanalysis mean. Differences (Right) between ERA-Interim, MERRA-2, JRA-55, NCEP/DOE R2 and multi reanalysis mean. (Bottom) Multi reanalysis spread.

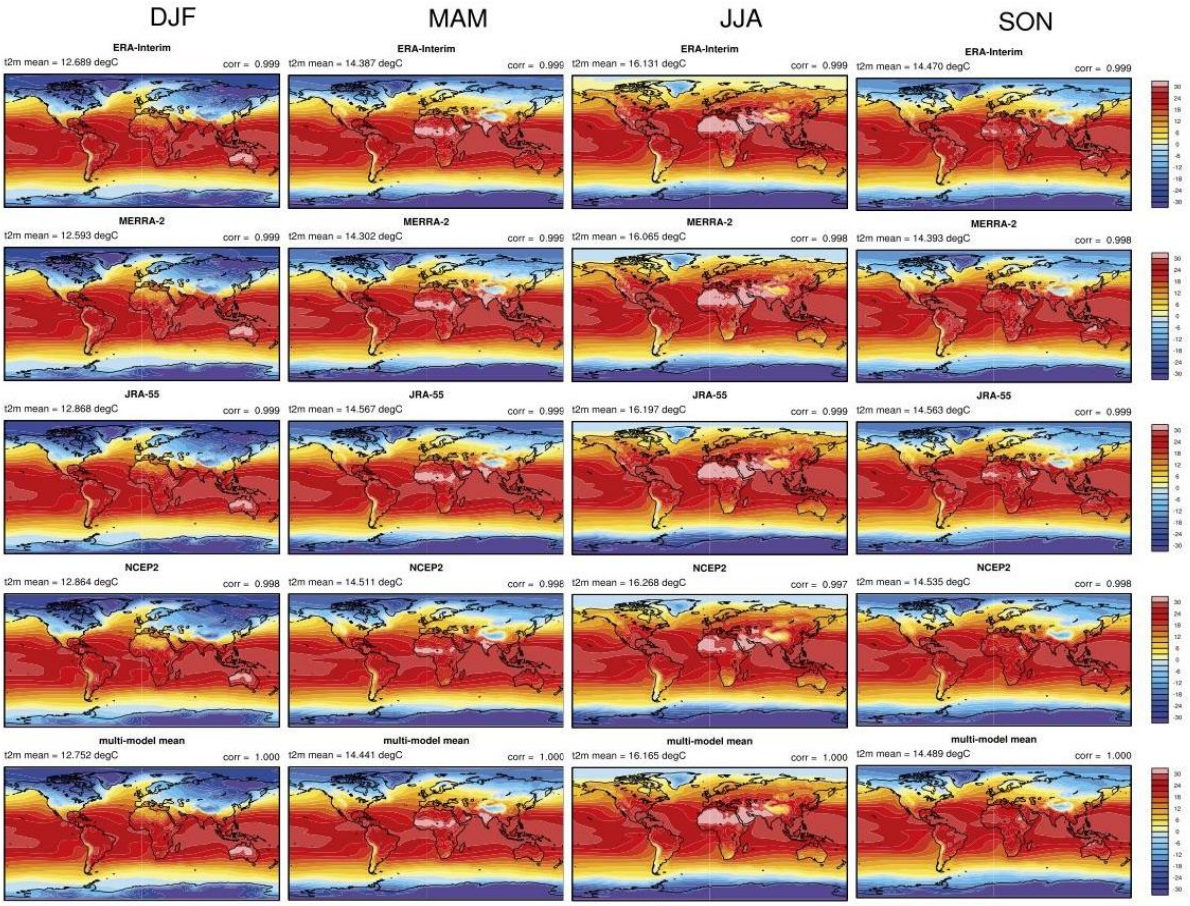

Figure S4: Seasonal (DJF, MAM, JJA, SON) climatological mean 1980-2017 of 2 m temperature of ERA-Interim, MERRA-2, JRA-55, NCEP/DOE R2 and multi reanalysis mean.

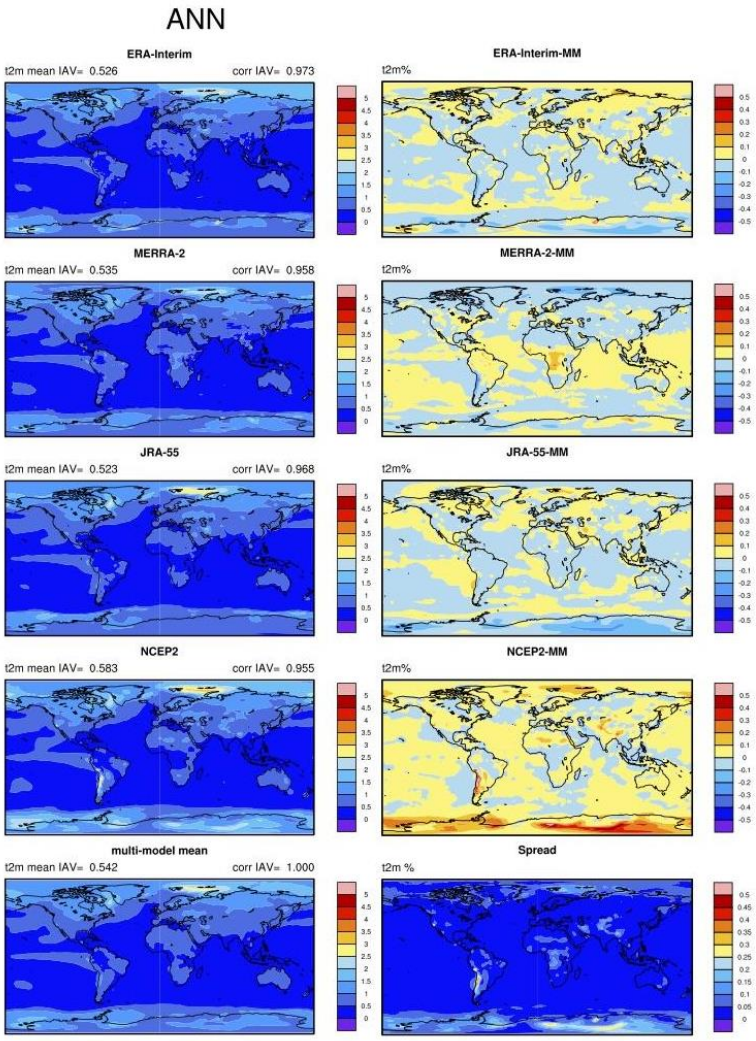

Figure S5: Interannual variability 1980-2017 (Left) of annual 2 m temperature in ERA-Interim, MERRA-2, JRA-55, NCEP2 and ensemble multi reanalysis mean. Differences (Right) between normalized interannual variability of ERA-Interim, MERRA-2, JRA-55, NCEP/DOE R2 and multi reanalysis mean. (Bottom) Multi reanalysis spread interannual variability.

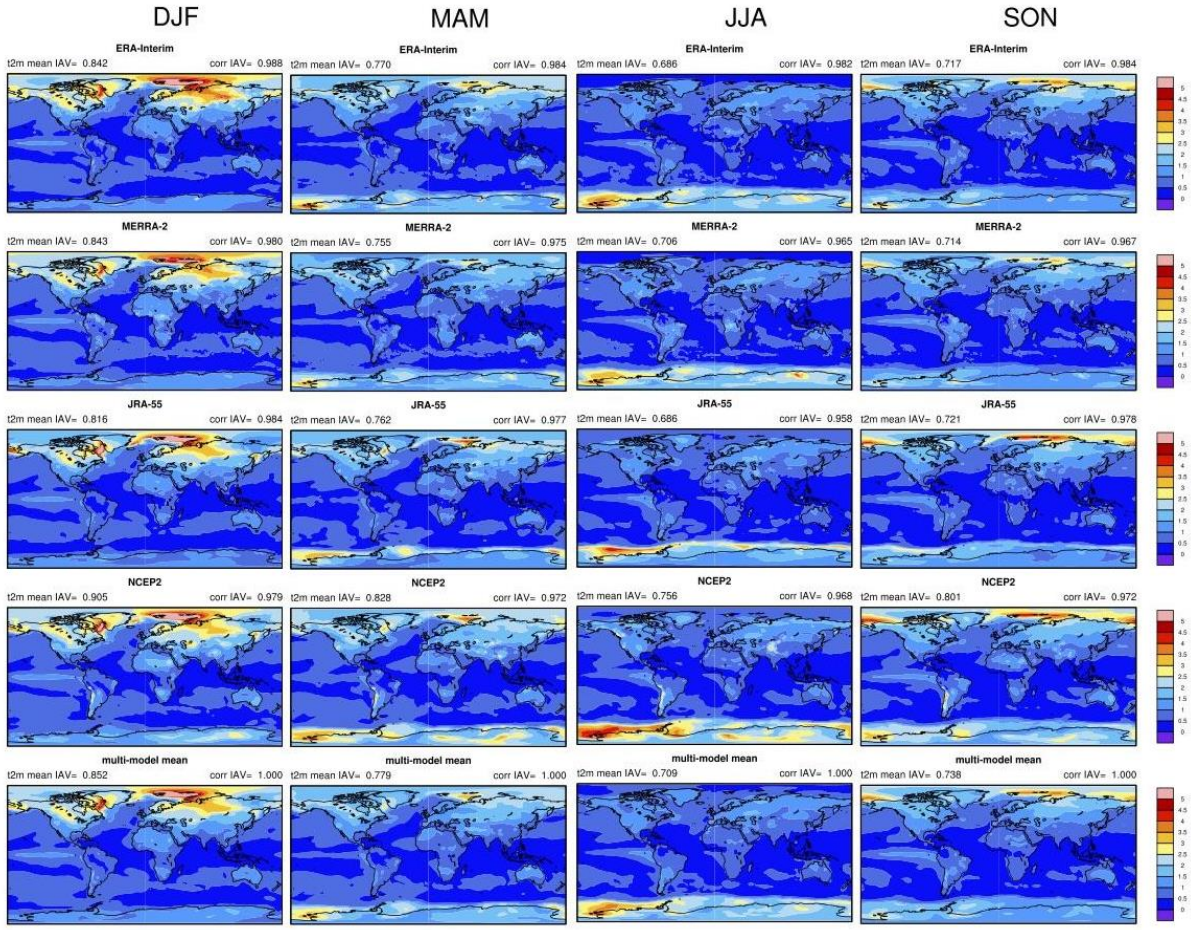

Figure S6: Interannual variability 1980-2017 of seasonal 2 m temperature in ERA-Interim, MERRA-2, JRA-55, NCEP/DOE R2 and ensemble multi reanalysis mean.

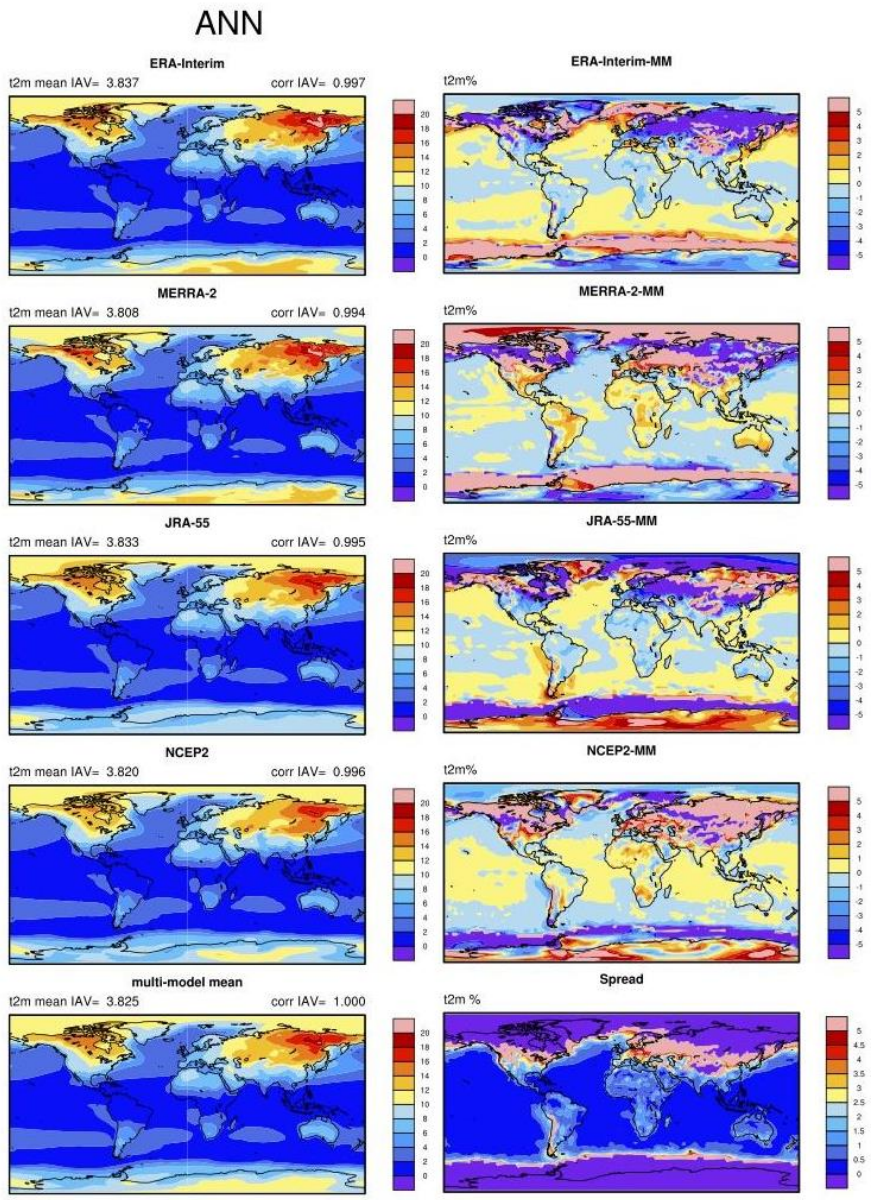

Figure S7: Intra-annual variability 1980-2017 (Left) of monthly 2 m temperature in ERA-Interim, MERRA-2, JRA-55, NCEP2 and ensemble multi reanalysis mean. Differences (Right) between normalized intra-annual variability of ERA-Interim, MERRA-2, JRA-55, NCEP/DOE R2 and multi reanalysis mean. (Bottom) Multi reanalysis spread of intra-annual variability.

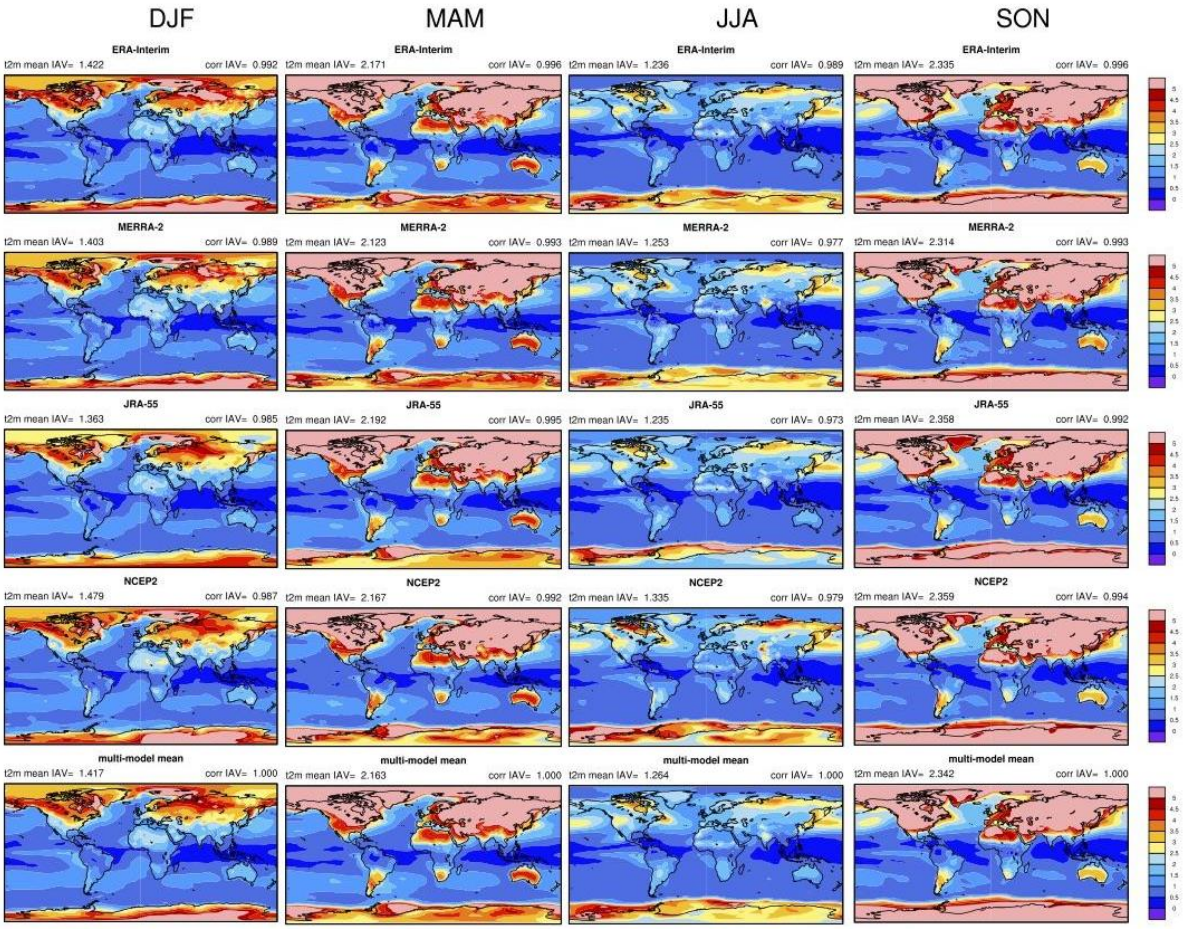

Figure S8: Intraseasonal variability 1980-2017 of monthly 2 m temperature in ERA-Interim, MERRA-2, JRA-55, NCEP/DOE R2 and ensemble multi reanalysis mean.

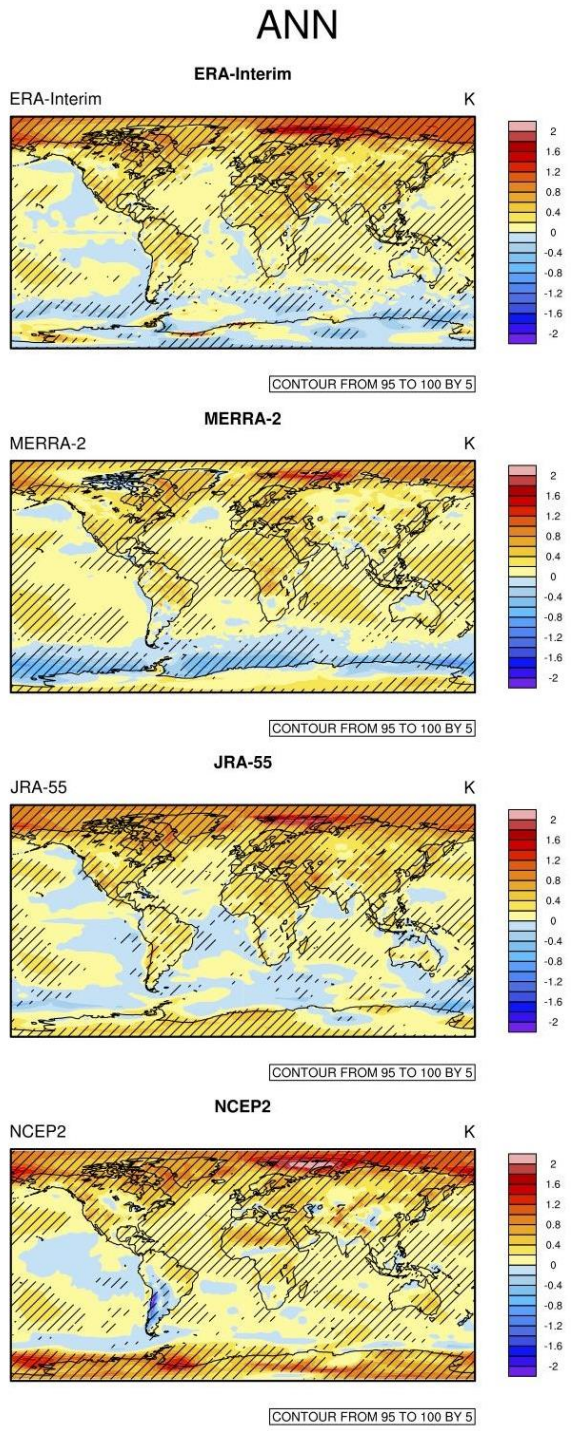

Figure S9: Trend 1980-2017 of 2 meters temperature in ERA-Interim, MERRA-2, JRA-55, NCEP/DOE R2.

Solar Radiation

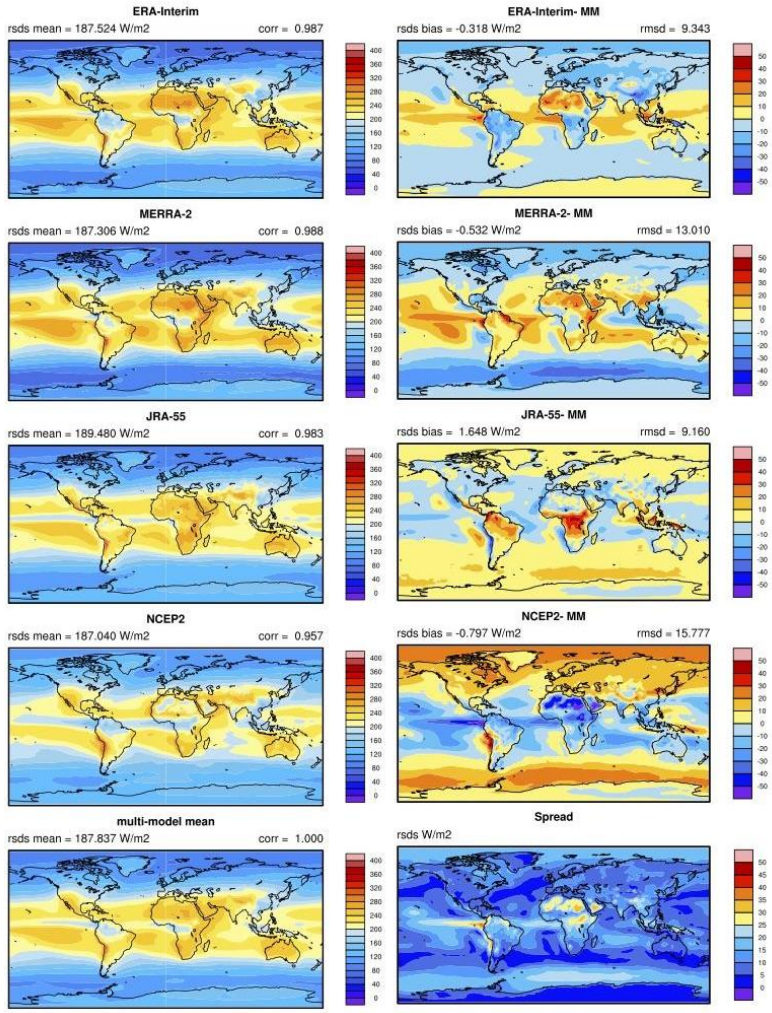

Figure S10: Climatological Mean 1980-2017 (Left) of solar radiation in ERA-Interim, MERRA-2, JRA-55, NCEP2 and ensemble multi reanalysis mean. Differences (Right) between ERA-Interim, MERRA-2, JRA-55, NCEP2 and multi reanalysis mean. (Bottom) Multi reanalysis spread.

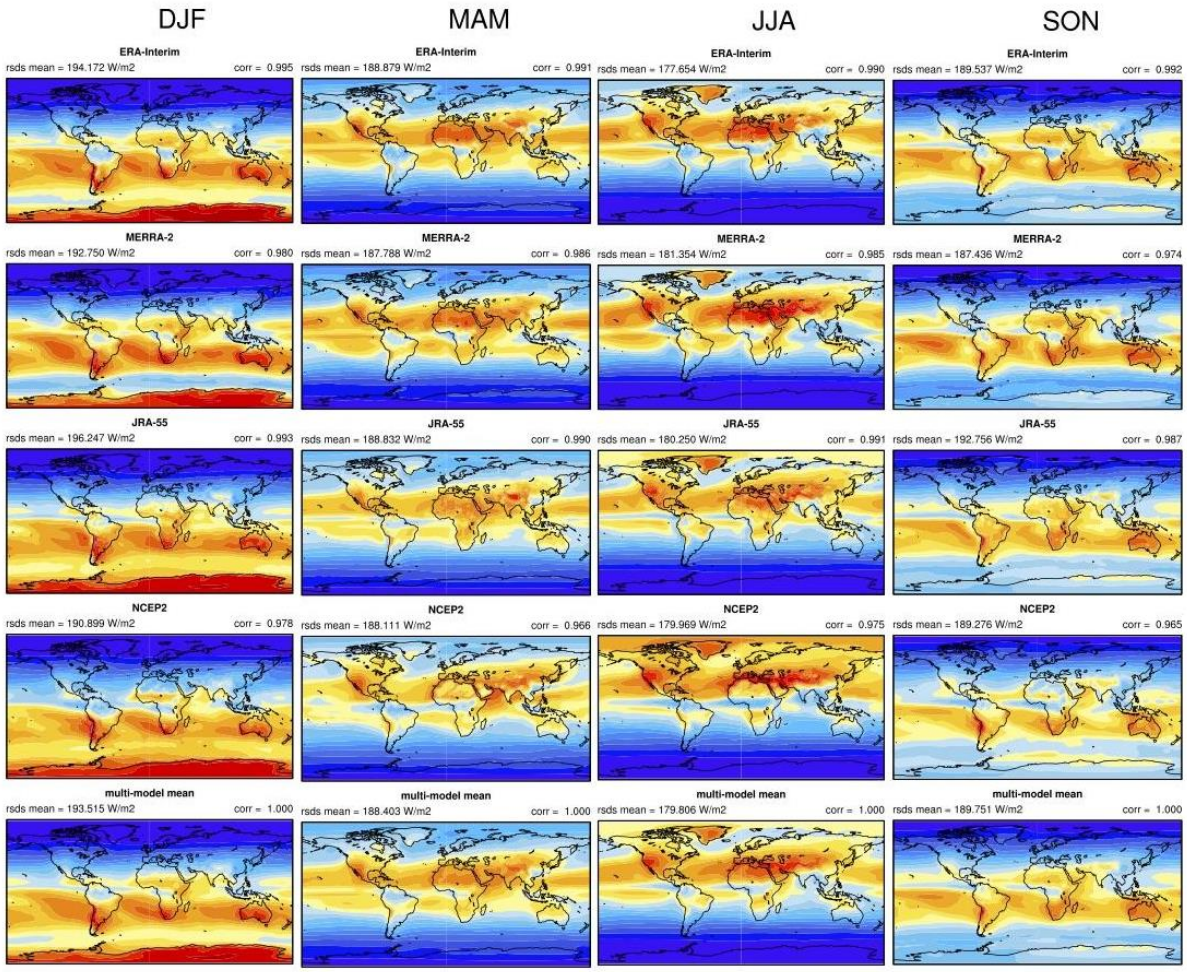

Figure S11: Seasonal (DJF, MAM, JJA, SON) climatological mean 1980-2017 of solar radiation in ERA-Interim, MERRA-2, JRA-55, NCEP/DOE R2 and multi reanalysis mean.

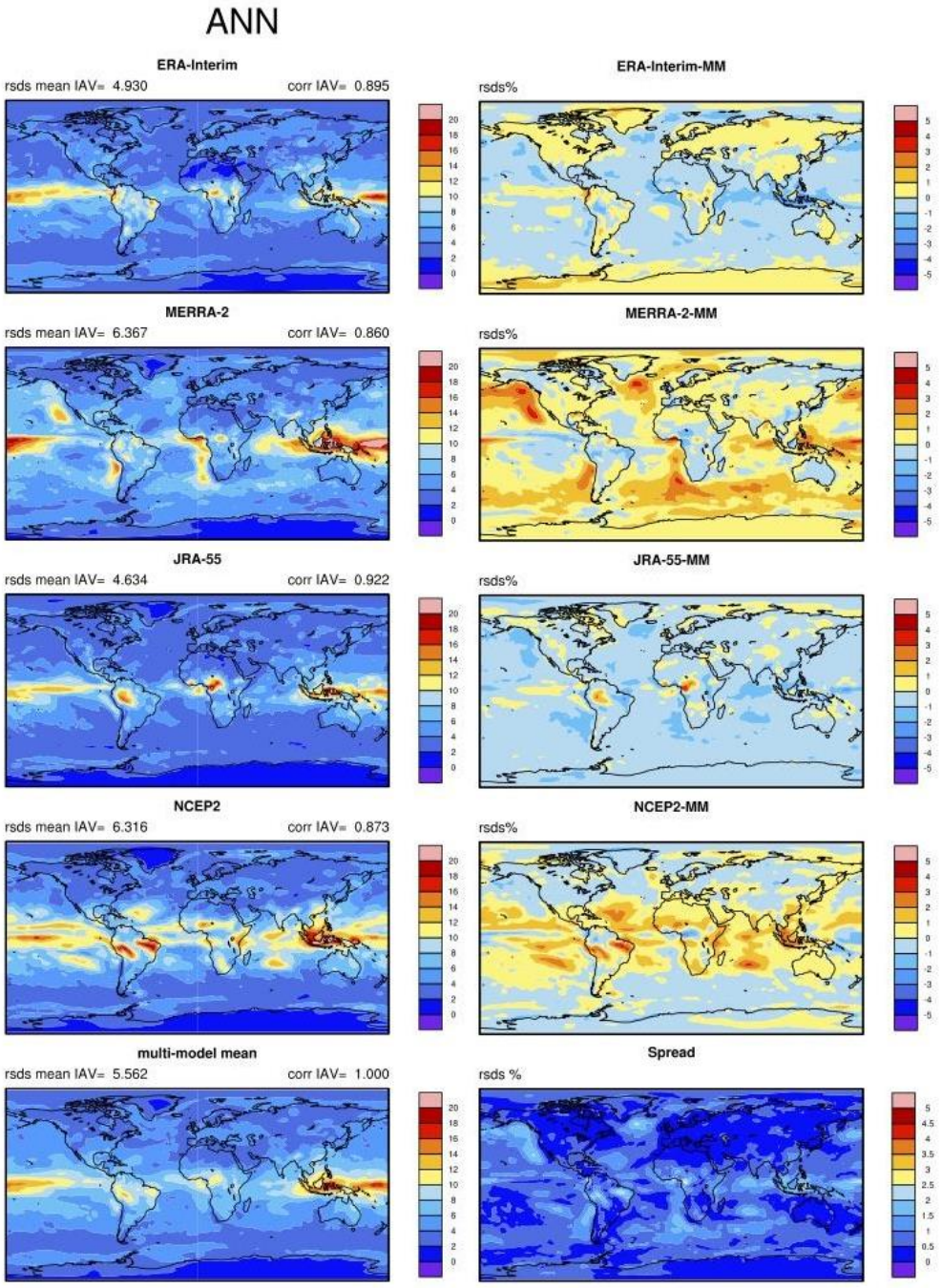

Figure S12: Interannual variability 1980-2017 (Left) of annual solar radiation in ERA-Interim, MERRA-2, JRA-55, NCEP/DOE R2 and ensemble multi reanalysis mean. Differences (Right) of normalized intreranual variability between ERA-Interim, MERRA-2, JRA-55, NCEP/DOE R2 and multi reanalysis mean. (Bottom) Multi reanalysis spread of interannual variability.

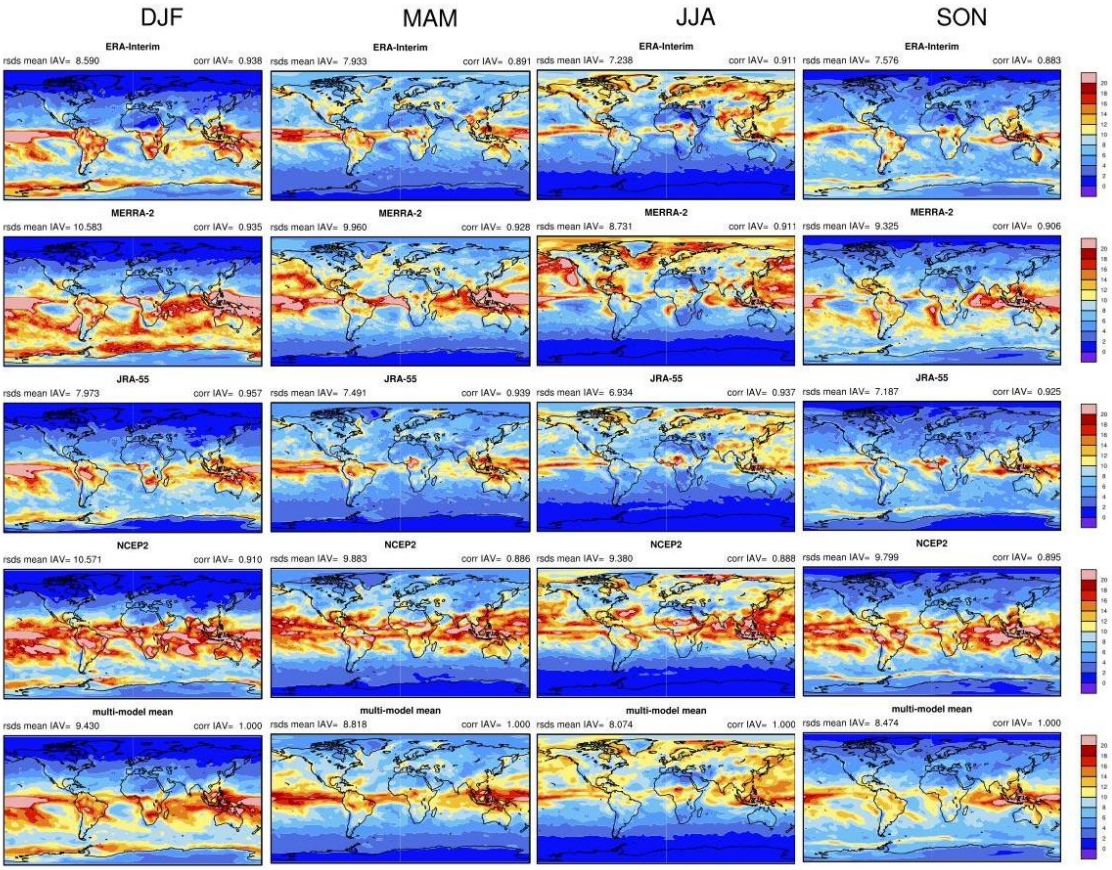

Figure S13: Interannual variability 1980-2017 of seasonal solar radiation in ERA-Interim, MERRA-2, JRA-55, NCEP/DOE R2 and ensemble multi reanalysis mean.

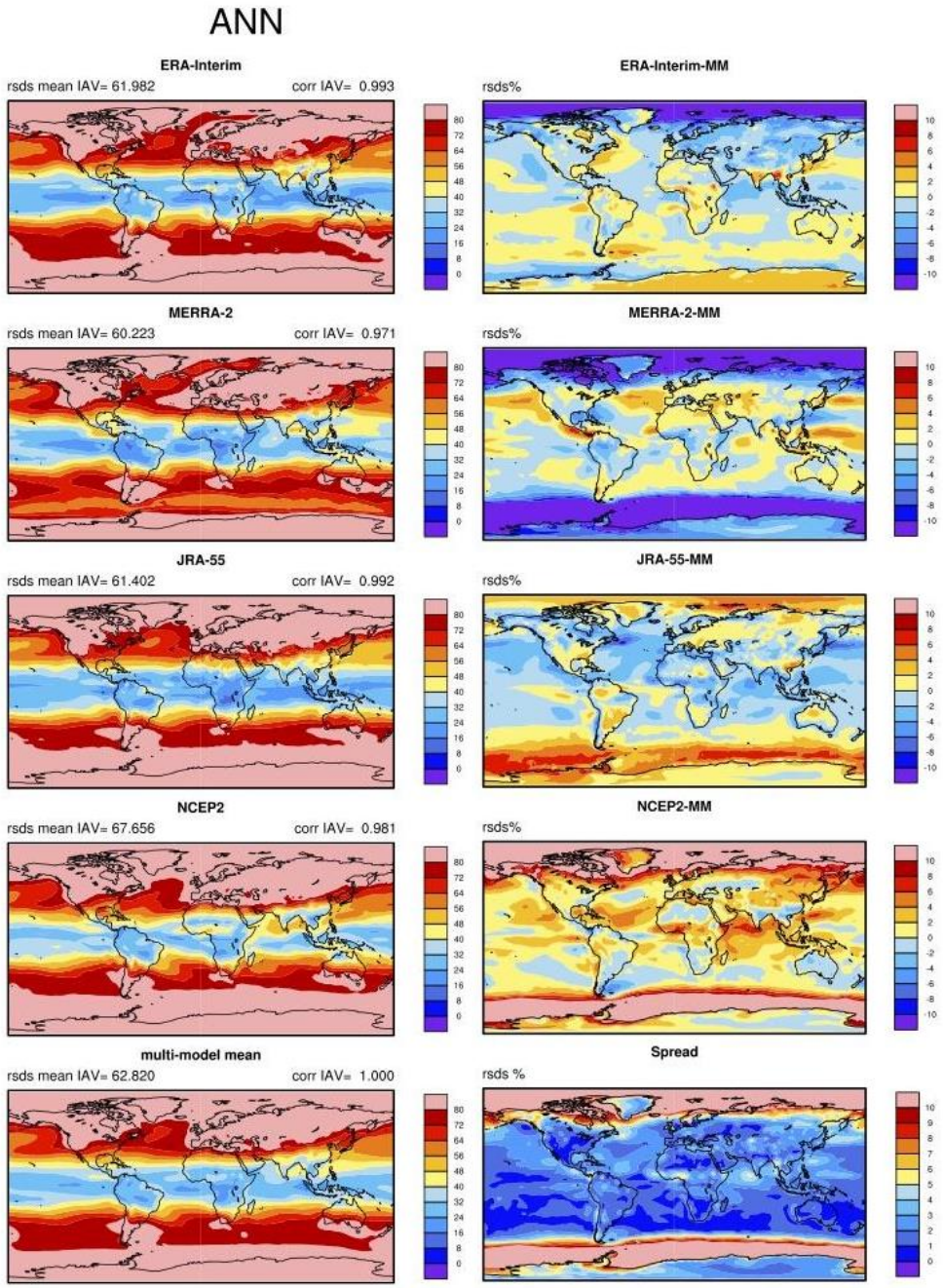

Figure S14: Intra-annual variability 1980-2017 (Left) of monthly solar radiation in ERA-Interim, MERRA-2, JRA-55, NCEP2 and ensemble multi reanalysis mean. Differences (Right) between normalized intra-annual variability ERA-Interim, MERRA-2, JRA-55, NCEP/DOE R2 and multi reanalysis ensemble. (Bottom) Multi reanalysis spread of intra-annual variability.

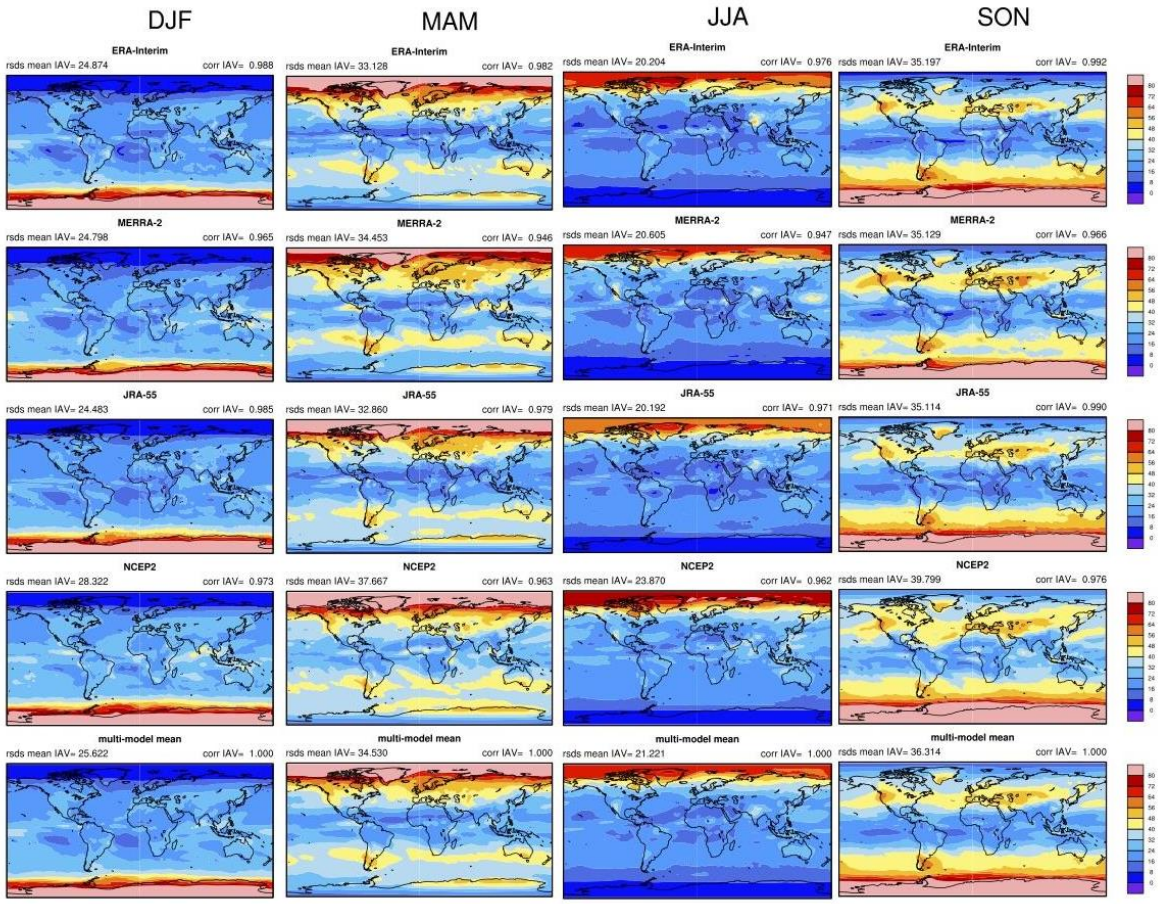

Figure S15: Intraseasonal variability 1980-2017 of monthly solar radiation in ERA-Interim, MERRA-2, JRA-55, NCEP/DOE R2 and ensemble multi reanalysis mean.

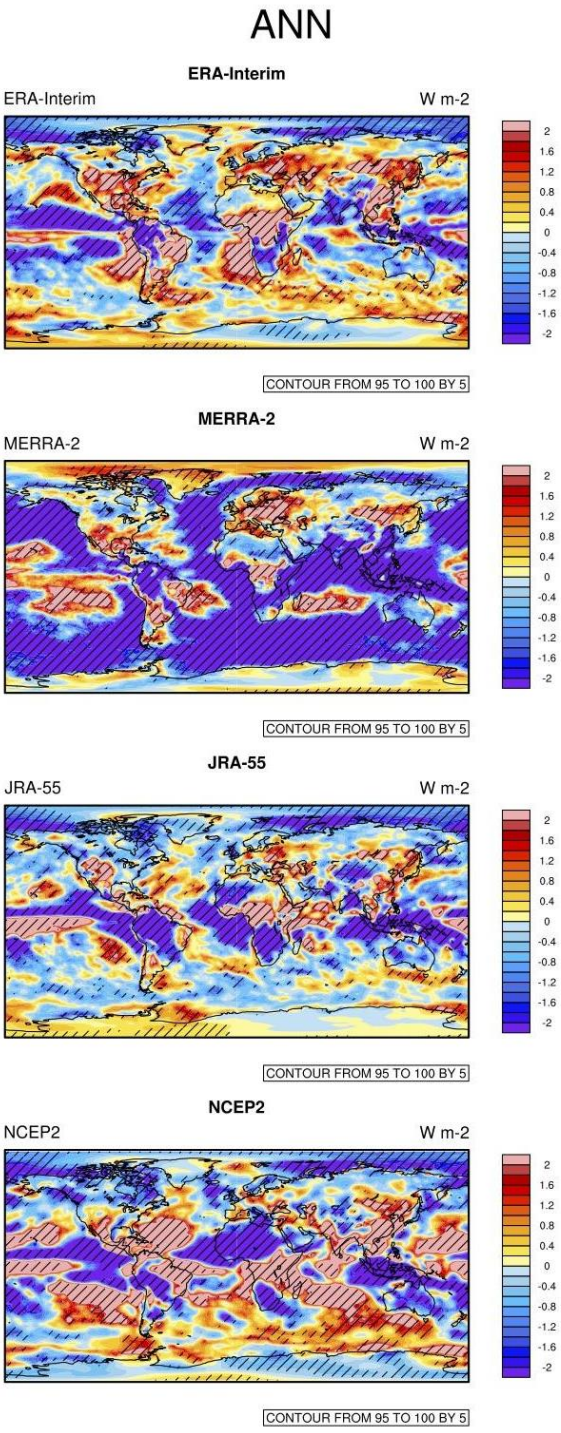

Figure S16: Annual trend 1980-2017 of solar radiation in ERA-Interim, MERRA-2, JRA-55, NCEP/DOE R2.

Precipitation

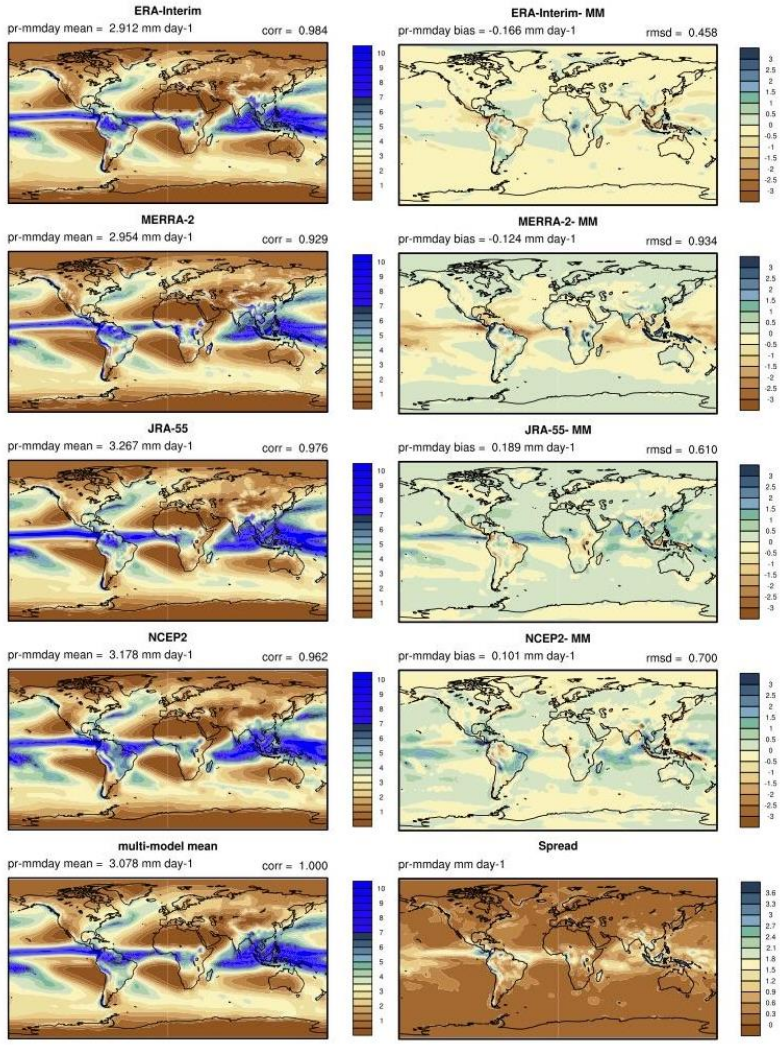

Figure S17: Climatological Mean 1980-2017 (Left) of precipitation in ERA-Interim, MERRA-2, JRA-55, NCEP/DOE R2 and ensemble multi reanalysis mean. Differences (Right) between ERA-Interim, MERRA-2, JRA-55, NCEP/DOE R2 and multi reanalysis mean. (Bottom) Multi reanalysis spread.

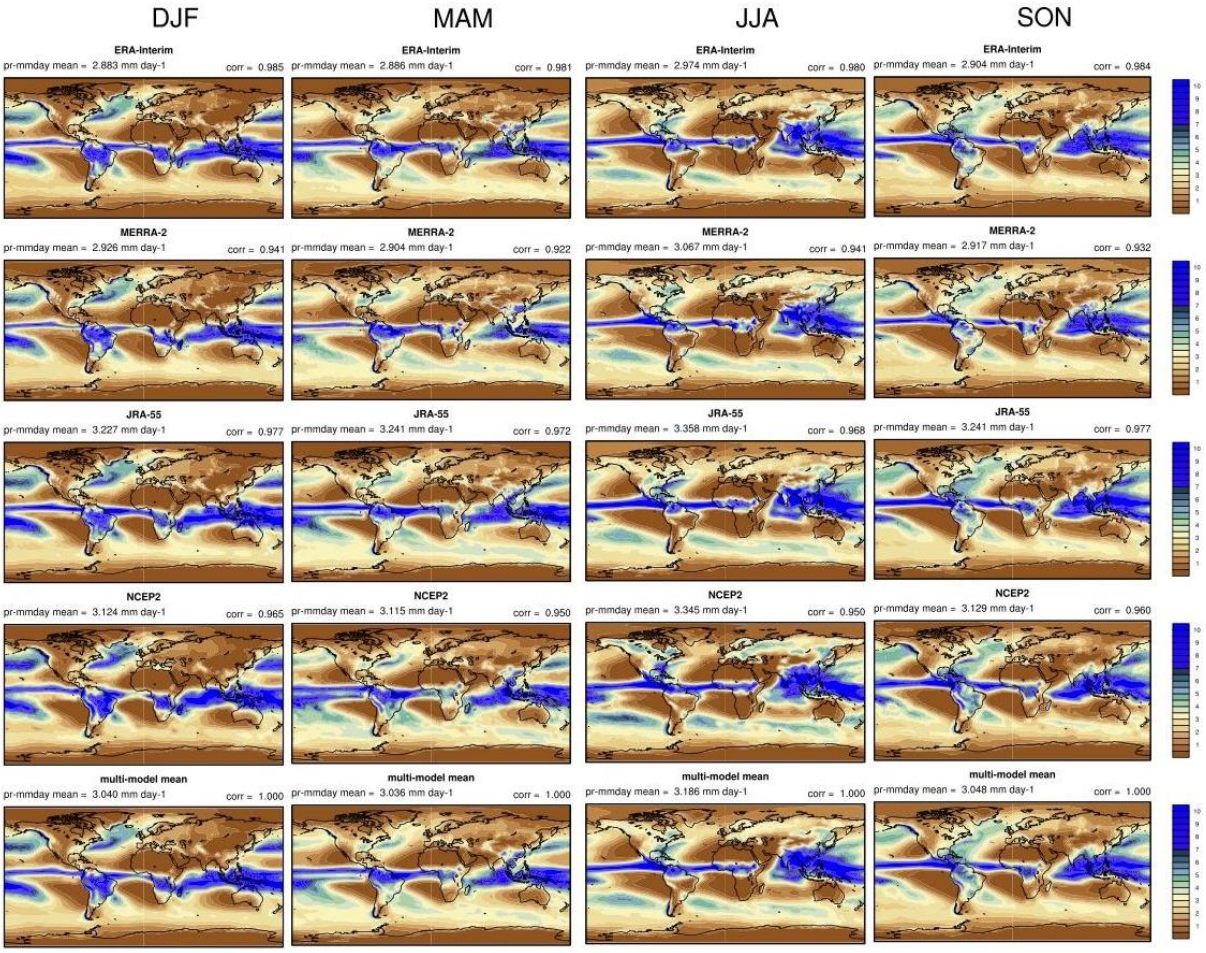

Figure S18: Seasonal (DJF, MAM, JJA, SON) climatological mean of precipitation 1980-2017 ERA-Interim, MERRA-2, JRA-55, NCEP/DOE R2 and multi reanalysis mean.

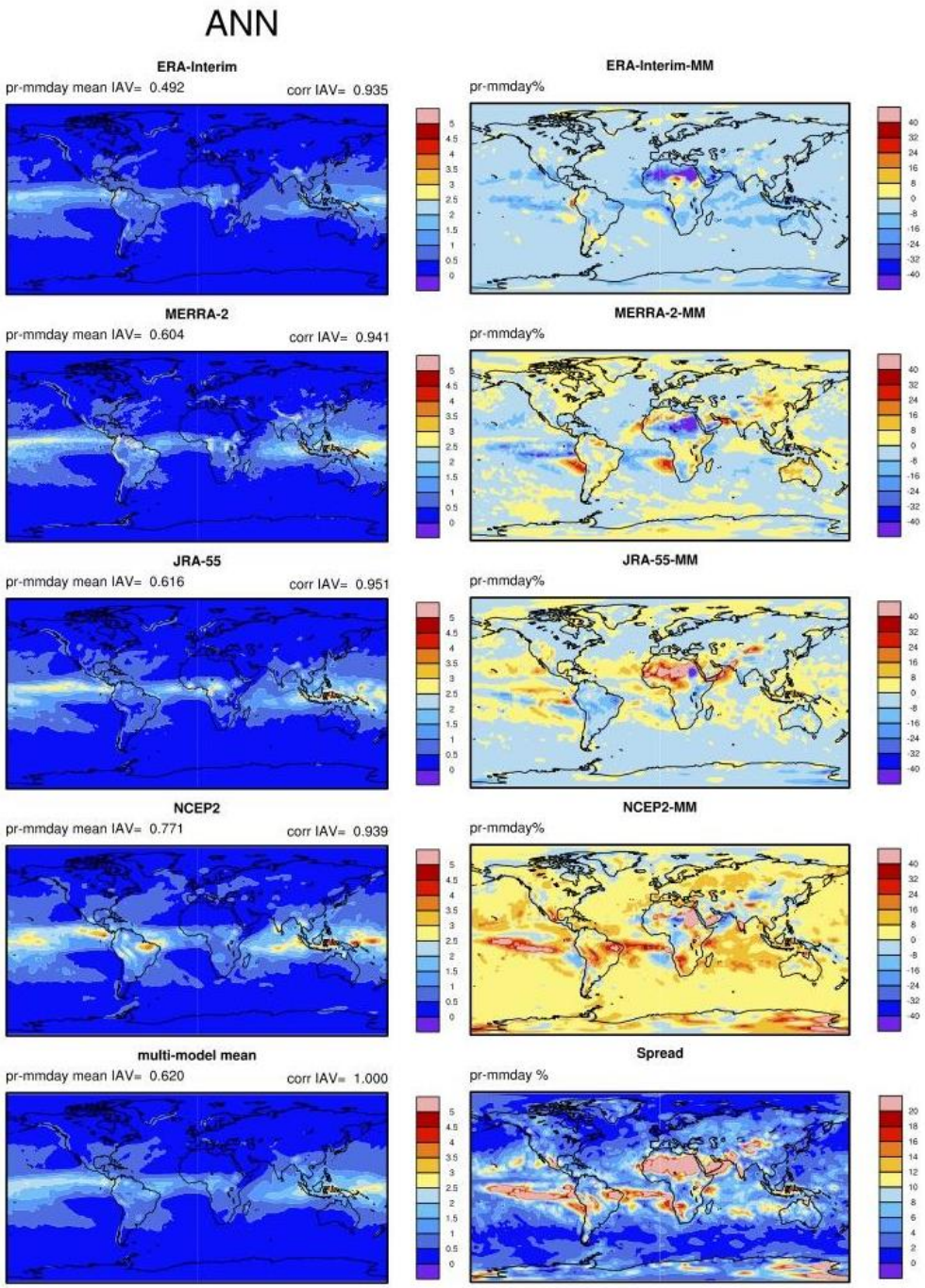

Figure S19: Interannual variability 1980-2017 (Left) of annual precipitation in ERA-Interim, MERRA-2, JRA-55, NCEP/DOE R2 and ensemble multi reanalysis mean. Differences (Right) between normalized interannual variability of ERA-Interim, MERRA-2, JRA-55, NCEP/DOE R2 and multi reanalysis mean. (Bottom) Multi reanalysis spread of interannual variability.

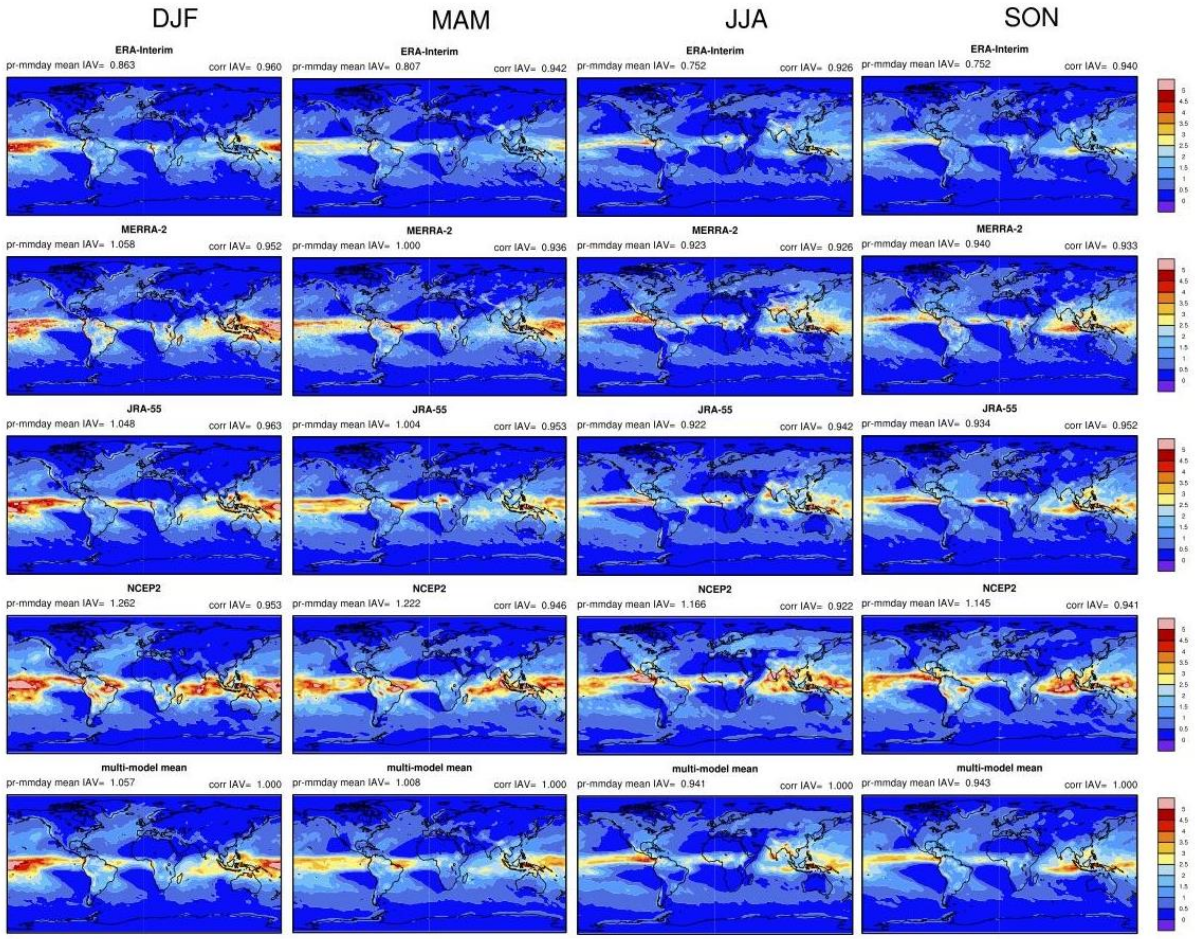

Figure S20: Interannual variability 1980-2017 of seasonal precipitation in ERA-Interim, MERRA-2, JRA-55, NCEP/DOE R2 and ensemble multi reanalysis mean.

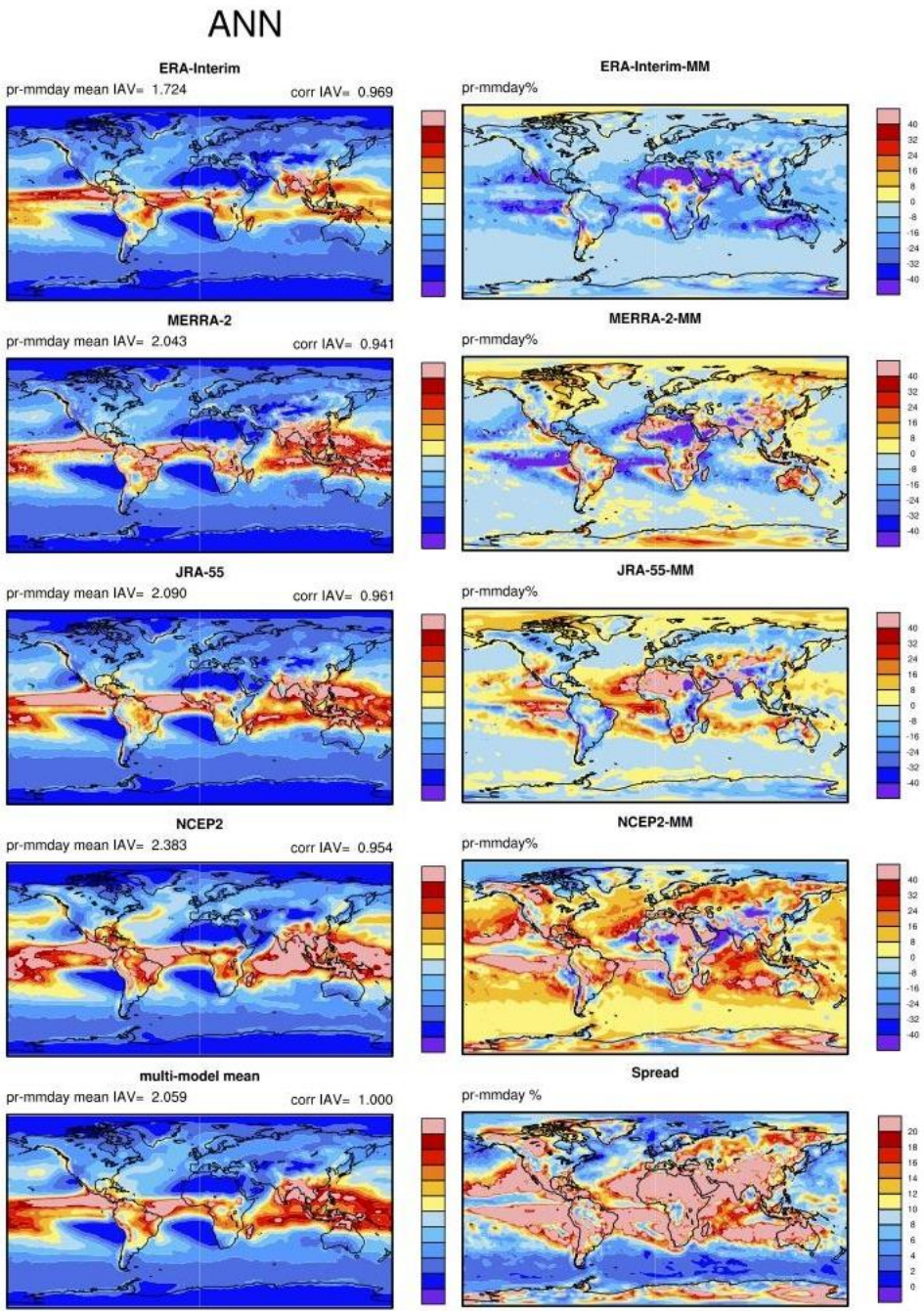

Figure S21: Intra-annual variability 1980-2017 (Left) of monthly precipitation in ERA-Interim, MERRA-2, JRA-55, NCEP/DOE R2 and ensemble multi reanalysis mean. Differences (Right) of normalized intra-annual variabiity between ERA-Interim, MERRA-2, JRA-55, NCEP/DOE R2 and multi reanalysis mean. (Bottom) Multi reanalysis spread of intra-annual variability.

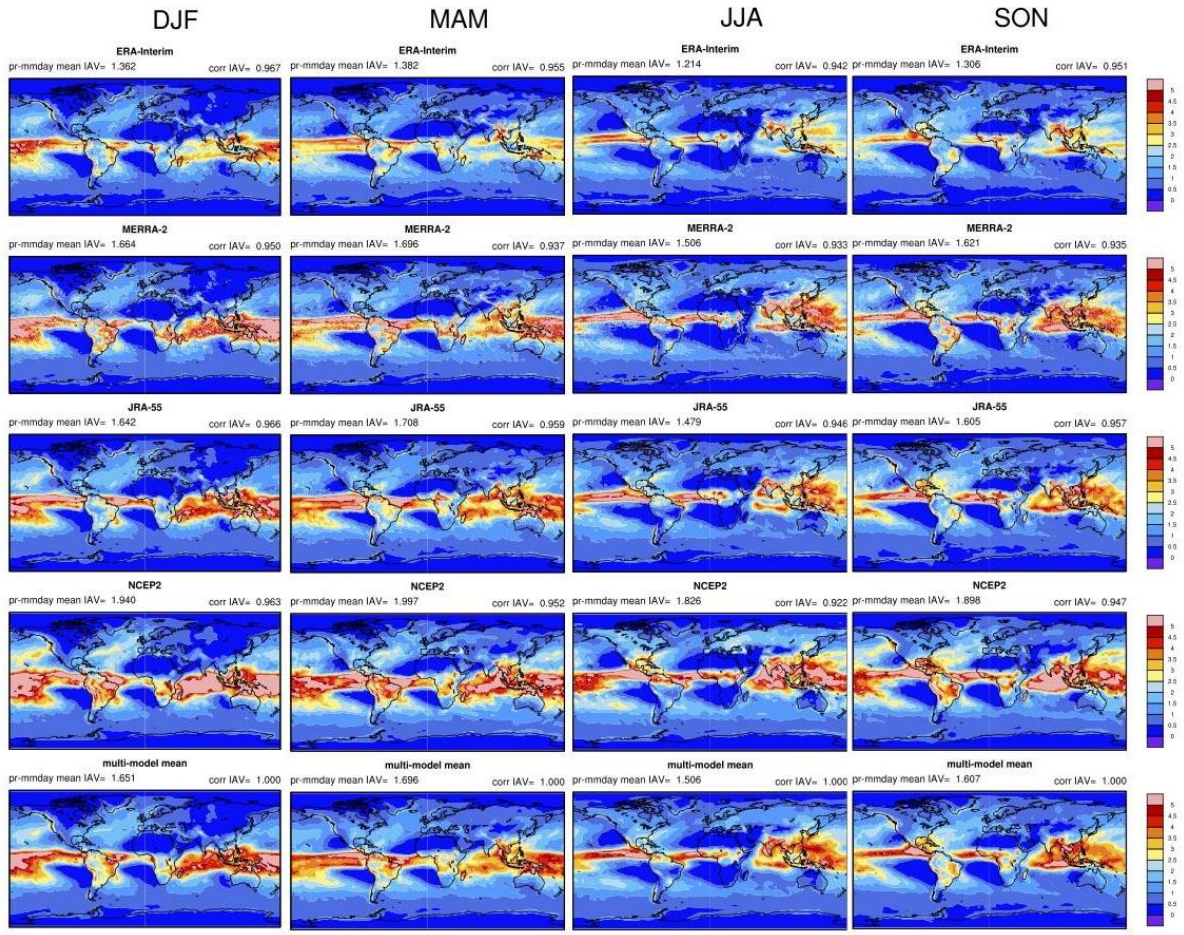

Figure S22: Intraseasonal variability 1980-2017 of monthly precipitation in ERA-Interim, MERRA-2, JRA-55, NCEP/DOE R2 and ensemble multi reanalysis mean.

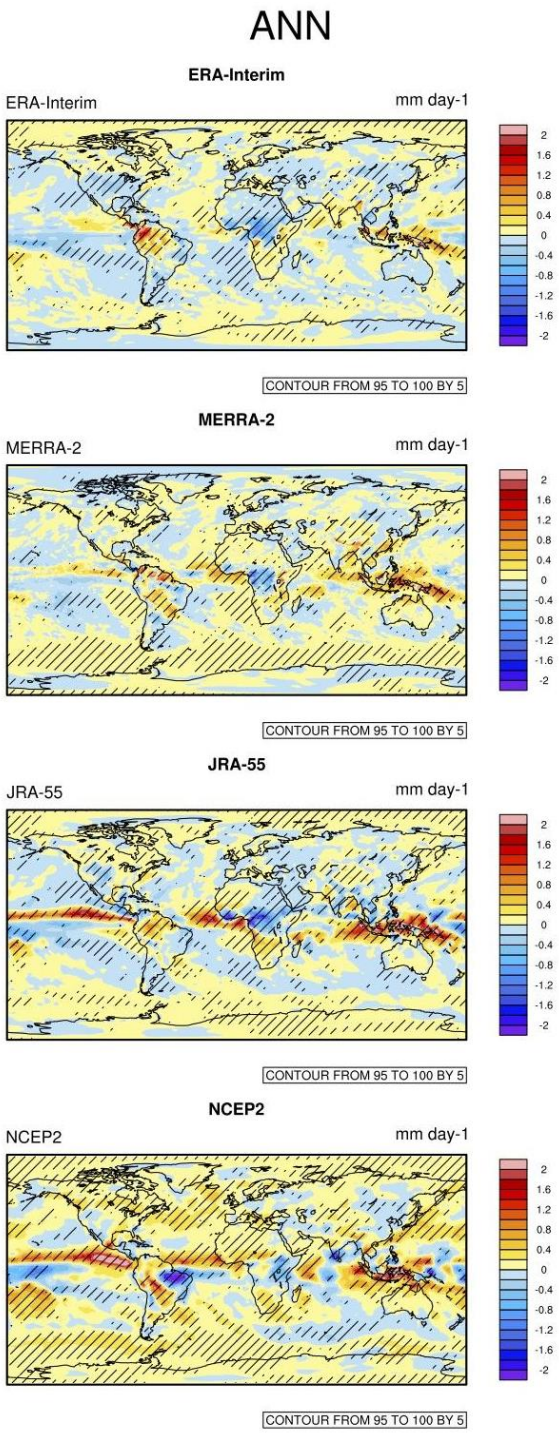

Figure S23: Trend 1980-2017 of precipitation in ERA-Interim, MERRA-2, JRA-55, NCEP/DOE R2.